Copyright Warning & Restrictions

The copyright law of the United States (Title 17, United States Code) governs the making of photocopies or other reproductions of copyrighted material.

Under certain conditions specified in the law, libraries and archives are authorized to furnish a photocopy or other reproduction. One of these specified conditions is that the photocopy or reproduction is not to be "used for any purpose other than private study, scholarship, or research." If a, user makes a request for, or later uses, a photocopy or reproduction for purposes in excess of "fair use" that user may be liable for copyright infringement,

This institution reserves the right to refuse to accept a copying order if, in its judgment, fulfillment of the order would involve violation of copyright law.

Please Note: The author retains the copyright while the New Jersey Institute of Technology reserves the right to distribute this thesis or dissertation

Printing note: If you do not wish to print this page, then select "Pages from: first page # to: last page #" on the print dialog screen

ABSTRACT

NUMERICAL INVESTIGATION OF FLOW THROUGH WIDE ANGLE DIFFUSERS

by
Moududur Rahman

This study is aimed at the development of a computational technique for the prediction of the flow field in wide angle diffusers. The finite element technique is used for the solution of the governing equations. A commercial software package, NISA/3D-FlUID, modified for this specific application was used. The parameters affecting the flow field have been identified. For a wide range of variation of these parameters, the effects on the flow field have been examined. This investigation is an exhaustive and comprehensive numerical study of diffuser flows. Such a study will result in substantial improvement in the understanding of the anatomy of the flow field. The creation of the current knowledge base will also enable a judicious selection of diffusers for industrial applications.

It was found that for laminar flow through wide angle diffusers the computational technique adequately predicted the qualitative and quantitative behavior of the flow field. Therefore new results, as predicted by the current computational technique have been presented. For example, it was found that the effective recirculation length varies exponentially with the angle of expansion of the diffuser. For

turbulent flow the standard k-ϵ model has been found to be qualitatively adequate in representing the flow field. However, the quantitative predictions are being compared with available experimental results and those obtained using other numerical schemes. A wide range of possibilities exist for the constants and boundary conditions employed in k-ϵ modeling. Such a numerical experimentation requires deep understanding of the equations governing the flow field. The validity and/or adjustments of these constants and boundary conditions for diffuser flow are investigated.

NUMERICAL INVESTIGATION OF FLOW THROUGH WIDE ANGLE DIFFUSERS

by
Moududur Rahman

A Dissertation
Submitted to the Faculty of
New Jersey Institute of Technology
in Partial Fulfillment of the Requirements for the Degree of
Doctor of Philosophy

Department of Mechanical and Industrial Engineering

January 1994

APPROVAL PAGE

NUMERICAL INVESTIGATION OF FLOW THROUGH WIDE ANGLE DIFFUSERS

Moududur Rahman

Dr. E.S. Geskin, Dissertation Advisor — Date
Professor of Mechanical Engineering
of The Department of Mechanical and
Industrial Engineering, NJIT

Dr. J.V. Droughton, Committee Member — Date
Professor of Mechanical Engineering
of The Department of Mechanical and
Industrial Engineering, NJIT

Dr. N. Levy, Committee Member — Date
Associate Professor of Mechanical Engineering
of The Department of Mechanical and Industrial
Engineering, NJIT

Dr. R.S. Sodhi, Committee Member — Date
Associate Professor of Mechanical Engineering
of The Department of Mechanical and Industrial
Engineering, NJIT

Dr. E. Gordon, Committee Member — Date
Distinguished Professor of Electrical Engineering
of The Department of Electrical and Computer
Engineering, NJIT

BIOGRAPHICAL SKETCH

Author: Moududur Rahman

Degree: Doctor of Philosophy in Mechanical Engineering

Date: January 1994

Undergraduate and Graduate Education :

- Doctor of Philosophy in Mechanical Engineering
  New Jersey Institute of Technology, Newark, New Jersey, 1994
- Master of Science in Mechanical Engineering
  New Jersey Institute of Technology, Newark, New Jersey, 1987
- Bachelor of Science in Mechanical Engineering
  Bangladesh University of Engineering and Technology, Dhaka, Bangladesh, 1983

Major: Mechanical Engineering

Presentations and Publications:

Rahman, M., 1987, "Finite Element Analysis of the temperature Field in the Course of Laser Heating", Master's Thesis, New Jersey Institute of Technology, Newark, New Jersey.

Rahman, M., Geskin, E.S., 1987, "Computer Modeling of Temperature Field in the Course of Laser Heat Treatment of Metals", Presented at the Annual Meeting of "The Metallurgical Society of AIME", Denver, Colorado.

Rahman, M., Geskin, E.S., 1987, "Computer Modeling of Surface Processing by High Energy Beams", Presented at the "Conference of The Technological Universities of New Jersey", held at Stevan's Institute of Technology, New Jersey.

BIOGRAPHICAL SKETCH
(Continued)

Rahman, M., Bhatia K., Geskin, E.S., 1993, "Finite Element Analysis of Turbulent Flow Through a Sapphire Nozzle for Waterjets", Presented at "9th International CAD/CAM, Robotics and Factories of the Future Conference", Newark, New Jersey.

Bhatia, K., Geskin, E.S., Rahman, M.,1993, "Evaluation of Turbulent Flow Through Expanding Axisymmetric Pipe", Presented at "Eastern Regional Rotating Machinery Conference", Newark, New Jersey.

Bhatia, K., Rahman, M., 1993, "Numerical Analysis of Turbulent Flow in Axisymetric Diffusers", Paper published in the "Proceedings of the Conference of the CFD Society of Canada", CFD93, held at Montreal, June 14-15, pp. 395-399.

Bhatia, K., Rahman, M., Agarwal, B., 1993, "Analysis of Three Banchmark Problems Using NISA/3D-FLUID", Paper published in the Proceedings of "The Fluids Engineering Conference of ASME", Washington D.C.

This dissertation is dedicated to
my parents

ACKNOWLEDGEMENT

I wish to sincerely acknowledge the guidance, patience and encouragement of my advisor, Professor Ernest S. Geskin, during this investigation.

I also wish to express my deepest gratitude to Dr. k. Bhatia, for his constant guidance and wise suggestions during the course of this study. This thesis could not be completed without his support.

I would like to thank Dr. J.V. Droughton, Dr. E. Gordon, Dr. N. Levy and Dr. R.S. Sodhi for serving as members of the committee.

Also thanks to my friend M.E.H. Khan for providing moral support during this work.

Finally, a grateful thank you to my wife for typing the dissertation as well as providing constant inspiration.

TABLE OF CONTENTS

TABLE OF CONTENTS
(Continued)

LIST OF TABLES

LIST OF FIGURES

LIST OF FIGURES
(Continued)

LIST OF FIGURES
(Continued)

LIST OF FIGURES
(Continued)

Figure **Page**

LIST OF SYMBOLS

$C_{\epsilon 1}$	First constant in dissipation equation
$C_{\epsilon 2}$	Second constant in dissipation equation
C_{μ}	Constant of eddy viscosity
d	diameter of inner tube or diffuser inlet
D	Diameter of the larger section of the diffuser
E	Expansion ratio (D/d)
$E^{'}$	Empirical constant in the log-law wall function
G	Production of turbulent kinetic energy
k	Kinetic energy of turbulence
L	Length scale of turbulence
L_e	Eddy center length
L_r	Effective recirculation length
l_m	Mixing length
P	Instantaneous/mean static pressure
Re	Reynolds number
r	Radial distance
x	Axial distance
U_o	Inlet axial velocity
U_1(U)	Instantaneous/mean velocity along axial direction
U_2(V)	Instantaneous/mean velocity along radial direction
U_p	Velocity parallel to the wall
u(u_1)	Fluctuating velocity in axial direction
v(u_2)	Fluctuating velocity in y or r direction
$V^{'}$	Velocity scale of turbulence
w(u_3)	Fluctuating velocity in z direction

LIST OF SYMBOLS
(Continued)

y_p	Distance perpendicular to the wall
ϵ	Dissipation of turbulent kinetic energy
μ	Molecular dynamic viscosity
μ_t	Turbulent dynamic viscosity
υ	Molecular Kinematic viscosity
υ_t	Turbulent kinematic viscosity
ρ	Density
σ_k	Diffusion constant in k equation
σ_ϵ	Diffusion constant in ϵ equation
κ	Von Karman's constant in log-law wall function
τ_w	Wall shear stress
θ	Half angle of expansion

CHAPTER 1

INTRODUCTION

Fluid flow diffusers are expanding axisymmetric geometries with a wide range of industrial applications. Based on the velocity and turbulence characteristics of axisymmetric expansions, they can be broadly classified into two groups. The first have expansions of small total angle (5-10^{o}) and the second are characterized by large total angles and separated flow (wide-angle diffusers). One typical reason for interest in wide-angle diffusers is the recirculation obtained downstream of the expansion. The engineering importance of separation in design of systems is to avoid separation while operating close to a separated state. The separated flow is sometimes called the "separated zone", "stalled region", "recirculation region" or misleadingly, "dead-water region". A separated region or stalled region is that part of the whole flow field adjacent to a free shear layer that separates the zone from the through flow, i.e., the flow that passes through the system from upstream.

Two-dimensional axisymmetric geometry is encountered in a large number of industrial and other processes, such as connection between pipes of different diameter, partial blockage of pipes due to sediment deposits, flow through engine inlet ports (Tsui, 1992), exhaust systems of gas turbine engines (Baskarone, 1991) etc.

Recently, abrasive water jet machining (AWJ) has evolved as a reliable manufacturing technique (Mosavi, 1987, Lai et al., 1991). Due to acceptable cutting speed, absence of heat-affected zones and thermal distortion, and the ability to cut all materials of interest, AWJ is widely used in a number of industrial applications. A typical setup for such an operation is shown in Figure 1. An effective design of the sapphire nozzle and the mixing chamber, where the water jet mixes with abrasive particles, is of critical importance for the whole operating system.

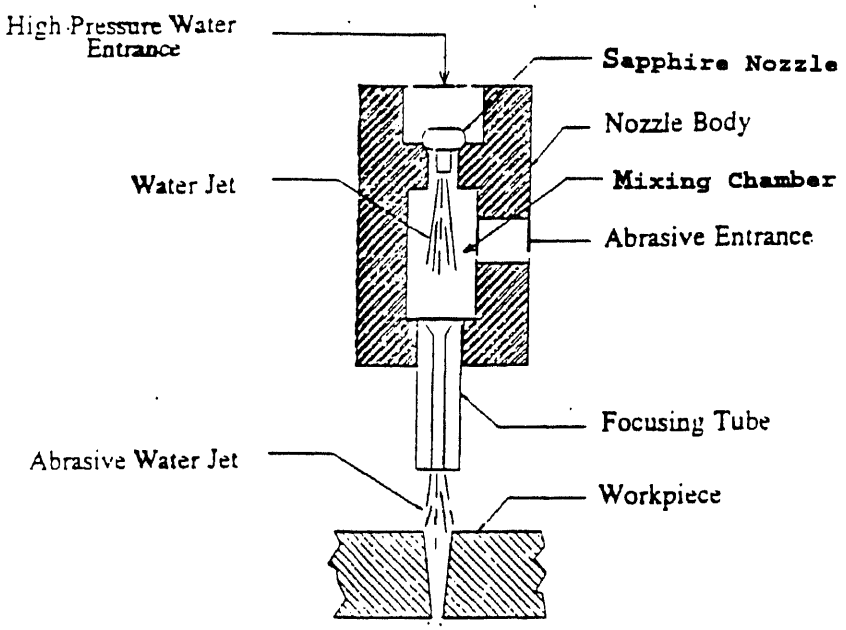

Figure 1 Schematic of Cutting Head.

Because of the simplicity of the suddenly expanding geometries (half angle of expansion of 90^{o}), it has been widely used for validation of complicated numerical fluid flow

solvers (especially the two-dimensional backward facing step). Although the geometry encountered is simple, the corresponding flow field is rather complex. For the industrial applications mentioned above, the Reynolds number encountered makes the flow field vary from a fully laminar case to a highly turbulent one. As will be shown in the review of the literature, attempts have been made in the past to solve the flow field for some specific Reynolds numbers and geometries, but no systematic study has been carried out for a wide range of variation of the above mentioned parameters.

The objective of the current study is to systematically investigate the flow through wide-angle diffusers for a wide range of variation of the parameters affecting the flow field. In case of tuurbulent flow, such a study will enable a better understanding of the physis of turbulence for flow through diffusers. This study will enable the creation of a knowledge base for more effective and efficient design of diffusers encountered in engineering applications. Such a knowledge base will also be helpful in avoiding costly experimentation to study the performance of diffusers.

CHAPTER 2

LITERATURE REVIEW ON DIFFUSER FLOWS

As mentioned in the previous chapter, the current study aims at investigating the flow through wide angle diffusers for a wide range of variation of the parameters affecting the flow field. One of the critical parameters affecting such flows is the Reynolds number ($U_o d/\upsilon$). Based on the Reynolds number the flow can be classified as laminar or turbulent. The current work will include both laminar and turbulent situations. A review of the literature indicates that previous studies on diffusers can be broadly classified based on this parameter. It is also noted that there is no demarkation (based on a single value of Re) when the flow changes from laminar to a fully turbulent one. In general the flow is expected to remain laminar for a Reynolds number below 200 and become fully turbulent for a Reynolds number more than 1000.

2.1 LAMINAR FLOW

Macagno and Hung (1967) performed both numerical and experimental investigation of flow through an axisymmetric conduit expansion. Steady and unsteady approaches were used to solve the stream function vorticity equations using the finite difference method. An expansion ratio of 2.0 was considered. A fully developed parabolic profile was used at the inlet. Oil was used as the fluid for experimental investigations and the

flow at the expansion was observed by means of fine tracers suspended in the oil. The photographic information was supplemented with direct visual observation of dyed oil coming into the flow through a series of small orifices bored through the walls of the conduit. The stream function and vorticity contours as obtained using a direct steady state approach have been reported for Reynolds numbers varying from a vanishingly small value up to 70. The same contours for Reynolds numbers of 100 and 200 were obtained using the unsteady approach. Also the eddy length, eddy center location, and the relative eddy intensity have been presented as functions of time as the Reynolds number was increased from 100 to 200. Comparisons were carried out between the experimental and numerical investigations with the obtained results for recirculation length, eddy center length, relative eddy intensity, and relative maximum vorticity in the backflow region for Reynolds numbers of up to 200.

Back and Roschke (1972) carried out experimental investigations of water flow through abrupt circular channel expansions over a Reynolds number range (based on inlet velocity and diameter) of 20 to 4000. The expansion ratio used was 2.6. The flow at the entrance of the abrupt channel expansion was nearly uniform. Dye injection technique was used for the flow visualization. For the range of Reynolds numbers mentioned above, the variation of recirculation length (normalized by the step height) has been reported as a

function of Reynolds number. For a range of Reynolds number from 20 to 200, the reattachment length was found to increase linearly. The slope of this linear increase was found to be different from that reported by Mecagno and Hung (1967). The reasons have been attributed to the difference in the ratio of step height to inlet diameter and the inlet velocity profile for the two cases. As the Reynolds number increased the reattachment length started to deviate from the linear variation and reached a peak value. This peak value was as large as 25 step heights (7.7 tube dia) and occurred at a Reynolds number of 250. For Reynolds number greater than 250, the recirculation length started decreasing, reaching a minimum near a Reynolds number of 1000 and then increasing again becoming almost invariant near a Reynolds number of 4000.

Fletcher et al. (1985) studied numerically the axisymmetric flow through sudden expansions using stream function vorticity formulation. A finite difference numerical technique was used to solve the differential equations. Computations were carried out for a Reynolds numbers varying from 25 to 1500 and expansion ratios from 1.5 to 6. The inlet velocity profile was changed from fully developed to an almost flat one. For an expansion ratio of 2.0 and the Reynolds number range mentioned above, the recirculation length was found to increase linearly. The location of the eddy center also increases initially with increasing Reynolds number, but for Re > 200, the ratio of L_e/L_r, i.e the relative location of

the eddy center, was found approximately to remain constant at 0.175. The following correlation was developed to describe the relation of recirculation length as a function of expansion ratio for a fixed Reynolds number (Re = 200) and a parabolic inlet profile.

$$L_r/d = 12.2\ (D/d) - 15.3$$

Fletcher et al. also established the strong effect of inlet velocity profile on the recirculation length. The recirculation length was found to have increased by almost 50% owing to the change in inlet profile from fully developed to a nearly flat one.

Laminar flow of a Newtonian fluid in both planar and axisymmetric abrupt expansions has been studied by Scott et al. (1986). Numerical computations were carried out by solving the Navier-Stokes equation using the finite element method. Galerkin's finite element formulation for the primitive variables was used to solve the continuity and momentum equations. Second order triangular elements were used for the velocities and linear variation of the pressure was considered within each element. Reynolds numbers ranging from 50 to 200 was considered with expansion ratios of 1.5, 2, 3 and 4. A parabolic velocity profile was used at the inlet. The Reynolds number dependence of reattachment lengths, eddy center location and relative eddy intensities for each of the above expansion ratios, were reported for both axisymmetric and two

dimensional cases. The reattachment and eddy center locations were reported to be varying linearly whereas the relative eddy intensity (ratio of the maximum amount of backflow in the recirculation region to the inlet mass flow) was found to vary exponentially with the Reynolds number within the range considered. The following relation was proposed relating the reattachment length, eddy center location and the Reynolds number.

$$L_e/L_r = ß + \lambda/Re$$

where L_e indicates eddy center location from the step, L_r the recirculation length; ß and λ are empirical constants.

More recently, Badekas and Knight (1992) carried out systematic numerical computation of flow through axisymmetric sudden expansion for a range of Reynolds number varying between 50 and 200 with expansion ratios (E) ranging from 1.5 to 6.0. A fully developed parabolic profile was used at the inlet. Navier Stokes equations were solved employing the primitive variables using the finite-difference-based SIMPLE algorithm.

Empirical equations were developed for eddy reattachment length, relative eddy intensity and location of the eddy center as functions of Reynolds number and expansion ratio.

The following equation was proposed relating the reattachment length with Reynolds number and expansion ratio

$$L_r/d = \alpha Re$$

where α is a parameter that depends on the expansion ratio. The value of α can be calculated from

$$\alpha = 0.0603 \ (E-1) \ - \ 0.0147$$

The above two equations are expected to hold for $1.5 \leq E \leq 6$ and $50 \leq Re \leq 200$.

The relative eddy intensity (I) is found to be an exponential function of Re, which was earlier realized by Scott and Mirza (1986) who proposed the following expression

$$I = \theta_1 [1 \ - \ e^{(-tRe)}]$$

where θ_1 is given by

$$\theta_1 = a_1 (E-1)^{a_2} + a_3$$

and t is given by

$$t = b_1 [1 - e^{-b_2 (E-1)}] + b_3$$

where the coefficients are found to be $a_1 = 0.17$, $a_2 = 1.27$, $a_3 = -0.37$, $b_1 = 0.054$, $b_2 = 0.86$, $b_3 = -0.008$

The location of eddy center L_e is found to follow the relation given below

$$L_e/d = \text{ß}Re$$

where ß is a parameter that depends on the expansion ratio. The value of ß can be calculated from

$$ß = a_1 [e^{a_2 (E-1)^{a_3}} - 1]$$

where $a_1 = 26$, $a_2 = 4 \times 10^{-4}$ and $a_3 = 1.4$. The higher the expansion ratio the better was the agreement of the above correlation with experimental data.

2.2 TURBULENT FLOW

One of the most thorough experimental & analytical investigations of flow through axisymmetric diffusers for various expansion angles has been carried out by Chaturvedi (1963). The Reynolds number considered was 200,000, based on the inlet condition, and the expansion ratio chosen was 1:2. Four discrete half angles of expansion were considered; 15^{o}, 30^{o}, 45^{o}, and 90^{o}. For analytic study, the Reynolds equations, expressing a balance between forces and mass acceleration, were used. Steady state incompressible flow conditions were assumed without the body force terms. Because of the high Reynolds number the viscous stresses were neglected in comparison with the Reynolds stresses. Since it was not possible to solve the equation for the dependent variables, they were used as a tool to clarify the details of motion by evaluating them on the basis of measured values of the terms involved. The equations were studied in their integral form to make them more convenient and meaningful. Similar approaches

were also used to evaluate the mean and turbulent energy of motion. These provided a valuable means of cross checking the obtained experimental results.

The measurements involved determination of the mean velocity and pressure and the characteristics of turbulence. The mean velocity and pressure measurements were made by stagnation tubes and pitot tubes respectively. The mean velocities were also measured by use of a hot-wire anemometer. The hot-wire anemometer was, however principally used for the measurement of the turbulence characteristics (fluctuating components in each direction and turbulent shear stress). An IIHR (Iowa Institute of Hydraulic Research) hot-wire anemometer, which operates on the principal of constant temperature, was used. Because of the high level of turbulence, the obtained experimental results were subject to certain minor discrepancies. Three types of discrepancies were mentioned and corrective actions were taken. Corrected values of mean velocity, mean pressure, axial turbulence intensity, radial turbulence intensity, and turbulent shear have been presented for different x/d values along the length of the diffuser. Other than turbulent shear, distribution along the centerline have also been reported for all of the above mentioned quantities.

Spatial distribution of stream lines have been reported for all four angles of expansion. As a result of momentum analysis, the centerline distribution of each individual term

has been reported. Similar results have also been reported due to energy analysis. At the end, a more vivid appreciation of the results is obtained due to the presentation of some of the more important factors, such as the kinetic energy of the mean motion, kinetic energy of turbulence, pressure distribution, turbulence production and turbulence shear in the form of their spatial distribution.

Moon & Rudinger (1977) carried out both experimental and numerical investigation of flow through a 90^{o} diffuser with expansion ratio of 1:1.428. The Reynolds number based on the inlet diameter was approximately 280,000. The laser doppler velocimeter was used for the measurement of the velocity field. Numerical computation was carried out using a k-ϵ turbulence model. Moon & Rudinger have presented experimental results from other investigators (Krall et al.,1966; Runchal, 1971; Back et al., 1972) along with their results to show the variation of recirculation length with Reynolds number. No definite conclusion can be made from these results other than that recirculation length varies from 6 to 9 step height for the Reynolds number range of 10^3 to $2.8x10^5$. Moon et.al (1977) iterates the fact that the uncertainty in the location of the reattachment point can be ascribed to both jet unsteadiness and measurement errors; also as the Reynolds number increases, the uncertainty in determination of the reattachment point appears to decrease. The above observation is also confirmed by Krall (1966). Axial velocity distributions as measured by a velocimeter have been provided at different sections

downstream of the step height. Comparisons have been made between the theory and experiment at X/D = 0.75 (D is the internal diameter of the larger tube). There is a good overall qualitative agreement between the two, but it is found that the predicted rate of spread of the round jet is too high, i.e the thickness of the recirculation zone is too small. Centerline velocity distribution obtained using the theory shows very good agreement with the experimental measurements. Attempts were made to adjust the length of the recirculation zone (which was initially further downstream compared to experiments) by changing the coefficients of the turbulence production and dissipation terms ($C_{\epsilon 1}$ and $C_{\epsilon 2}$). However, it was found that these adjustments resulted in poor recirculation zone thicknesses and centerline velocity decay. Nevertheless, the co-efficient of dissipation ($C_{\epsilon 2}$) used by the author was 1.7 instead of 1.94 as recommended by Launder (1974) .

Sala et al. (1980) also studied the flow characteristics of axisymmetric diffusers with half angles of 15^{o}, 30^{o}, 45^{o}, and 90^{o} by means of two equations; the (k-ϵ) turbulence model in conjunction with the finite difference method. The obtained results were compared with those reported by Chaturvedi (1963). Integral analysis of the momentum, mean kinetic and turbulence kinetic energy equation were also carried out. The expansion ratio considered was 2.0. A uniform velocity U_o , a turbulence kinetic energy of 0.014 U_o^2 and a uniform length scale of 0.05 d (d is the inlet diameter) were used as the

boundary conditions at the inlet. The wall-function method (Launder et al., 1974) was used for setting the boundary conditions for the momentum equations and calculating k-generation terms near the wall. A different relation for the shear stress at the wall has been used in place of that derived from the logarithmic velocity profile (Launder et al,1974) i.e..

$$\tau_w = \rho C_\mu^{1/4} k_p^{1/2} \kappa U_p$$

in which, subscript p = the adjacent node to the wall; κ = von Karman's constant; U_p = the velocity parallel to the wall under consideration. The above equation is obtained under the assumption that the mean turbulent dissipation near the wall is fixed at a value given by

$$\epsilon = C_\mu^{3/4} k_p^{3/2} / \kappa y_p$$

and the hypothesis of a uniform shear region.

Sala et al. have presented the results for centerline velocity and pressure distribution. Large disagreement was found to occur near the recirculation region. Axial velocity profiles as a function of radial distance have been reported at different downstream stations for an expansion angle of 45^o. In the recirculation region, the maximum return-flow velocity location is predicted nearer the wall than observed experimentally. Serious discrepancy is found in the computed

recirculation lengths compared to the corresponding experimental results. Experimental results (Chaturvedi, 1963) indicate that the recirculation length in case of 15^{o} is significantly less compared to the other angles of expansion, but in the computation of Sala et al., in the case of 15^{o} the recirculation length is found to be slightly higher than the others. Spatial distribution of turbulent kinetic energy, turbulence production, turbulent shear stress and mean kinetic energy have been reported for angles of expansion of 45^{o} and 90^{o}. Turbulent kinetic energy distributions indicate that the location of this maxima are predicted reasonably well with the magnitude well within 15%, but centerline velocity distributions are in gross disagreement with each other. Contours of turbulent production depict that the location of maxima are predicted much closer to the inlet compared to the experiments. Contours of turbulent shear stress show a reverse trend compared to the turbulent production as the maxima are predicted further downstream compared to the experimental values. Though the mean kinetic energy contours show reasonably good agreement near upstream (both in magnitude and location) they begin to differ as one moves downstream of the diffuser. Shear stress distribution as reported for a half-angle of expansion of 45^{o} at different axial locations indicates better agreement in the shear layer upstream and downstream of the recirculation region. Author (Sala et al., 1980) has also reported the results of integral analysis of

momentum, mean kinetic & turbulent kinetic energy as was also done by Chaturvedi (1963).

Habib & Whitelaw (1982) described a method of calculating the properties of axisymmetric swirling and nonswirling turbulent recirculating flows in wide-angle diffusers. The study is based on the numerical solution of two equation (k-ϵ) (Jones, 1971) turbulence model in orthogonal curvilinear coordinates using finite difference method. The angles of expansion considered were 20^{o} and 45^{o} with an expansion ratio of 2.0. The boundary conditions required for the solution at the inlet were taken from measurements where possible. The rate of dissipation at the inlet section was estimated using the relation $\epsilon = c_{\mu}k^{3/2}/L$ where $L = 0.3r$ and r is the radius of the pipe upstream of the expansion. All the axial gradients were presumed to be zero in the exit plane of the confining tube. The wall function approach was used to bridge the wall with the fully turbulent region. The inlet distribution of kinetic energy of turbulence was presumed to be similar to that of the normal stress with the value of k at the centerline taken equal to $0.003U_{o}^{2}$, where U_{o} is the mean velocity at the centerline. For an angle of expansion of 20^{o} the results obtained were compared with the experimental results obtained by the same authors. The width of recirculation was predicted correctly, and the agreement was found to be better in the downstream region where a maximum discrepancy of 8% was obtained. A maximum discrepancy of 14% was obtained in cases of mean velocity results with a maximum

occurring close to the region of maximum normal stresses. The calculated kinetic energy distribution was also compared with the experimental results, which was based on the measurement of normal stress u with the values of v and w taken equal to 0.60u. Although the location of maximum kinetic energy was predicted correctly its magnitude at different axial locations differed by as much as 30%. The reason for this was attributed partly to the overprediction in the rate of dissipation due to the incorrect representation of the source term in its transport equation and partly to the effects of the extra strain terms in the calculation of Reynolds stress and the dissipation rate.

In the case of 45^{o}, the results were compared with the experimental results of Chaturvedi (1963). The general features of the flow were found to be correctly predicted. The disagreement in the kinetic energy solution in the recirculation region was severe.

Benim and Zinser (1985) studied axisymmetric flow through sudden expansion using the finite element method and adopting a primitive-variable formulation. An expansion ratio of 6.6 and a Reynolds number of 3×10^{5} were considered. The standard k-ϵ equation was used for turbulence modeling with wall-function approach near solid boundaries. A modified expression for estimating wall function had also been proposed. In the analysis, rectangular isoparametric elements were used. The velocity components as well as k and ϵ were interpolated linearly while the pressure was assumed to be constant in each

element. Finite element equations were derived using the Galerkin method. The obtained results were compared with experimental as well as finite difference predictions (Pai et al., 1975).

The velocity profile at the inlet was approximated using the following expression

$$U/U_{oc} = (y/r)^{1/n}$$

where, U_{oc} is the velocity at the center and r is the radius of the inlet section. Inlet boundary conditions for k and ϵ were derived by assuming a turbulence intensity of six percent and a length scale of

$$L = 0.1\ (0.99)^{n}r$$

A value of 40 was used for n, since the inlet profile for the experimental setup was not fully developed. A constant eddy viscosity model and jet profile were also used to compare with the other models.

Axial velocity distributions along the centerline show good correlation between the experimental, current numerical scheme, and other numerical schemes. The constant eddy viscosity model failed to provide good correlation throughout the whole domain. The free jet profile was found to perform well for x/d of up to 10. The effect of variation of n was also studied; a value of n = 10 (fully developed profile at

inlet) failed to predict the initial core region. Axial velocity profiles for different x/d locations were also presented. Good agreement between the numerical schemes and experiments were reported.

It was concluded that the finite element method is as effective as other numerical schemes, with the added advantage of allowing a flexible mesh for complex geometries.

Numerical studies of turbulent flow in an axisymmetric 45^{o} expansion combustor and bifurcated diffuser has been carried out by Yung et al. (1989). The Navier-Stokes equation along with the k-ϵ model were solved in a non-orthogonal curvilinear co-ordinate system. A zonal grid method, where the flow field is divided into several subsections was developed. This approach allows different computational schemes in different zones. A finite volume method was used to solve the equations in the transformed co-ordinate system incorporating the SIMPLE algorithm. In this study three differencing methods-hybrid, quadratic upwind (Leonard,1979), and skew upwind (Raithby,1976), were used for the convective flux.

For the 45^{o} combustor, the inlet boundary conditions were taken from experimental conditions of Chaturvedi. The inlet velocity profile was flat and the Reynolds number was $2.5x10^{5}$. The expansion ratio was 2.0. Inlet boundary conditions for k and ϵ were chosen as $k = 0.03U_{o}^{2}$, $\epsilon = k^{1.5}/0.005D$ where, U_{o} is the velocity at inlet and D is the diameter of the larger pipe.

The reattachment length of the recirculation calculated with for various computational schemes and meshes were tabulated. The experimental value of the reattachment length is 4.5 times the inlet diameter (Chaturvedi,1963). The differences between the predicted and measured lengths range from 10% to 30% depending upon the numerical methods considered. The hybrid scheme produced the most accurate results among the three differencing schemes. The velocity decay for the three differencing schemes were also compared with the experimental data. Good agreement was found within the recirculation region, but produced overestimated results farther downstream for the three differencing methods used. The radial distribution of turbulence intensity ($u = \sqrt{(2k/3)}$) was also compared at different locations. The predictions were not good at the upstream locations but satisfactory agreement was found at downstream locations (X/D = 8.0). Contour plots as obtained by the hybrid scheme have been reported for streamline, axial velocity, and turbulence intensity respectively. The maximum reverse flow was found to be about 18% of the total mass flow rate at a location about one inlet diameter downstream of the inlet.

CHAPTER 3

STATEMENT OF THE PROBLEM

In the previous section, the importance of the understanding of fluid flow through diffusers has been emphasized. It was found that there are wide ranges of applications starting from very low speed flow to a highly turbulent one. It has been well documented (Fletcher et al., 1985) that the parameters affecting the performance of a suddenly expanding diffuser are the inlet Reynolds number, inlet velocity profile, and the expansion ratio. To the best of our knowledge, no study has been presented in the literature investigating the effect of angle of expansion on the flow field in the case of laminar flow in combination with other factors. The current study shows that angle of expansion has a strong effect on the recirculation length.

In this study, a systematic investigation of flow through expanding axisymmetric pipe has been undertaken. A typical sketch of the flow domain is shown in Figure 2. The required differential equations describing this kind of flow are compiled in Chapter 6. In brief, momentum, continuity, and k-ϵ equations are to be solved. The effect of different angles of expansion, expansion ratios and Reynolds numbers (both laminar and turbulent) have been examined. For the turbulent flow case, the effect of inlet boundary conditions, wall boundary conditions and empirical coefficients used in the k-ϵ

equations have also been studied. The inlet velocity boundary condition was kept constant for all flow situations. The variation of Reynolds number was obtained by changing the molecular viscosity of the fluid considered.

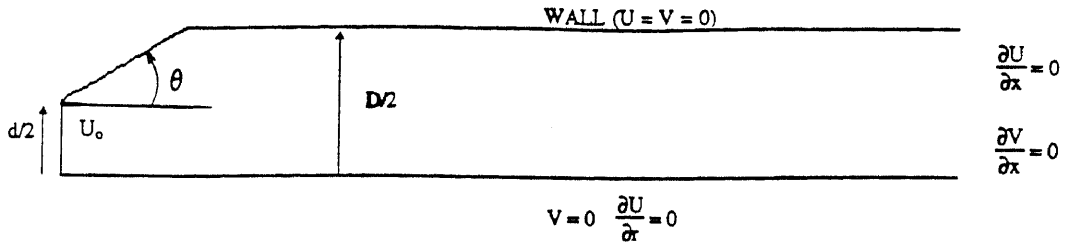

Figure 2 The Computational Domain and the Prescribed Boundary Conditions

As shown in Figure 2, at the inlet a fixed axial velocity $U = U_o$ has been specified, with the radial velocity (V) considered as zero. On the walls, the no-slip boundary condition (U = V = 0) has been specified. On the axis of symmetry, the radial velocity V and the radial derivative of the axial velocity have been considered as zero. At the exit, the axial derivatives of both axial and radial velocities are taken as zero. For turbulent flow, the wall function approach (Tong, 1983) has been used to bridge the solution obtained in the fully turbulent region with that near the physical wall. The following relation (Launder et al., 1974) was used to obtain the turbulent kinetic energy boundary condition at the inlet.

$$k = CU_o^2 \qquad (3.1)$$

where C is an empirical constant. The boundary condition for turbulent dissipation energy at the inlet is obtained using the following relation :

$$\epsilon = \frac{C_\mu k^{3/2}}{L} \qquad (3.2)$$

where C_μ is another empirical constant and L is known as the length scale of turbulence.

CHAPTER 4

MOMENTUM EQUATION AND TURBULENCE

In the previous chapter the problem of obtaining a flow field for a range of Reynolds numbers had been identified. In this chapter, the equations required to solve the flow field will be presented. The basic principles are the well known conservation of mass and conservation of momentum. The first one gives rise to the continuity equation the second one to the momentum or Navier Stokes equation. The following assumptions are used to derive and simplify the equations to the forms given below

1) Flow is homogeneous, isotropic, incompressible.

2) Continuum principle is satisfied.

3) Valid for both laminar and turbulent flows.

4) No body force considered.

5) Fluid is Newtonian.

Under the above assumptions the equation of continuity can be written as (Schlichting, 1979) :

$$\frac{\partial U_i}{\partial x_i}=0 \qquad (4.1)$$

and the momentum equation takes the form

$$\rho\left[\frac{\partial U_i}{\partial t}+U_j\frac{\partial U_i}{\partial x_j}\right]=-\frac{\partial P}{\partial x_i}+\frac{\partial}{\partial x_j}\mu\left[\frac{\partial U_i}{\partial x_j}+\frac{\partial U_j}{\partial x_i}\right] \qquad (4.2)$$

Note that summation convention for repeated indices is

assumed above. The first term on the left hand side is the unsteady term, followed by the convection terms. Pressure gradient is the first term on the right hand side and the second term is known as the diffusion term.

As mentioned previously the Reynolds numbers for the problem to be analyzed range from laminar to fully turbulent situations. Although the equations of motion stated above are applicable to both situations, due to computational limitations (Launder et al., 1974), it is not possible to use the above equations directly for a turbulent flow situation. A detailed description of turbulent flow simulation is given next.

4.1 TURBULENCE

Turbulence is a highly complex nonlinear, time dependent and three-dimensional phenomenon. The most important characteristic of turbulent motion is its ability to diffuse momentum, heat, and mass far more effectively than molecular diffusion. It is an eddying motion which, at high Reynolds numbers, usually prevailing, has a wide spectrum of eddy sizes and a corresponding spectrum of fluctuation frequencies; it's motion is always rotational and can be thought of as a tangle of vortex elements whose vorticity vectors can be aligned in all directions and are highly unsteady. The larger eddies, which are associated with the low frequency of fluctuations, are determined by the boundary conditions of the flow and their size is of the same order of magnitude as the flow

domain. The smaller eddies, associated with high frequency of fluctuations, are determined by viscous forces. The width of the spectrum and thus the difference between the largest and smallest eddies increase with the Reynolds number. It is mainly the large scale turbulent motion that transports momentum and heat.

The large eddies interact with the mean flow (because the scales of both are similar), thereby extracting kinetic energy from the mean motion and feeding it into the large scale turbulent motion. The eddies can be considered as vortex elements which stretch each other. Due to this vortex stretching, which is an essential feature of the turbulent motion, the energy is passed on to smaller and smaller eddies until viscous forces become active and dissipate the energy. This process is called energy cascade. The rate at which mean-flow energy is fed into the turbulent motion is determined by the large scale motion; only this amount of energy can be passed on to smaller scale and finally be dissipated. Therefore, the rate of energy dissipation is also determined by the large-scale motion although dissipation is a viscous process and takes place at the smallest eddies. It is important to note that viscosity does not determine the amount of dissipated energy but only the scale at which dissipation takes place. The smaller the viscosity (i.e. the larger the Reynolds number), the smaller are the dissipative eddies relative to the large-scale eddies.

The instantaneous velocity field in a turbulent flow is

described by the Navier-Stokes equation. However, even today's super computers are not fast enough nor do they have the storage capacity to solve these equations directly for the required range of length and time scales. Hence it is of practical importance to describe turbulent motion in terms of time average quantities rather than instantaneous ones.

A statistical approach is used and each of the field variables (velocity, pressure, and temperature) is separated into mean and fluctuating quantities. Thus mean values of the field variables (U_i and P) are used to model the large scale flow characteristics. For an arbitrary field variable Γ, we define its mean value as

$$\overline{\Gamma} = \frac{1}{\Delta t}\int_{t}^{t+\Delta t} \Gamma d\tau \qquad (4.3)$$

where the averaging time t is long compared with the time scale of the turbulent motion. The variable Γ is then decomposed into mean and fluctuating components as follows

$$\Gamma = \overline{\Gamma} + \gamma \qquad (4.4)$$

This decomposition is directly applied to the equations of motion (4.1 and 4.2) given earlier. For brevity, the overbars indicating averaged value will be dropped from U_i and P from here on. The resulting equations are integrated over the interval (t, t + Δt) yielding the following field equations.

$$\frac{\partial U_j}{\partial x_j}=0 \qquad (4.5)$$

$$\rho\left[\frac{\partial U_i}{\partial t}+U_j\frac{\partial U_i}{\partial x_j}\right]=-\frac{\partial P}{\partial x_i}+\frac{\partial}{\partial x_j}\left[\mu\left(\frac{\partial U_i}{\partial x_j}+\frac{\partial U_j}{\partial x_j}\right)-\rho\overline{u_i u_j}\right] \qquad (4.6)$$

These are the equations governing the mean flow quantities U_i and P .

The averaging process has introduced unknown correlations between fluctuating velocities $\overline{u_i u_j}$ and the mean velocity U_i. The term $-\rho\overline{u_i u_j}$ is known as "apparent" or Reynolds stresses of turbulent flow. From now on the overbar from the Reynolds stress term will be dropped when it appears within the text.

Equations (4.5) - (4.6) can be solved for the mean values of velocity and pressure only when the turbulence correlations can be determined in some way. Basically, the determination of these correlations is the main problem in calculating turbulent flows.

Exact transport equations can be derived for $u_i u_j$, but these equations contain turbulence correlations of the next higher order. Therefore, closure of the equations cannot be obtained resorting to equations for correlations of higher and higher order; instead, a turbulence model must be introduced which approximates the correlations of a certain order in terms of lower order correlations and/or mean-flow equations.

4.2 Eddy-Viscosity Concept

The mostly-used approach to modeling the Reynolds stresses is due to Boussinesq (Rodi, 1980); his eddy-viscosity concept assumes that, in analogy with the viscous stresses in laminar flow, the components of the Reynolds stress tensor are proportional to the mean velocity gradient, i.e

$$-\rho\overline{u_i u_j}=\mu_t\left(\frac{\partial U_i}{\partial x_j}+\frac{\partial U_j}{\partial x_i}\right)-\frac{2}{3}k\delta_{ij} \qquad (4.7)$$

The proportionality parameter μ_t is termed the eddy viscosity and unlike the conventional shear viscosity μ, depends on the turbulence of the flow and hence is a flow property.

The eddy-viscosity concept was conceived by presuming an analogy between the molecular motion, which leads to Stoke's viscosity law in laminar flow, and the turbulent motion. The turbulent eddies were thought of as lumps of fluid which, like molecules, collide and exchange momentum. The molecular viscosity is proportional to the average velocity and mean free path of the molecules; accordingly the eddy viscosity is considered proportional to a velocity characterizing the fluctuating motion and to a typical length of this motion which Prandtl called mixing length (Schlichting, 1979).

4.3 Model classification

Turbulence models were developed which do not make use of the turbulent viscosity concept but employ differential transport

equations for the turbulent momentum $u_i u_j$. One possible way of classification of turbulence models would be according to whether (or not) the models use the eddy viscosity concept. However, there are such large differences between the simplest and the most advanced eddy-viscosity models that a finer subdivision seems appropriate. For example, the use of constant eddy viscosity tuned to suit the problem has little to do with turbulence modeling, it does not account for changes in local turbulence structure, whence it cannot in general describe correctly the details of the mean flow field. The simplest models relate the eddy viscosity μ_t directly to the mean velocity distribution.

$$\frac{\mu_t}{\rho} = \upsilon_t \alpha V'L \qquad (4.8)$$

These models assume that the turbulence is in local equilibrium (generation = dissipation), which means there is no transport of turbulence in the flow field.

In order to account for the transport of turbulence, models have been developed which employ transport equations for quantities characterizing the turbulence. These equations contain terms representing both the convective transport by the mean motion and diffusive transport by the turbulent motion. Some models use only a transport equation for the single velocity scale V' (one equation model) assumed to characterize the fluctuating velocities, while others also use an equation for length scale L (two equation model). Still

more complex models solve equations for more than one velocity scale, namely the transport equations for $u_i u_j$.

4.3.1 Zero equation / Mixing-Length Model

The first model to describe the distribution of the eddy viscosity, and thus the first proper turbulence model, was suggested by Prandtl (1925) and is known as the Prandtl mixing length hypothesis. Stimulated by kinetic gas theory Prandtl assumed that the eddy viscosity μ_t is proportional to a mean fluctuating velocity V´ and a "mixing length" l_m (similar to equation 4.8).

Considering the shear layers with only one significant turbulent stress ($u_1 u_2$) and velocity gradient $\partial U/\partial y$, he then postulated that V´ is equal to the mean velocity gradient times the mixing length l_m

$$V' = l_m \left| \frac{\partial U}{\partial y} \right| \qquad (4.9)$$

with this relation, the eddy viscosity can now be expressed as

$$\upsilon_t = l_m^2 \left| \frac{\partial U}{\partial y} \right| \qquad (4.10)$$

This is Prandtl mixing length theory; it relates the eddy viscosity to the local mean-velocity gradient and involves as single unknown parameter the mixing-length l_m.

The mixing length model has been applied with a

considerable success, at least for relatively simple flows, because l_m can be specified by simple empirical formulae in many situations. In free layers, l_m can be assumed constant across the layer and proportional to the local layer width δ.

The mixing length model is not suitable when processes of convective or diffusive transport of turbulence are important; examples are rapidly developing flows, heat transfer across planes with zero velocity gradient, and recirculating flows. More generally the model is of little use in complex flows because of the great difficulties encountered in specifying l_m, and the simplicity with which it is derived.

4.3.2 One Equation Model

In order to overcome the above mentioned limitations of the mixing length hypothesis, turbulence models were developed which account for the transport of turbulence equations by solving differential transport equations for them. An important step in the development was to give up the direct link between the fluctuating velocity scale and the mean-velocity gradients and to determine this scale from a transport equation.

If the velocity fluctuations are to be characterized by one scale, the physically most meaningful scale is $\sqrt{k}$, where k is the kinetic energy of the turbulent motion (per unit mass) defined as follows.

$$k = 1/2\ (u_1^2 + u_2^2 + u_3^2) \qquad (4.11)$$

According to this equation k is a direct measure of the

intensity of the turbulence fluctuations in the three directions. When this scale is used in the eddy viscosity relation (4.8), it results in

$$\upsilon_t = C_\mu' \sqrt{k} L \tag{4.12}$$

where C_μ' is an empirical constant. This formula is known as Kolmogorov-Prandtl expression because Kolmogorov (1968) and Prandtl (1945) introduced it independently. They also suggested to determine the distribution of k by solving a transport equation for this quantity. Such an equation can be derived in exact form from the Navier-Stokes equation. For high Reynolds numbers the equation reads

$$\frac{\partial k}{\partial t} + U_i \frac{\partial k}{\partial x_i} = \frac{\partial}{\partial x_i} \overline{[u_i (\frac{u_i u_j}{2} + \frac{P}{\rho})]} - u_i u_j \frac{\partial U_i}{\partial x_j} - \upsilon \overline{\frac{\partial u_i}{\partial x_j} \frac{\partial u_i}{\partial x_j}} \tag{4.13}$$

The rate of change of k is balanced by the convective transport due to the mean motion, the diffusive transport due to velocity and pressure fluctuations, the production of k (G) by interaction of Reynolds stresses and mean-velocity gradients, and the dissipation of k by viscous dissipation into heat.

The exact k equation (4.13) is of no use in a turbulence model because new unknown correlations appear in the diffusion and dissipation terms. To obtain a closed set of equations, model assumptions are made for these terms. The diffusion flux of k is often assumed proportional to the gradient of k.

$$\overline{u_i\left(\frac{u_i u_j}{2}+\frac{P}{\rho}\right)}=\frac{\upsilon_t}{\sigma_k}\frac{\partial k}{\partial x_i} \qquad (4.14)$$

where σ_k is an empirical diffusion constant. The dissipation ϵ is usually modeled by the expression

$$\epsilon=C_D\frac{k^{3/2}}{L} \qquad (4.15)$$

where C_D is a further empirical constant.

With the above model assumptions and eddy-viscosity and diffusivity expressions for u_iu_j and using equation (4.8), the k equation reads

$$\rho\left[\frac{\partial k}{\partial t}+U_i\frac{\partial k}{\partial x_i}\right]=\frac{\partial}{\partial x_i}\left(\frac{\mu_t}{\sigma_k}\frac{\partial k}{\partial x_i}\right)+\mu_t\left(\frac{\partial U_i}{\partial x_j}+\frac{\partial U_j}{\partial x_i}\right)\frac{\partial U_i}{\partial x_j}-C_D\frac{k^{3/2}}{L} \qquad (4.16)$$

This is a high Reynolds number form of the transport equation for k used in most one equation models. $C_\mu' C_D \approx 0.08$ and $\sigma_k \approx 1$ appear to be reasonable values of empirical constants (Launder et al., 1972). It should be noted that it is not the individual values of C_μ' and C_D that are important but only their product; the individual values determine the absolute value of the length scale L which is normally not of interest.

The Kolmogorov-Prandtl expression (4.12) and the dissipation term of the k-equation (4.15) contain the length scale L which needs to be determined. This determination

distinguishes the various one-equation models that use equation, (4.12) and (4.15). In most models L, is determined from simple empirical relations similar to those given for the mixing length l_m. Unfortunately, L is no easier to prescribe than l_m; its ratio to the shear layer width S also depends on the type of flow, and in flows that are more complex than shear layers there is little empirical information available on the length scale distribution.

4.3.3 Two-Equation Models

The length scale L characterizing the size of the large, energy-containing eddies is subject to transport processes in a similar manner to the energy k. For example, the eddies generated by a grid are convected downstream so that their size at any station depends very much on their initial size. Other processes influencing the length scale are dissipation, which destroys the small eddies and thus effectively increases the eddy size, and vortex stretching connected with the energy cascade, which reduces the eddy size. The balance of all these processes can be expressed in a transport equation for L which can then be used to calculate the distribution of L.

A length scale equation need not necessarily have the length scale itself as dependent variable; any combination of the form $Z = k^m L^n$ will suffice because k is known from solving its own transport equation. In fact most equations proposed so far do not use L as a variable (Rodi, 1980) : Chou (1945), Davidov (1961), Harlow and Nakayama (1967) and Launder (1972)

suggested an equation for the dissipation rate $\epsilon \alpha k^{1.5}/L$, Rotta (1968) proposed an equation for kL, Kolmogorov (1968) an equation for the frequency $k^{0.5}/L$, and Spading (1971) and Saffman (1970) an equation for a turbulence vorticity k/L^2. Even though these equations express different physical processes and may not have been intended as length-scale equations, this is effectively what they all are. Some of the equations were derived first in exact form by manipulation of the Navier-Stokes equations and were then turned into a tractable form by model assumptions; other were conceived heuristically. The results are very similar; in fact all the equations possess a common form which reads

$$\frac{\partial Z}{\partial t}+U_i\frac{\partial Z}{\partial x_i}=\frac{\partial}{\partial x_i}\left(\frac{\sqrt{k}L}{\sigma_z}\frac{\partial Z}{\partial x_i}\right)+C_{z1}\frac{Z}{k}G-C_{z2}\frac{Z\sqrt{k}}{L}+S \qquad (4.17)$$

The first term on the left hand side indicates rate of change whereas the second term indicates convection. On the right hand side, the first term indicates diffusion, the second term indicates production whereas the last two terms indicate distribution of the variable Z; where , C_{z1}, C_{z2} and σ_z are empirical constants.

4.3.3.1 The ϵ equation

At high Reynolds numbers where local isotropy prevails, the rate of dissipation is equal to the (molecular) kinematic viscosity times the fluctuating vorticity $(\partial u_i/\partial x_i)^2$. An exact transport equation can be derived from the Navier-Stokes equations for the fluctuating vorticity, and thus for the

dissipation (Tenneskes, et al., 1972). This equation contains complex correlations whose behavior is little known and for which fairly drastic model assumptions must be introduced in order to make the equation tractable. The equation contains terms representing the rate of change, convection, diffusion, generation of vorticity due to vortex stretching connected with the energy cascade, and viscous destruction terms that require model assumptions. Usually, the diffusion is modeled with the gradient assumption. The generation and destruction terms cannot be modeled with gradient assumptions. They cannot be modeled separately. It is their difference that is modeled (Rodi, 1971). The outcome of the modeling is the equation presented below

$$\rho\left[\frac{\partial \epsilon}{\partial t}+U_i\frac{\partial \epsilon}{\partial x_i}\right]=\frac{\partial}{\partial x_i}\left(\frac{\mu_t}{\sigma_e}\frac{\partial \epsilon}{\partial x_i}\right)+C_{\epsilon 1}\frac{\epsilon}{k}G-C_{\epsilon 2}\frac{\epsilon^2}{k} \qquad (4.18)$$

where G is the production term which is also used in the k equation.

4.3.4 Reynolds-Stress Equations

The first suggestion to determine u_iu_j from a transport equation was already made by Keller and Friedmann (1924). These authors showed how (under certain assumptions) equations for u_iu_j can be derived, but they did not give the equations explicitly. Chou (1945) was the first to derive and present the exact u_iu_j equation given below.

The exact equation for the Reynolds-Stress u_iu_j can be

derived in the following way. The time-averaged momentum equation (4.6) is subtracted from the time dependent Navier-Stokes equation (4.2) for both the x_i and the x_j momentum. The resulting equation for the component i is then multiplied with the fluctuating velocity u_j, and the equation for the component j is multiplied with u_i. Summation of the two equations and subsequent time-averaging yields the u_iu_j equation (Hinze, 1959).

$$\frac{\partial \overline{u_iu_j}}{\partial t}+u_1\frac{\partial \overline{u_iu_j}}{\partial x_1}=-\frac{\partial}{\partial x_1}(\overline{u_1u_iu_j})-\frac{1}{\rho}(\frac{\partial \overline{u_jP}}{\partial x_i}-\frac{\partial \overline{u_iP}}{\partial x_j})-\overline{u_iu_1}\frac{\partial u_j}{\partial x_1}$$

$$-\overline{u_ju_1}\frac{\partial u_i}{\partial x_1}+\frac{P}{\rho}(\overline{\frac{\partial u_i}{\partial x_j}+\frac{\partial u_j}{\partial x_i}})-2\upsilon\overline{\frac{\partial u_i}{\partial x_1}\frac{\partial u_j}{\partial x_1}} \qquad (4.19)$$

The contraction of this equation, that is when the three equations for the three normal stress (i = j = 1, 2, 3) are summed up, yields the exact turbulent kinetic energy equation (4.16), presented already ($k = 1/2u_iu_i$). The physical meaning of the individual terms of the k-equation was described before and equivalent terms appear in equation (4.19), which represent the rate of change, convective and diffusive transport, and viscous destruction of u_iu_j. Equation (4.19) contains an additional term (fifth term on right hand side) denoted "pressure strain" term because it involves correlations between fluctuating pressure and strain rates. Summation of the pressure strain term for i = j over 1, 2, and 3 yields $2\overline{\frac{P}{\rho}\frac{\partial u_i}{\partial x_i}}$ which is zero because of the continuity condition. That is why this term is absent in the k equation.

4.3.5 Algebraic Stress / Flux Models

In general flows, there are six components of the Reynolds stress $u_i u_j$. A turbulence model employing transport equations for all this components, would therefore require the solution of 10 partial differential equations. This is not a trivial task even with modern numerical schemes and computing facilities, and it renders the models rather uneconomical. Suggestions were therefore made to simplify the equations such that they reduce algebraic expressions but still retain most of their basic features.

Gradient of their dependent variables appear in the transport equations only in the rate of change, convection and diffusion terms. Hence, when these gradients can be eliminated by model approximations, the differential equations can be converted into algebraic expressions. The simplest model is to neglect the rate of change and transport terms, and this appears to be a sufficiently accurate approximation in many cases. However, a more generally valid approximation was proposed by Rodi (1976), who assumed that the transport of $u_i u_j$ is proportional to the transport of k, the proportionality factor being the ratio $u_i u_j/k$ (which is not a constant).

$$\frac{D\overline{u_i u_j}}{Dt} - Diff(\overline{u_i u_j}) = \frac{\overline{u_i u_j}}{k}\left(\frac{Dk}{Dt} - Diff(k)\right) = \frac{\overline{u_i u_j}}{k}(G-\epsilon) \qquad (4.20)$$

The second equality follows from the k equation (4.13). Equation (4.20) is a good approximation when the temporal and

spatial change of $u_i u_j/k$ is small compared with the change of $u_i u_j$ itself (Rodi, 1976). When 4.20 is incorporated into the $u_i u_j$ equation (4.19) together with some model approximations, the following is obtained.

$$\overline{u_i u_j} = k\left[\frac{2}{3}\delta_{ij} + \frac{(1-\gamma)\left(\frac{P_{ij}}{\epsilon} - \frac{2}{3}\delta_{ij}\frac{G}{\epsilon}\right)}{C_1 + \frac{G}{\epsilon} - 1}\right] \qquad (4.21)$$

where, P_{ij} is the stress production term in the Reynolds stress equation (third and fourth term on the right hand side of equation 4.19)

4.4 The k-ϵ Model of Turbulence

In section 4.2 the concept of eddy-viscosity has been elaborated. In this concept the components of the Reynolds stress tensor are assumed to be proportional to the mean velocity gradient (equation 4.7). The proportionality parameter μ_t is termed the eddy viscosity.

The turbulence models utilizing the eddy-viscosity concept can be further classified based on the number of equations used in determining the eddy-viscosity (which is proportional to the velocity and the length scales of turbulence).

The most simple eddy viscosity model is known as the mixing length or zero equation model (section 4.3.1) in which no differential equation is solved to obtain the velocity and the length scales of turbulence. In one equation model of

turbulence a differential equation is solved to obtain the velocity scale of turbulence whereas the length scale is determined from simple empirical relations.

The k-ϵ two equation model of turbulence determines both the velocity scale ($\sqrt{k}$) and the length scale of turbulence by solving partial differential equations. In these equations both convective and diffusive transports of the kinetic energy and the dissipation rate are taken into account. Such consideration is needed when solving rapidly developing flows, recirculating flows etc.

While the higher order equations (e.g. The Reynolds stress model) take into consideration the anisotropic effects of turbulence; enormous amount of computational resources required for their solution limits their practical application. The exact form of the k equation as derived from the Reynolds stress equations under the assumption of isotropic turbulence is given in section 4.3.2. Under some model assumptions (section 4.3.2) the high Reynolds number k equation of turbulence takes the form.

$$\rho\left[\frac{\partial k}{\partial t}+U_i\frac{\partial k}{\partial x_i}\right]=\frac{\partial}{\partial x_i}\left(\frac{\mu_t}{\sigma_k}\frac{\partial k}{\partial x_i}\right)+\mu_t\left(\frac{\partial U_i}{\partial x_j}+\frac{\partial U_j}{\partial x_i}\right)\frac{\partial U_i}{\partial x_j}-\epsilon \qquad (4.16)$$

The first term on the left hand side is the unsteady term and the second term is known as the convection term. On the right hand side the first is the diffusion term, the second term is the production of turbulent kinetic energy (G) and the last term is the dissipation of turbulent kinetic energy.

The length scale (L) as mentioned before is obtained by solving for the dissipation rate of turbulence and then using equation (4.15). The complete equation is given below.

$$\rho\left[\frac{\partial \epsilon}{\partial t}+U_i\frac{\partial \epsilon}{\partial x_i}\right]=\frac{\partial}{\partial x_i}\left(\frac{\mu_t}{\sigma_\epsilon}\frac{\partial \epsilon}{\partial x_i}\right)+C_{\epsilon 1}\frac{\epsilon}{k}G-C_{\epsilon 2}\frac{\epsilon^2}{k}$$

The physical interpretation of the terms in the dissipation equation is similar to that of the k equation.

Once the k and ϵ are obtained the eddy-viscosity is solved for using the following relation

$$\upsilon_t = C_\mu\frac{k^2}{\epsilon}$$

4.5 Wall Function

At a boundary wall the no slip condition leads to predominantly viscous behavior and is thus termed the viscous sublayer. For turbulent flows it is often desirable not to compute the flow right up to the wall. When boundary conditions are specified right at the wall, the equation must be integrated through the viscous sublayer present near the wall, which is undesirable because of two reasons. Firstly, very steep velocity gradients prevail in the viscous sublayer so that, for proper resolution, many mesh points have to be placed in this layer and the computation would be prohibitively expensive; secondly, viscous effects are important in this layer so that the high Reynolds number k-ϵ turbulence model is not applicable in this region. Solution of

the flow in this viscous sublayer is normally not necessary because empirical laws of sufficient generality are available that connect the wall conditions (e.g., wall shear stress and heat flux, temperature) to the dependent variables just outside the viscous sublayer. Thus the finite element mesh is not extended completely to the wall, rather an empirical law is employed to connect the computational point to the wall conditions.

The function used is logarithmic and is written as (Tong, 1983)

$$U^+ = \frac{1}{\kappa} \ln(E' y^+) \qquad for \quad 12 < y^+ < 100 \tag{4.22}$$

$$U^+ = y^+ \qquad for \quad y^+ < 12 \tag{4.23}$$

where

$$U^+ = \frac{U_p}{U_\tau} \ , \quad y^+ = \frac{y_p U_\tau}{\upsilon} \ , \quad U_\tau = \sqrt{\frac{\tau_w}{\rho}}$$

where κ and E' are empirical constants. τ_w is the wall shear stress and U_τ is known as the friction velocity.

The boundary condition for k and ϵ at the wall is evaluated using the following relations

$$k = \frac{U_\tau^2}{\sqrt{C_\mu}} \ , \quad \epsilon = \frac{U_\tau^3}{\kappa y} \tag{4.24}$$

The values of κ and E' (Tong, 1983) used in the current computations are 0.435 and 9.0 respectively.

CHAPTER 5

FINITE ELEMENT ANALYSIS TECHNIQUE

The finite element method (FEM) is an approximate method of solving equations of boundary and/or initial value problems in engineering and mathematical physics. In this method, a continuum is divided into many small zones (called elements) of convenient shapes, triangular, quadrilateral etc. Choosing suitable points called "nodes" within the elements (figure 3), the variable in the differential equation is written as a linear combination of appropriately selected interpolation functions and the values of the variable or its various derivatives specified at the nodes. Using variational principle or weighted residual methods, the governing differential equations are transformed into "finite element equations" governing all isolated elements. These local elements are finally collected together to form a global system of differential or algebraic equations with proper boundary and/or initial conditions imposed. The nodal values of the variable are determined from this system of equations.

Among the approximate method of analysis, the finite-difference method (FDM) and the variational methods such as the Ritz and Galerkin methods are more frequently used in the literature.

In the finite-difference approximation of a differential equation, the derivatives in the equations are replaced by

difference quotients which involve the values of the solution at discrete mesh points of the domain. The resulting discrete equations are solved, after imposing the boundary conditions, for the values of the solution at the mesh points. Although the finite-difference method is simple in concept, it suffers from several disadvantages. The most notable are the derivatives of the approximated solution, the difficulty in imposing the boundary conditions along nonstraight boundaries, the difficulty in accurately representing geometrically complex domains, and the difficulty in employing nonuniform and nonrectangular meshes.

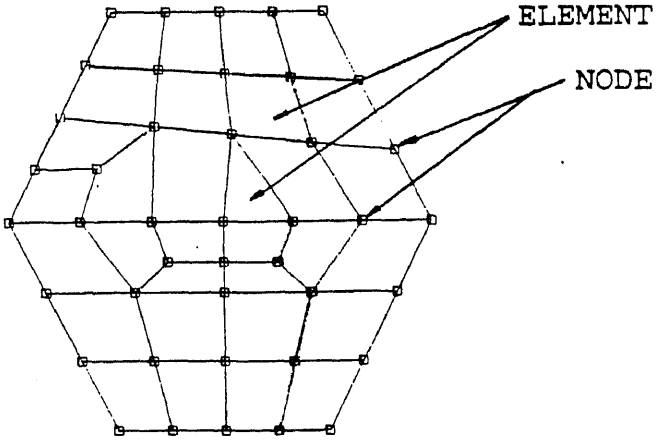

Figure 3 Finite Element Entities

The finite-element method is endowed with two basic features which accounts for its superiority over other competing methods. First, a geometrically complex domain of the problem can be represented as a collection of geometrically simple subdomains (elements). Second, over each

finite element the approximation functions are derived using concepts from interpolation theory (interpolation functions).

The interpolation functions are algebraic polynomials and the undetermined parameters represent the values of the solution at a finite number of nodes, on the boundary and in the interior of the element. From interpolation theory one finds that the order of the interpolation function depends on the number of nodes in the element. Another advantage of FEM, again over FDM and especially over analytical solution techniques (as opposed to numerical techniques) is the ease with which nonhomogeneous and anisotropic materials may be handled. Very little extra effort is required in the FEM formulation when heterogeneous and/or anisotropic materials are to be modeled, even when some parts of the structure or body are made of one material and other parts are made of different materials.

All the various types of boundary conditions that one may encounter in a typical FEM application except those that require prescribed values of the field variables (Dirichlet boundary condition) themselves are automatically included in the formulation. Among the boundary conditions that are automatically included (Natural or Neumann type boundary condition) are convection, radiation, applied heat fluxes and insulation in case of thermal analysis and pressure and velocity gradients in case of fluid flow analysis. In all cases, these conditions need not be constant. When these boundary conditions or other properties are functions of the

field variable, the problem becomes nonlinear. Special solution techniques must be applied in these cases. The basic finite element method is applicable, however, for both linear and nonlinear problems.

Another advantage of FEM is that higher order elements may be implemented with relative ease. Higher order elements require the use of higher-order interpolating polynomials. In fact by using isoparametric elements, curved sides may actually be used thereby allowing very close fits to essentially all irregular geometries.

5.1 BRIEF HISTORY OF FEM

Hrenikoff (1941) introduced the so called framework method, in which a plane elastic medium was represented as a collection of bars and beams. The use of piecewise continuous functions defined over a subdomain to approximate the unknown function dates back to the work of Courant (1943), who used an assemblage of triangular elements and the principal of minimum potential energy to study the St. Venant torsion problem. Although certain key features of the finite-element method can be found in the works of Hrenikoff (1941) and Courant (1943), the formal presentation of the finite-element method is attributed to Argyris and Kelsey (1960) and to Turner, Clough, Martin and Topp (1956). However, the term "finite element" was first used by Clough (1960).

Zienkiewicz and Cheung (1965) and Visser (1965) were among the first to apply the finite element method to generate

solutions to the problems described by Laplace's and Poisson's equations in 1965. The application at that particular time happened to be in conduction heat transfer, but it was immediately recognized that the procedure was applicable to all problems that could be stated in a variational form.

Other researchers, such as Szabo and Lee (1969), showed how the method of weighted residuals, particularly the Galerkin method, could be used in the study of nonstructural applications to retain the basic finite element process. Zienkiewicz (1971), in a second edition of an earlier book, was evidently the first to include in one book the general applicability of the finite element method to problems describable by ordinary and partial differential equations, or field problems in general.

CHAPTER 6

FINITE ELEMENT FORMULATION OF GOVERNING EQUATIONS

In Chapter 4, the equations required for the solution of flow through a diffuser have been obtained in tensor notation. For laminar flow only the solution of continuity and momentum equations are required, whereas for turbulent flow additional equations are needed to be solved to obtain the Reynolds stress terms appearing in the momentum equation. As mentioned earlier, the two-equation k-ϵ model, which uses the eddy viscosity concept will be employed in this regard. The k-ϵ model obtains the velocity and the length scale by solving the turbulent kinetic energy and dissipation of turbulent kinetic energy equations respectively. Since the geometry considered is axisymmetric the relevant equations are summarized and presented as follows :

$$\frac{\partial U}{\partial x} + \frac{V}{r} + \frac{\partial V}{\partial r} = 0 \qquad (6.1)$$

$$\rho\left(U\frac{\partial \phi}{\partial x}+V\frac{\partial \phi}{\partial r}\right)-\frac{\partial}{\partial x}\left(\Gamma_\phi\frac{\partial \phi}{\partial x}\right)-\frac{\partial}{r\partial r}\left(r\Gamma_\phi\frac{\partial \phi}{\partial r}\right)+A'\frac{\partial P}{\partial x}+B\frac{\partial P}{\partial r}+C\frac{V}{r^2}=S_\phi \qquad (6.2)$$

where, ϕ is the dependent variable (U, V, k, or ϵ). A' is nonzero (A'=1.0) only for the U equation, B and C are nonzero (1.0) only for the V equation. For momentum equations Γ_ϕ is the molecular viscosity.

for the U equation

$$S_\phi = -\frac{\partial}{\partial x}(\rho\overline{u^2}) - \frac{1}{r}\frac{\partial}{\partial r}(r\rho\overline{uv})$$

for the V equation

$$S_\phi = -\frac{\partial}{\partial x}(\rho\overline{uv}) - \frac{1}{r}\frac{\partial}{\partial r}(r\rho\overline{v^2})$$

where

$$-\rho\overline{u^2} = 2\mu_t\frac{\partial U}{\partial x} - \frac{2}{3}\rho k \; ; \quad -\rho\overline{uv} = \mu_t\left(\frac{\partial U}{\partial r} + \frac{\partial V}{\partial x}\right)$$

$$-\rho\overline{v^2} = 2\mu_t\frac{\partial V}{\partial r} - \frac{2}{3}\rho k \; ; \quad \mu_t = \rho C_\mu\frac{k^2}{\epsilon}$$

for the k and ϵ equations

$$S_k = G - \rho\epsilon \; ; \quad \Gamma_\phi = \frac{\mu + \mu_t}{\sigma_k}$$

$$S_\epsilon = C_{\epsilon 1}\epsilon\frac{G}{k} - C_{\epsilon 2}\rho\frac{\epsilon^2}{k} \; ; \quad \Gamma_\phi = \frac{\mu + \mu_t}{\sigma_\epsilon}$$

$$G = \mu_t 2\left\{\left[\left(\frac{\partial U}{\partial x}\right)^2 + \left(\frac{\partial V}{\partial r}\right)^2 + \left(\frac{V}{r}\right)^2\right] + \left(\frac{\partial U}{\partial r} + \frac{\partial V}{\partial x}\right)^2\right\}$$

The constants in the above equations are chosen as (Launder, 1974)

C_μ=0.09, σ_k=1.0, σ_ϵ=1.3, $C_{\epsilon 1}$=1.44, $C_{\epsilon 2}$=1.92

Since the governing equation mentioned above are nonlinear, a symmetric variational form and the associated functional do not exist. Therefore, Galerkin's weighted residual scheme is used to obtain the finite element formulation of the above equations.

6.1 GALERKIN METHOD

The objective of the finite element method is to approximate the differential equations by a system of algebraic equations. This is achieved by discretizing the flow domain into a number of elements. Within each element, the dependent variables are approximated by simple polynomial functions as described earlier. The coefficients of these polynomials are obtained from nodal values of the dependent variable. Mathematically, the dependent variable in an element can be written as (Chung, 1978).

$$\phi_1(x) = \psi^T \phi_1$$

$$P(x) = \theta^T P$$

where the unknowns ϕ_1, P are column vectors of nodal points ψ and θ are column vectors of the shape functions. Substituting these into the governing equations yields a set of equations of the form

$$f(\psi, \phi, \theta, P) = R$$

where R is the residual resulting from the use of the approximations of the variables in equations (6).

The Galerkin form of the method of weighted residuals

seeks to reduce the error (residual) R to zero. This is done by achieving orthogonality between the residual and weighting functions of the element which is expressed as

$$\int_{\Omega_E} (f.w)\, d\Omega = \int_{\Omega_E} (R.W)\, d\Omega = 0$$

where Ω_E is the element domain.

6.2 ELEMENT SHAPE FUNCTION

Four noded isoparametric quadrilateral elements have been used for all the computations. The shape functions used are given in terms of the natural coordinates of the elements, i.e ξ and η

$$\psi_1 = 1/4(1-\xi)(1-\eta)$$

$$\psi_2 = 1/4(1+\xi)(1-\eta)$$

$$\psi_3 = 1/4(1+\xi)(1+\eta)$$

$$\psi_4 = 1/4(1-\xi)(1+\eta)$$

6.3 FINITE ELEMENT FORMULATION

Using Galerkin's method of weighted residual, equation 6 becomes

$$[\int_A \psi \frac{\partial \psi^T}{\partial x} dA]\, U + [\int_A \frac{\psi \psi^T}{r} dA]\, V + [\int_A \psi \frac{\partial \psi^T}{\partial r} dA]\, V = 0 \qquad (6.3.1)$$

In case of the momentum equation the pressure term (included

$$\left[\int_A \rho\psi U\frac{\partial\psi^T}{\partial x}dA\right]\phi+\left[\int_A \rho\psi V\frac{\partial\psi^T}{\partial y}dA\right]\phi+\left[\int_A \Gamma_\phi\frac{\partial\psi}{\partial x}\frac{\partial\psi^T}{\partial x}dA\right]\phi+$$
$$\left[\int_A \Gamma_\phi\frac{\partial\psi}{\partial y}\frac{\partial\psi^T}{\partial y}dA\right]\phi+A'\left[\int_A \frac{\partial\theta}{\partial x}\psi^T dA\right]P+B\left[\int_A \frac{\partial\theta}{\partial y}\psi^T dA\right]P+C\left[\int_A \psi\frac{\psi^T}{r^2}dA\right]\phi$$
$$=\int_A S_\phi\psi dA+\int_l \Gamma_\phi\psi n_x\frac{\partial\phi}{\partial y}dl+\int_l \Gamma_\phi\psi n_r\frac{\partial\phi}{\partial x}dl \qquad (6.3.2)$$

in the source term) is handled using the penalty method (Hughes et al. 1979), where the continuity equation is replaced by a perturbed equation :

$$p = -\lambda(\partial u/\partial x + v/r + \partial v/\partial r)$$

For further details see NISA/3D-Fluid user's manual.

Equation 6.3 results in a system of algebraic equations of the form

$$[K]\,[\phi] = [F\}$$

where, [K] is the stiffness matrix, [ϕ] is the column vector of unknowns {U,V,k,ϵ} and [F] is the source term.

NISA/3D-FLUID uses successive Picard iteration scheme to solve the system of nonlinear equation given above.

6.4 WAVEFRONT SOLVER

For the solution of the overall finite element equilibrium equations, which are in the form of simultaneous linearized algebraic equations, the wavefront technique (Irons, 1970) is used. For most practical problems the computer time required for the solution of system of equations represent a substantial portion of the total computational time of the run. In the wavefront (frontal) technique, the solution time is proportional to the square of the wavefront size. Therefore it is important to minimize the wavefront size by resequencing

the elements, which is carried out in NISA/3D-FLUID as a prefrontal operation.

CHAPTER 7

RESULTS AND DISCUSSIONS

7.1 Laminar Flow

In this section, the results obtained by the numerical (finite element method) solution of the Navier Stokes and continuity equations for expanding axisymmetric laminar flows will be presented. A typical geometry for this study and boundary conditions have already been discussed in Chapter 3. The parameters affecting the performance of a diffuser are the inlet Reynolds number, inlet velocity profile, angle of expansion and the expansion ratio . As discussed in Section 3.1, a few numerical and experimental results are available for flow through axisymmetric suddenly expanding geometries with fully developed parabolic velocity profile specified at the inlet. Validation of the current code for laminar two dimensional situations have already been reported (Bhatia et al., 1993). For the sake of comparison and validation of axisymmetric geometries, the results obtained by applying the above mentioned boundary condition at the inlet will be compared with the available results.

In this study, in addition to the comparison of results mentioned above, more results (not reported in literature thus far) are obtained by studying the effect of the above mentioned parameters on the flow field for a flat specified

inlet velocity profile. Quadrilateral, isoparametric, first order elements are used for all computations.

In the results reported, all velocities and distances are non-dimensionalized with respect to inlet average velocity (U_o) and inlet diameter (d) respectively.

7.1.1 The Effect of Reynolds Number

The effect of Reynolds number on the flow field has been studied for the following configurations :

1) 90^o half expansion angle with fully developed parabolic velocity profile specified at the inlet.

2) 90^o half expansion angle with flat velocity profile specified at the inlet.

3) 30^o, 45^o, 60^o and 75^o half expansion angles with flat velocity profile specified at the inlet.

For all of the above three cases the expansion ratio D/d had been chosen as 2.0 with the Reynolds number ranging from 50 to 200.

Figure 4 shows the variation of recirculation length as a function of Reynolds number for the first configuration mentioned above. Also shown in this Figure are the experimental results of Macagno et al. (1967). The number of elements used in this case to achieve mesh independence was 11960. It is found that the current computations correctly predict the linear variation of recirculation length with the Reynolds number. Solutions showing better agreement with the above mentioned reference are obtained when the inlet

prescribed velocity boundary condition is specified at 5 diameters upstream from the inlet section, also shown in Figure 4. Figure 5 shows the comparison of the current results with the computational results obtained by Fletcher et al. (1985), Scott et al. (1986) and Badekas et al. (1992). Back and Roschke (1972) have mentioned that linear increase in recirculation zone length with Reynolds number can be explained if the flow is considered to be a jet mixing with a fluid at rest, since the spread of the shear layer between the central jet and the reverse flow is solely by molecular diffusion. Another interesting comparison can be made by measuring the location of eddy center, which is defined as a distance between the eye of the recirculation zone and edge of the step. Figure 6 shows the variation of eddy center location with Reynolds number for the same configuration. Current numerical scheme predicts correctly both the qualitative and quantitative behavior by agreeing closely with those reported in other references mentioned above. As can be noted from this Figure, there is large disagreement between the results obtained by Scott et al. (1986) with those reported by others. This can be partly attributed to the inadequate mesh used in their computation. This is evidenced by the fact that in the present study a total number of nearly 13,000 nodes were required against 945 nodes used by Scott et al. (1986).

Variation of recirculation zone length with Reynolds number for the second and third configurations (30^{o}, 60^{o} and 90^{o}) have been shown in figure 7. The number of elements used

for the 30^{o} half expansion angle was 12250. For all other angles of expansion 9800 elements were used. For all angles of expansion considered, a linear variation is obtained but with different slopes. The reason for this (linear variation) may be the same as that of the case with specified parabolic inlet velocity profile. For any fixed Reynolds number the recirculation length is always found to be less for the geometry with the smaller half angle of expansion. These results have not been previously reported in literature. The linear variation of recirculation length can be expressed as

$$L_r/d = A_1(Re-50) + B_1 \qquad (7.1)$$

The above relation is valid for $50 \leq Re \leq 200$. The coefficients A_1 and B_1 for various half angles of expansion have been tabulated in table 7.1

For the second configuration, Figures 8 to 11 show the velocity profiles for different Reynolds numbers at various cross sections (x/d of 1.0, 2.0, 4.0, 16.0). Figures 8 and 9 indicate that with the increase in Reynolds number the reverse flow speed increases. Also the curve for Reynolds number of 50 is almost normal to the wall depicting the fact that the recirculation length for this case is close to 1.0. Similar behaviors for Reynolds numbers of 100 and 200 are found to occur for x/d of 2.0 and 4.0 (Figures 9 and 10) respectively. As the axial length increases, the velocity profile in each case tends to become parabolic. The larger the Reynolds number, the larger is the length required for the flow to

become fully developed (Figure 11) for the range of Reynolds number being considered.

Table 7.1 Empirical coefficients of equation 7.1

Half Angle of Expansion	Coefficient A_1	Coefficient B_1
30	0.01467	0.996
45	0.01621	1.005
60	0.01742	1.0287
75	0.0180	1.0803
90	0.01806	1.157

7.1.2 The Effect of Inlet Velocity Profile

A comparison between Figures 4 and 7 shows that, for a parabolic inlet velocity profile, the recirculation length is more than twice of that obtained with a flat inlet velocity profile. This may be due to the fact that the vorticity near the step edge is high for the flat profile, causing increasing spread of the shear layer between the jet and the reverse flow regime. Figures 12 to 15 show the comparison of velocity profiles at various axial locations (x/d = 1.0,4.0,8.0,16.0) for the two different specified inlet velocity profiles mentioned above.

7.1.3 The Effect of Angle of Expansion

Figure 16 shows the variation of recirculation length as a function of half angle of expansion for a specified flat inlet velocity profile and a fixed Reynolds number of 200. The expansion ratio considered for this case is 2.0 with the half angles of expansion varying from 10^{o} to 90^{o}. The number of elements used for angles of expansion of 15^{o} and 30^{0} were 14700 and 12250 respectively. For all other half angles of expansion ($10^{o}, 20^{o}, 45^{o}, 60^{o}, 75^{o}, 90^{o}$) the number of elements used were 9800. It is found that a half angle greater than 20^{o}, a smooth curve between recirculation length and angle of expansion is obtained which is exponential in nature. But the recirculation length for 15^{o} does not follow this curve and the value at 15^{o} is more than that of 20^{o}. The same trend is found for 10^{o} also. The reason for this may be the fact that as the angle decreases below a certain limit the detachment point moves downstream much faster than the reattachment point (Figure 17). The effective recirculation zone length (axial distance between the reattachment and the detachment point) variation with half angle of expansion for this case is shown in Figure 18. The curve is exponential in nature for the whole range of angles considered.

Figure 19 shows the centerline velocity distribution for three half angles of expansion (15^{o}, 30^{o}, and 90^{o}) for the same Reynolds number and inlet boundary conditions mentioned above. Figures 20 and 21 show the corresponding centerline pressure (non-dimensionalized with $\rho U_{o}^{2}/2$) and axial velocity

distributions along the shear layer respectively. From Figure 19 it is found that, although there is no significant difference between the 15° and 30° cases, the 90° case shows a distinct difference from the other two cases. The centerline velocity for this case tries to hold for a small distance which is not observed in the other cases.

Figure 20 shows that, as expected, lower the angle of expansion higher the recovery of pressure. Peaks for all the three curves are found to be occuring almost at the same axial location just downstream of the step edge.

Figure 21 shows the sharp gradients that exist along the shear layer. The magnitude of maximum axial velocity is significantly higher in case of 90° in comparison with the other two angles of expansion.

7.1.4 The Effect of Expansion Ratio

Variation of recirculation zone length with expansion ratio is shown in Figure 22. The half-angle of expansion considered for this case was 90°. The Reynolds number used was 100 with the velocity profile specified at the inlet being a flat one. The expansion ratio varies from 1.5 to 4.0. The number of elements used for expansion ratio of 1.5, 1.75, and 2.0 were 8960, 9800, and 9800 respectively. 12800 elements were used for other expansion ratios (2.5, 3.0 and 4.0). A linear variation of recirculation zone length with expansion ratio is obtained for the expansion ratio range of 2 to 4. Below an expansion ratio of 2.0, the recirculation length does not vary linearly.

It needs to be mentioned here that a linear relationship between the recirculation length and expansion ratio (varying from 1.5 to 6.0) has been proposed by Badekas et al. (1992) for a parabolic inlet velocity profile (Section 2.1). It has also been indicated that this proposed correlation shows poor agreement with the experimental results as the expansion ratio decreases. This may be due to the fact that below a certain expansion ratio the relation is no longer a linear one (also for a parabolic inlet profile).

7.2 Turbulent Flow

In the previous section, computational results for laminar flow through expanding axisymmetric geometries have been reported. In this section, results for turbulent flow through similar geometries will be considered. In addition to the continuity and momentum equations, more equations are required to be solved for determining the Reynolds stresses in the momentum equations which arise due to the time averaging of the Navier Stokes equations. Since the eddy viscosity concept is used to model the Reynolds stress terms, additional equations to determine the eddy viscosity are required. A two equation k-ϵ turbulence model is employed in this regard. A review of literature in Section 2.2 have shown that a few computational and experimental results are available for some of the geometries considered here.

The parameters affecting the performance of axisymmetric diffusers have already been identified which are mainly angle

of expansion, expansion ratio, velocity profile at inlet and the Reynolds number. In addition to these parameters, variables affecting the performance of the k-ϵ equations need to be considered. Similar to the previous section, before presenting new results, comparison with available results will be carried out.

In the results reported, all velocities and distances have been non-dimensionalized with inlet uniform velocity (U_o) and inlet diameter (d) respectively.

7.2.1 Effects of Angle of Expansion

To study the effect of angle of expansion on the flow field, three discrete half angles of expansion (15^o, 30^o, and 90^o) have been considered. The expansion ratio chosen is 2.0 with a Reynolds number of 200,000, based on the inlet conditions. The boundary condition for k at the inlet was chosen according to equation 3.1, with the value of C chosen as 0.014. The dissipation inlet boundary condition was based on equation 3.2, with the value of the length scale L chosen as 0.05d. The number of elements required for the 15^o, 30^o and 90^o angles of expansion were 2415, 2940, and 2525 respectively. Figures 23 through 25 show the centerline axial velocity distributions for the above three angles. Also presented in theses Figures are the experimental results of Chaturvedi (1963) and computational results of Sala et al. (1980) . Figure 23 (half angle of expansion of 90^o) shows that both the computational

schemes predict correctly the qualitative nature of the curve obtained experimentally. The recirculation length obtained by the current scheme is 3.6 which is underpredicted compared to the experimental value of 4.6 reported by Chaturvedi (1963). Figure 24 shows the centerline axial velocity distribution for 30^{o} half angle of expansion. Better correlation is obtained with the experimental results compared to the other numerical scheme (Sala, et al.,1980). The recirculation length obtained is 2.6, which is also an underpredicted one. Figure 25 shows the results for 15^{o} case. Although good correlation is obtained with the experimental results, the current scheme fails to capture any recirculation. As can be seen from Figures 24 and 25 gross difference exist between the predictions of Sala et al. (1980) and the reported experimental results, although his predictions of recirculation length are better than the current scheme. This can be attributed to the different shear stress relation used in conjunction with the wall function (see section 2.2). It has already been mentioned in Section 2.2 that gross anomaly exist in the qualitative nature of his predictions (recirculation length obtained by 15^{o} is more than that of 90^{o}).Figure 26 shows the profiles of the fluctuating axial components of velocity at different cross sections for the 90^{o} case. Comparison with Figure 27 (results of Chaturvedi) shows a good qualitative agreement between the two.

Figures 28 to 30 show the profiles of turbulent kinetic energy (non-dimensionalized with U_o^2) and Figures 31 to 33

show the profiles of dissipation of turbulent kinetic energy (non-dimensionalized with U_o^3/d) at different axial sections of the above mentioned geometries.

Figure 34 shows the pressure distribution along the centerline for all three angles of expansion mentioned above. Good qualitative results are obtained, which follows the trend of the laminar case.

In a bid to improve the recirculation length, the effects of following parameters on the flow field have been studied.

7.2.2 Effects of inlet kinetic energy boundary condition

The geometry considered in this case is the 15^o angle of expansion with the same expansion ratio and Reynolds number mentioned above. Three different values of the constant C of equation (3.1) were chosen (0.005, 0.014, and 0.025). Figure 35 shows the centerline axial velocity distribution for this case. It can be seen from the presented results that for the range of kinetic energy considered, the centerline velocity does not show any significant change. The recirculation length also remained unchanged. Since there was no difference in the recirculation length for this particular geometry considered effect of this boundary condition was not examined for the other two geometries. It can be mentioned here that the experimental results of Chaturvedi (1963) were obtained with no turbulence at the inlet. To simulate this computationally one needs to apply zero value for turbulent kinetic energy at

inlet. But this makes the computational scheme totally unstable.

7.2.3 Effects of inlet boundary condition of dissipation

It has been observed that several estimates for boundary conditions for dissipation of turbulent kinetic energy at the inlet have been tried (Benim et al.,1984; Habib et al,1982). In order to study its effect on the flow characteristics in a diffuser, prescribed ϵ at the inlet is increased by an order of magnitude (L = 0.005d) while the k boundary condition remained unchanged. The geometry and Reynolds number considered are the same as were used to study the effect of inlet k boundary condition (half angle = 15^{o}). The centerline velocity for this case is shown in Figure 36. The recirculation length improves dramatically (for this case it changed from no circulation to 3.2). However, the centerline velocity shows a marked difference in comparison with the experimental results. Effects of considering this boundary condition on the resulting axial velocity distribution of other two geometries are shown in Figures 37 and 38. The recirculation length for 30^{o} changes from 2.8 to 3.60 and that for 90^{o} becomes 3.99 from 3.6. The centerline velocity deteriorates for both these cases.

7.2.4 Effects of empirical constant C_{μ}

As discussed in the previous section, in case of laminar flow the spreading of the incoming jet to the diffuser; which,

primarily determines the recirculation length is because of molecular diffusion. For turbulent flow the turbulent diffusion is expected to be one of the key factor affecting the spreading. In addition to the turbulent kinetic energy and turbulent dissipation, the coefficient that directly affects the turbulent diffusion is C_μ. Attempt have been made in the past to study the effect of this coefficient on the recirculation region in case of turbulent flow through backward facing step (Autret et al.,1987) and improved recirculation length have been obtained. In the current investigation the value of C_μ was reduced from 0.09 to 0.045. All three expansion angles were used for this investigation. In case of 15°, a very small recirculation length was obtained. For 30° the recirculation length increased from 2.6 to 3.7. In the case of 90° the effect was very pronounced. The recirculation length jumped from 3.6 to 4.99 which is slightly more than that obtained experimentally. The centerline axial velocity distributions for these cases are shown in Figures 39 to 41. In all three cases, the centerline velocities are found to be significantly different from the experimental ones. It can be noticed that the effect of C_μ is more significant as the angle of expansion increases. The reverse is true for the inlet boundary condition of dissipation. A summery of the results obtained for various conditions mentioned above has been tabulated in table 7.2

7.2.5 Effects of coefficients $C_{\epsilon 1}$ and $C_{\epsilon 2}$

It has been already noticed that increasing the dissipation energy boundary condition at the inlet improves the recirculation length significantly. Another way of obtaining an increased level of dissipation in the flow domain is to manipulate the first ($C_{\epsilon 1}$) and the second ($C_{\epsilon 2}$) coefficients in the dissipation equation.

To study the effects of the above coefficients on the flow field the value $C_{\epsilon 2}$ was changed from 1.92 to 1.42. Figure 42 shows the centerline velocity in this case for the geometry with 15° half expansion angle. It is found that the centerline velocity is overpredicted substantially for most of the domain, although the recirculation length improved to 3.43. Similar effects were also obtained for the coefficient $C_{\epsilon 1}$.

Table 7.2 Comparison of recirculation lengths for turbulent flow

HALF ANGLE OF EXPAN-SION	CHATURVEDI	SALA	STANDARD	REDUCED C_{μ}	INCREASED DISSIPA-TION
15°	3.55	4.60	X	SMALL	3.20
30°	4.20	4.50	2.60	3.70	3.60
90°	4.65	4.45	3.60	4.99	3.99

7.2.6 Effects of Turbulent kinetic energy Boundary Condition on the wall

A boundary condition for k at the wall, different from that of equation 4.24 has been reported (Betts et al., 1985). In this reference, the gradient of k $\{\partial k/\partial r\}$ at the wall has been set

to zero. Figure 43 shows the centerline axial velocity for the 15^{o} diffuser which had been used to study the effect of the above mentioned boundary condition. Figure 44 shows a comparison of the turbulent kinetic energy along the centerline of this diffuser with the prescribed boundary condition of k. Upon close examination of the results obtained using $\partial k/\partial r = 0$ at the wall, it can be concluded that no significant differences are observed. The reattachment length is still underpredicted by almost the same margin as in the case where k was computed using equation 4.24.

7.2.7 Effects of Reynolds Number

To study the effect of Reynolds number on the flow field, the Reynolds number was varied from 4000 to 200,000 (Figure 45). The geometry considered was the 90^{o} half angle of expansion with expansion ratio 2.0. It is found that the recirculation length remains almost constant for the Reynolds number range from 10,000 to 200,000. This may be due to the fact that at higher Reynolds numbers the decrease in diffusivity is offset by the higher level of mixing due to turbulence. Below 10,000, the recirculation length reduces slightly for the turbulent flow case.

7.2.8 Effects of expansion ratio

Thus far numerical results and their comparisons with the corresponding experimental results have been reported for diffusers with different angles for an expansion ratio of 2.0.

Similar results for any other expansion ratio are not available. The angle of expansion considered is 30^{o}. The number of elements employed for expansion ratios of 4.0 and 6.0 were 3439 and 4521 respectively. A Reynolds number of 200,000 were used. Figure 46 shows a comparison of the centerline axial velocities for expansion ratios of 2.0, 4.0 and 6.0. Figure 47 shows the kinetic energy profile (non-dimensionalized with U_o^2) for x/d of 4, 8, 12 and 16 for the expansion ratio of 6.0. It can be noted that the behavior of this quantity is similar to that obtained with an expansion ratio of 2.0 but the maximum for example is obtained at a different value of the radius.

CHAPTER 8

FURTHER NUMERICAL EXPERIMENTATION

In section 7.2 results of numerical experimentation has been reported by modifying some of the standard co-efficients and also the boundary conditions for k and ϵ at the inlet. Some of the changes have shown insignificant effects while others have shown improved localized results. While manipulating the co-efficients, a constant value throughout the flow field has been assumed. As mentioned earlier, the co-efficient that directly affects the turbulent diffusion is C_μ. A variation of C_μ in the flow field as a function of the ratio of production of turbulent kinetic energy (G) and its dissipation has been proposed by Rodi (1972) and investigated by Autret et al. (1987) for a two-dimentional backward-facing step. It is interesting to see the effect of such spatial variation of C_μ in the present case of diffuser flows. The expression employed is as follows :

$$C_\mu = \frac{2}{3}\frac{1-\alpha}{\omega}\frac{1-\frac{1}{\omega}(1-\alpha\frac{G}{\epsilon})}{[1+\frac{1}{\omega}(\frac{G}{\epsilon}-1)]^2}$$

The coefficents in the above expression have been taken as $\omega = 2.8$, $\alpha = .549$ as suggested by the author. The graphical representation of the above expression is given in Figure 48.

To test the performance of this model the geometry with

half angle of expansion of 15° was considered. The centerline velocity distribution for this case is shown in Figure 49. It can be seen that the centerline velocity in this case is very much similar to that obtained with a constant value of C_μ of 0.045, although the recirculation length improved to 3.2 from a very small recirculation length (obtained with C_μ of 0.045).

CHAPTER 9

CONCLUSIONS AND RECOMMENDATIONS

1) The current investigation has resulted in the development of a comprehensive computational procedure for solving flow through diffusers over a wide range of variation of the parameters affecting the flow field. Such a computational procedure can be utilized for effective design of diffusers by the creation of a database covering all practical range of variation of the design parameters.

2) For laminar flow, the current numerical scheme can predict both the qualitative and quantitative behavior accurately. A mathematical model has been proposed showing the variation of recirculation length with Reynolds number for various angles of expansion.

3) The recirculation length for half angle of expansion of 90^{o} shows linear variation with expansion ratio for a certain range .

4) The recirculation length does not show a monotonic variation with half expansion angle. There is an inflection point giving a minimum reattachment point location.

5) Effective recirculation length shows an exponential variation with half angle of expansion.

6) The standard k-ϵ model of turbulence in conjunction with current numerical scheme can adequately predict the qualitative behavior of the flow field.

7) The standard k-ϵ model is unable to predict the quantitative behavior of the flow field adequately.

8) Changing the kinetic energy boundary condition on the wall does not show any significant effect on the computed flow field.

9) Increasing the dissipation rate boundary condition at the inlet yields better recirculation length for all expansion angles.

10) Manipulation of the coefficients resulted in significant improvement of recirculation lengths in most cases. However, there is room for improvement in the overall prediction of the flow field.

11) The current study has elaborated a procedure for selection of proper boundary conditions while solving turbulent flow through diffusers.

12) The current study has resulted in a deep and thorough understanding of the physics of turbulence in diffuser flows in conjunction with the k-ϵ model.

13) The finite element method is an effective numerical tool for predicting the flow field in diffuser flows.

Recommendations for Further Work

Further numerical experimentation can be carried out to study the effect of variation of empirical coefficients simultaneously.

The higher order turbulence model can be examined to

check for any improvement in the prediction of flow field due to a consideration of anisotropic turbulence.

More exhaustive experimental results with state-of-the-art equipment are required to have better insight of the flow field and creation of a database to enable further tuning of the empirical constants.

APPENDIX I

RESULTS FOR LAMINAR FLOW

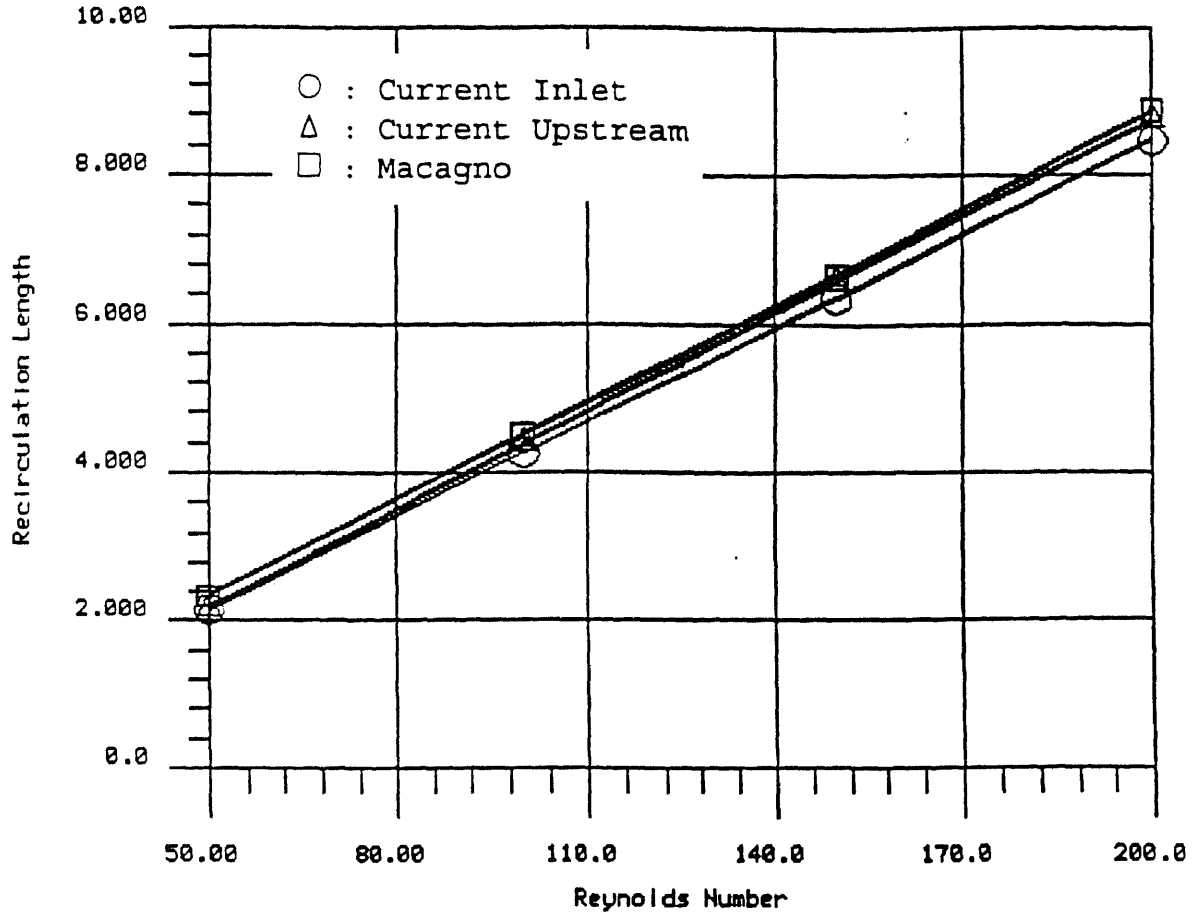

Figure 4 Variation of recirculation length with Reynolds number for a parabolic inlet velocity profile

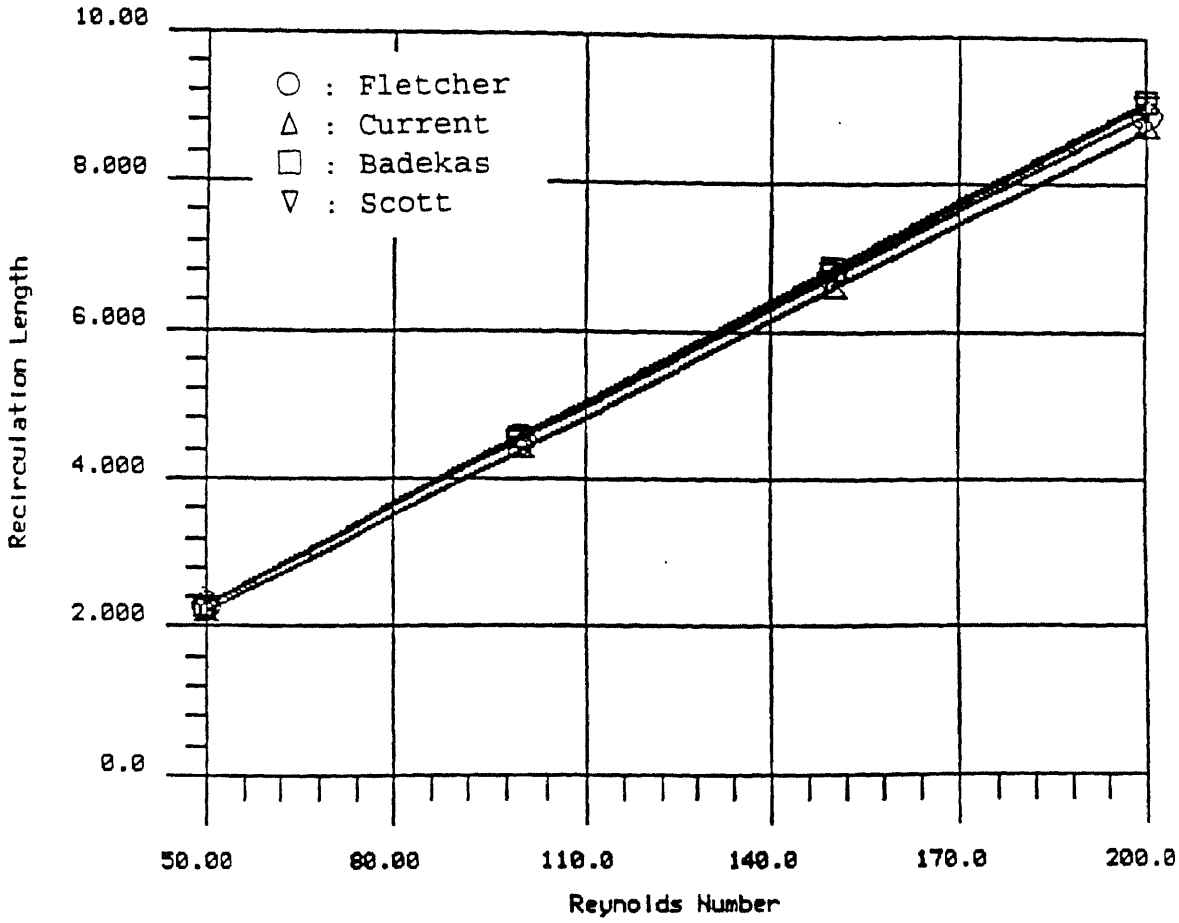

Figure 5 Variation of recirculation length with Reynolds number for a parabolic inlet velocity profile

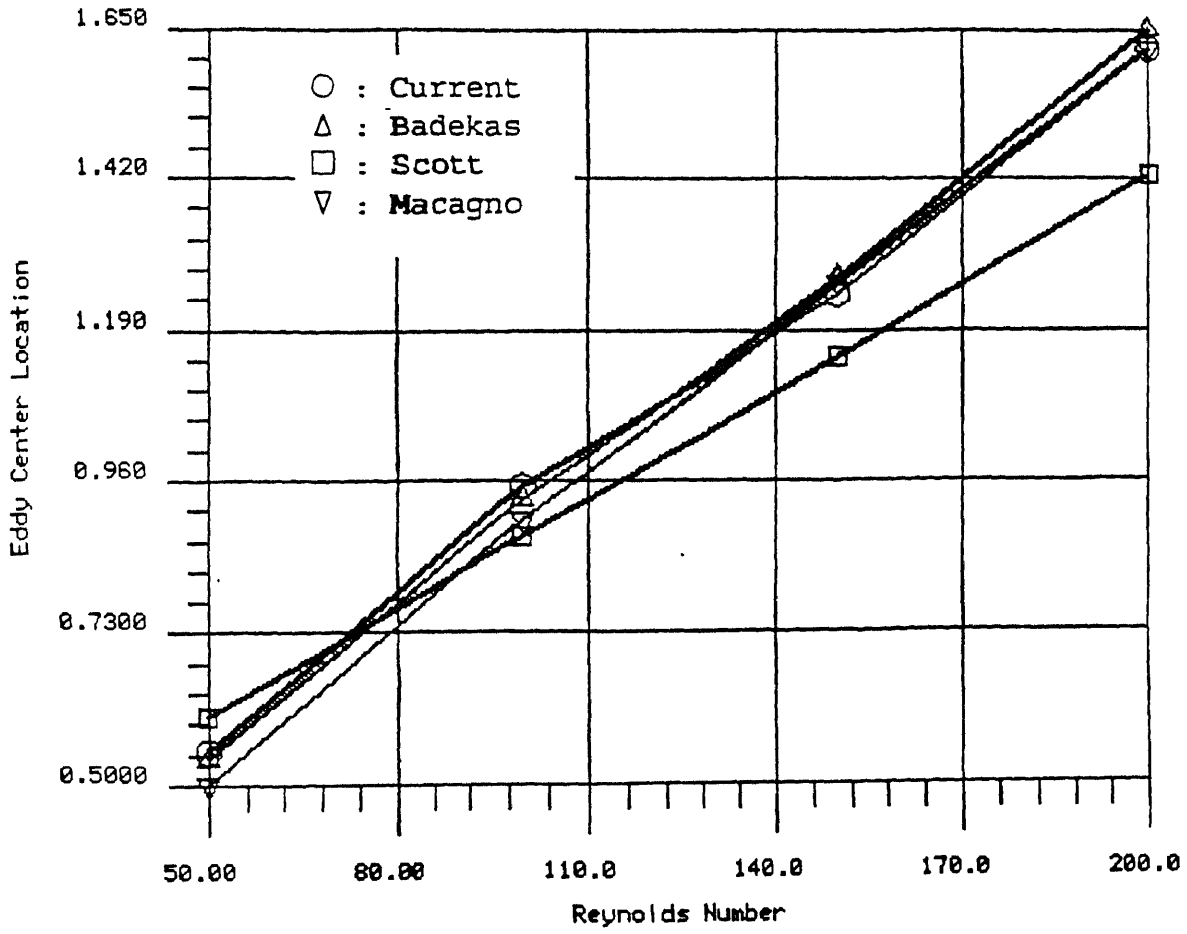

Figure 6 Variation of eddy center location with Reynolds number for a parabolic inlet velocity profile

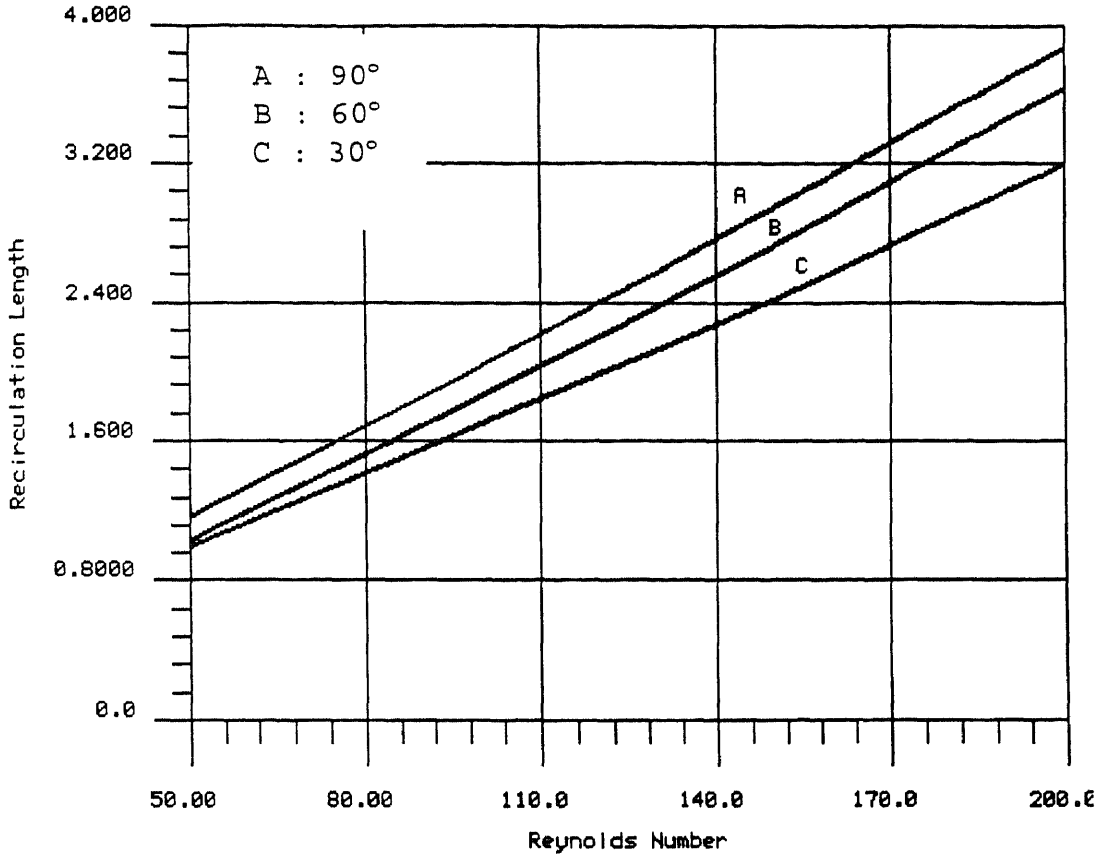

Figure 7 Variation of recirculation length with Reynolds number for a uniform inlet velocity profile

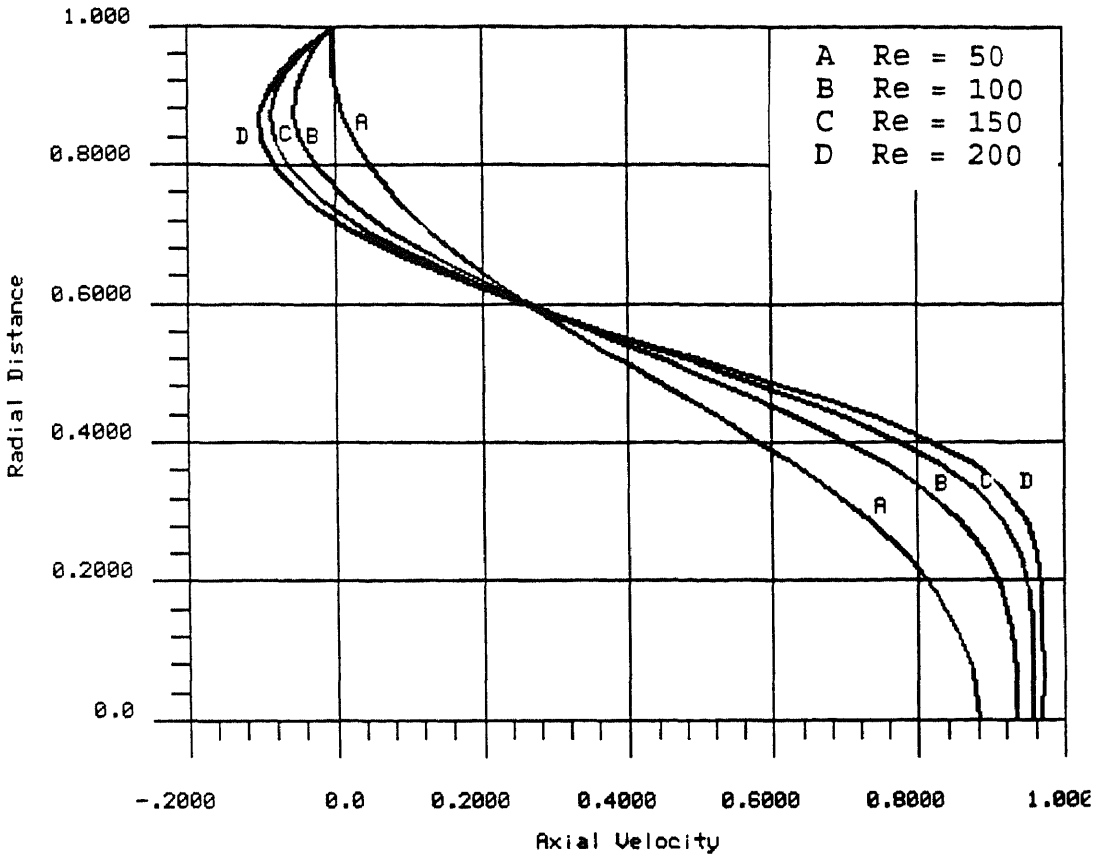

Figure 8 Velocity profiles at a fixed cross section (x/d = 1) for different Reynolds numbers for a uniform inlet velocity profile

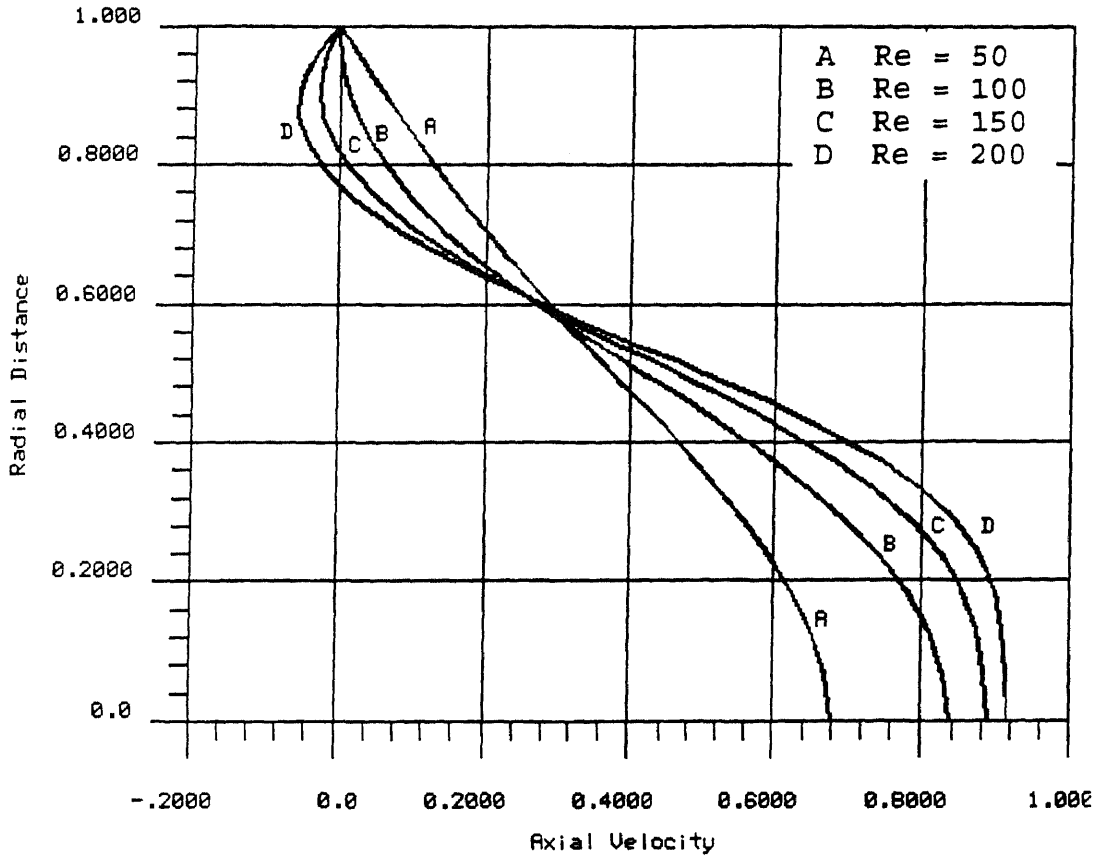

Figure 9 Velocity profiles at a fixed cross section (x/d = 2) for different Reynolds numbers for a uniform inlet velocity profile

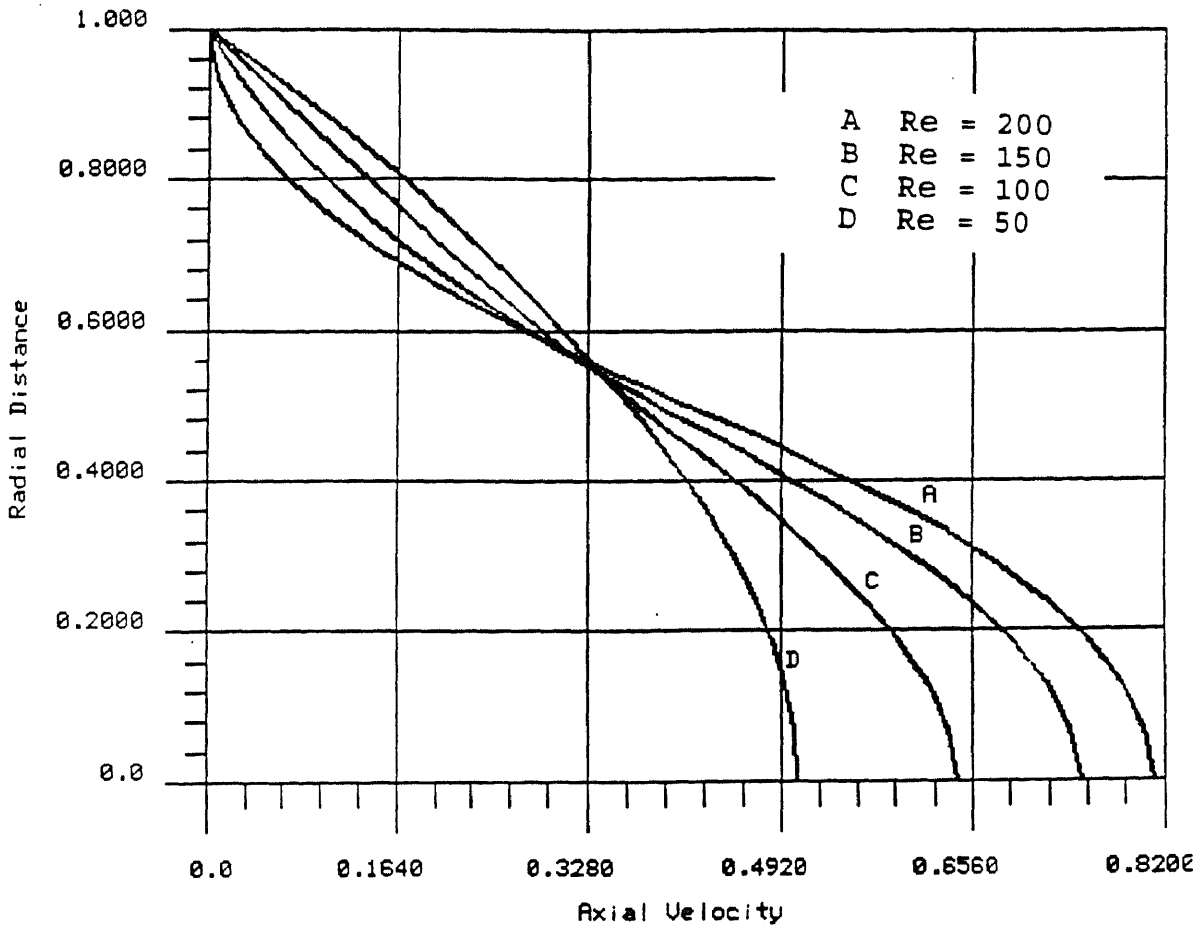

Figure 10 Velocity profiles at a fixed cross section (x/d = 4) for different Reynolds numbers for a uniform inlet velocity profile

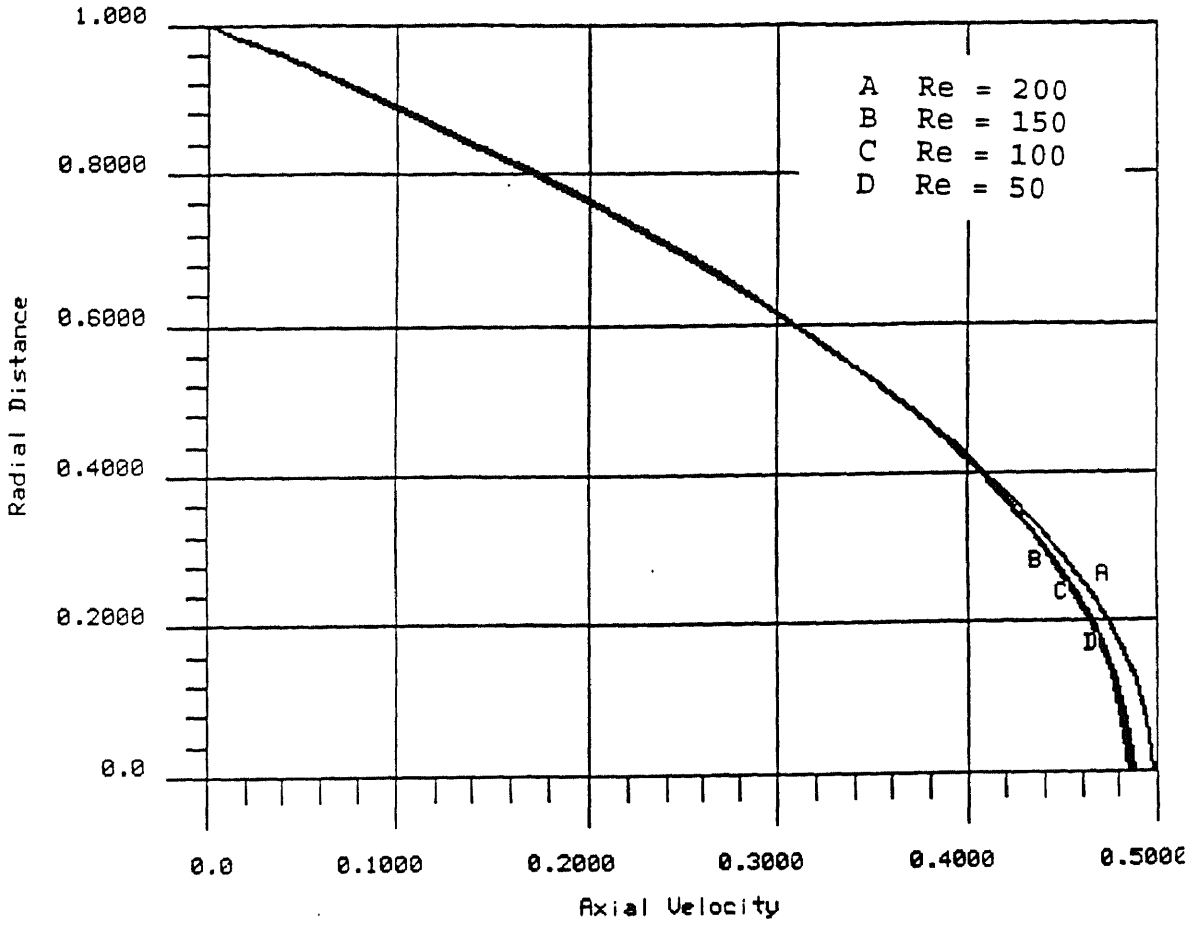

Figure 11 Velocity profiles at a fixed cross section (x/d = 16) for different Reynolds numbers for a uniform inlet velocity profile

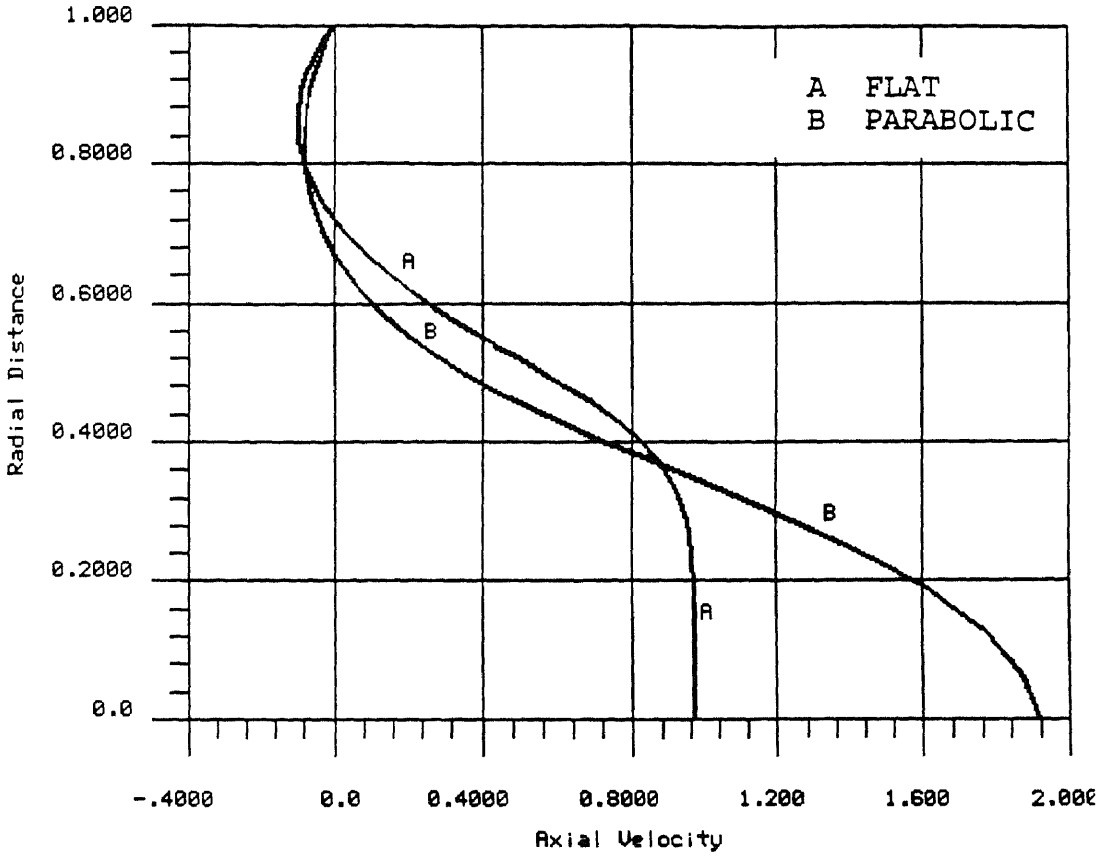

Figure 12 Comparison of velocity profiles at a fixed cross section (x/d = 1) for uniform and parabolic inlet velocity profiles

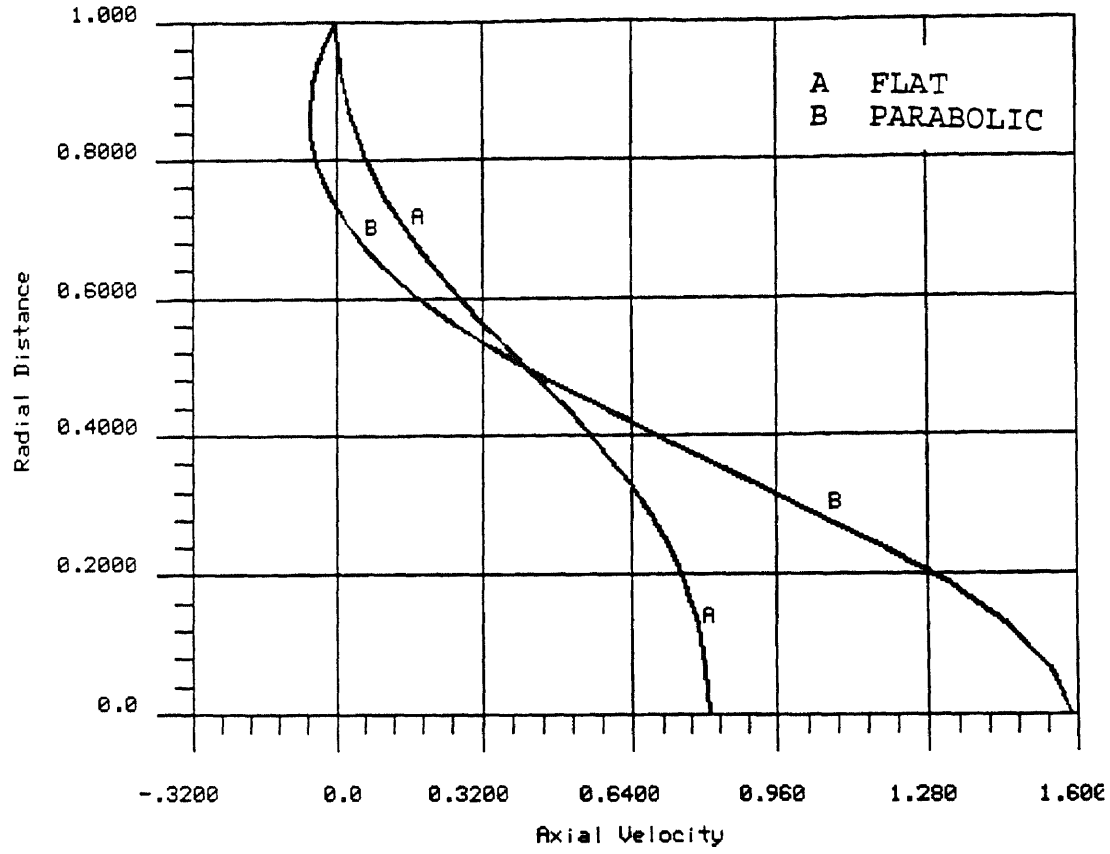

Figure 13 Comparison of velocity profiles at a fixed cross section (x/d = 4) for uniform and parabolic inlet velocity profiles

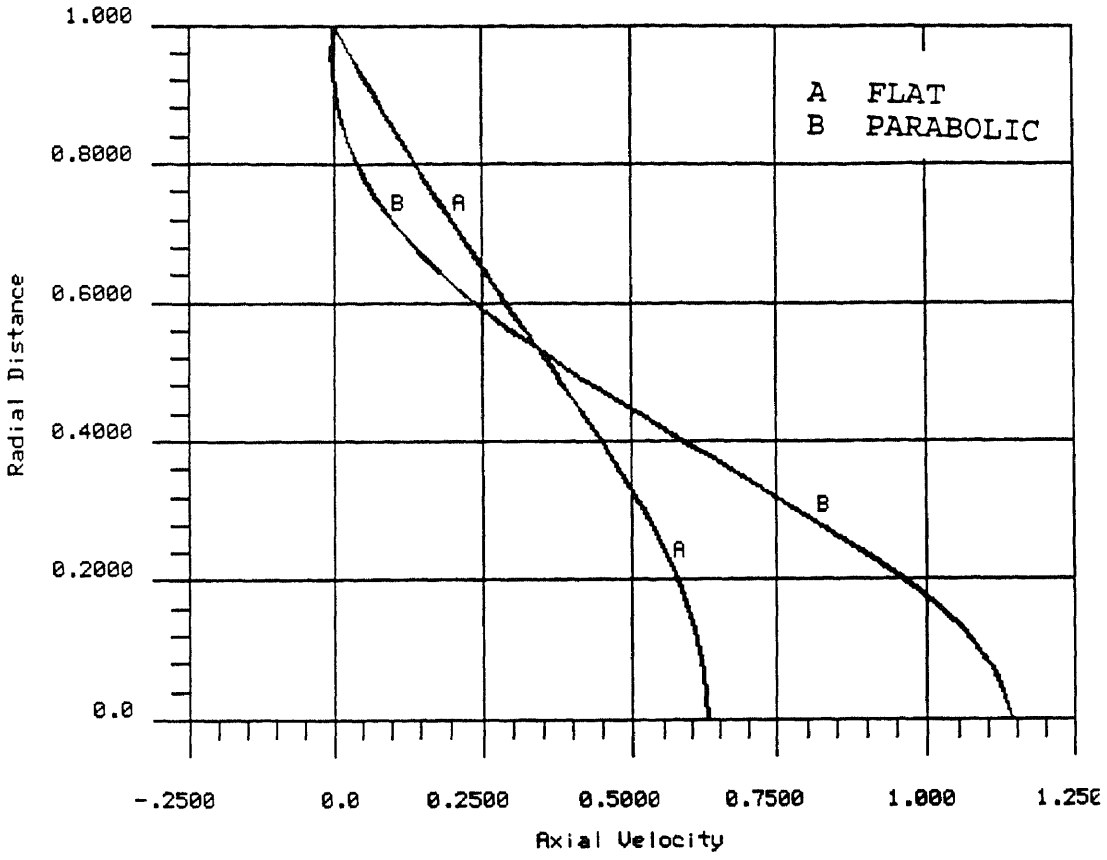

Figure 14 Comparison of velocity profiles at a fixed cross section (x/d = 8) for uniform and parabolic inlet velocity profiles

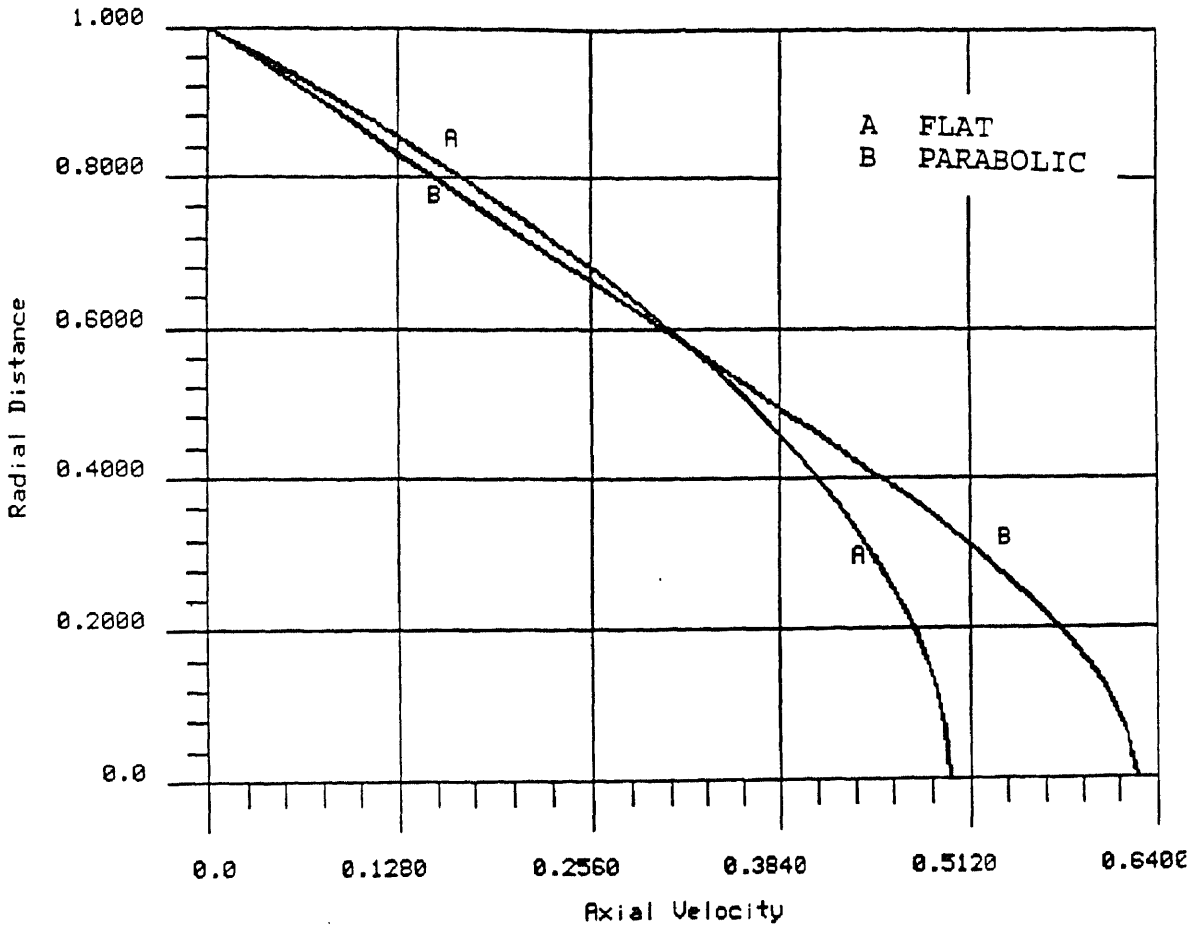

Figure 15 Comparison of velocity profiles at a fixed cross section (x/d = 16) for uniform and parabolic inlet velocity profiles

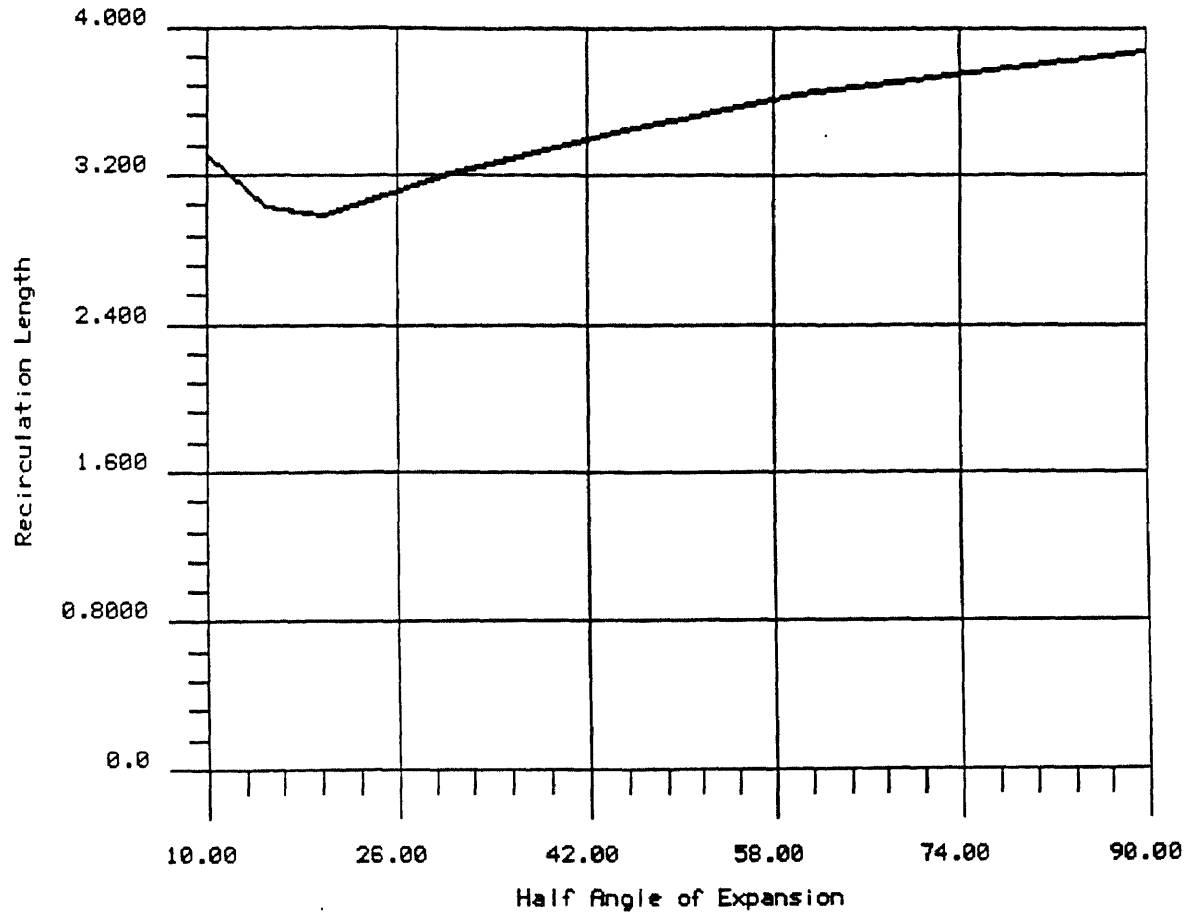

Figure 16 Variation of recirculation length with half angle of expansion

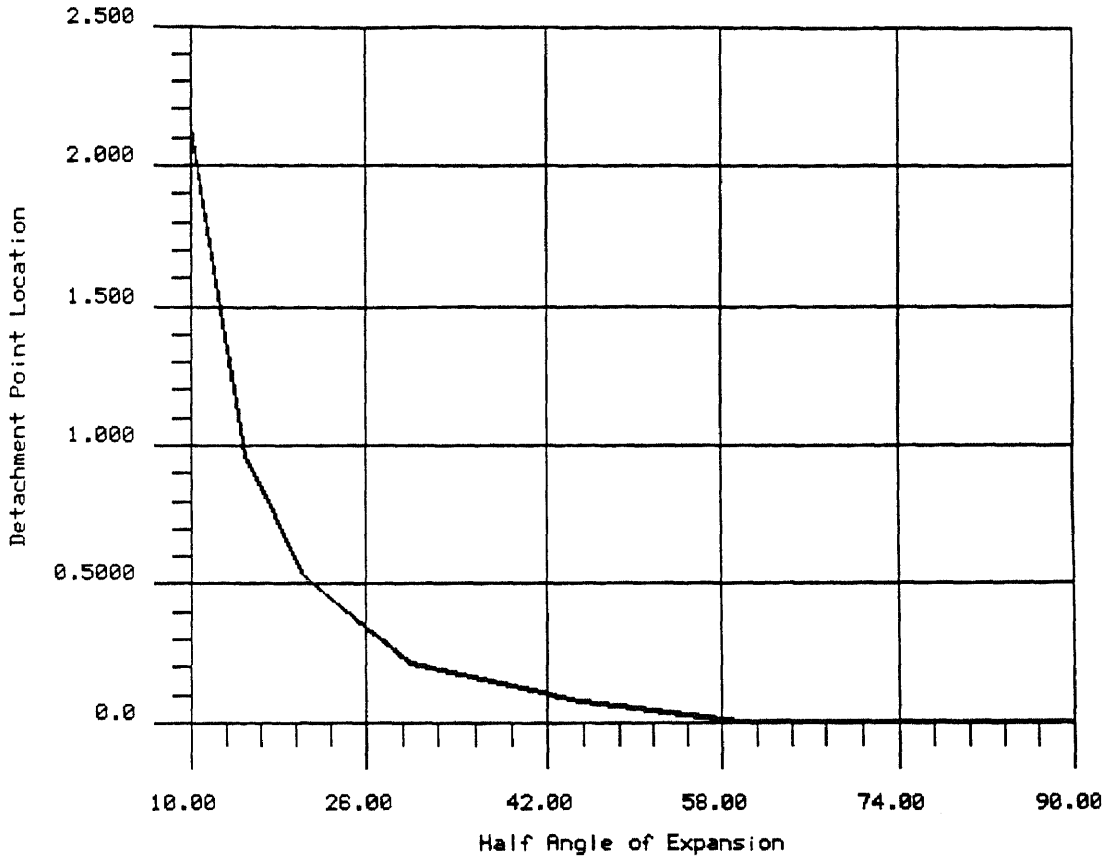

Figure 17 Variation of detachment length with half angle of expansion

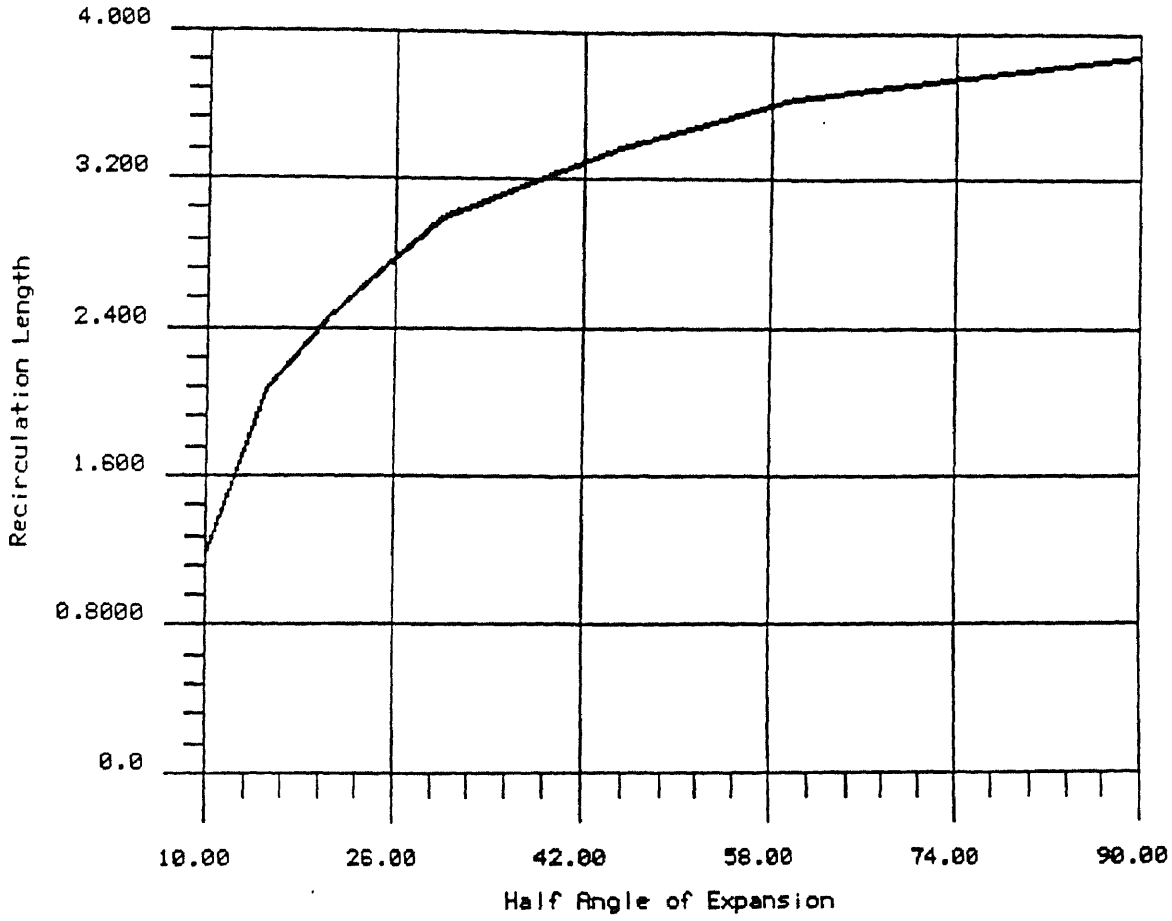

Figure 18 Variation of effective recirculation length with half angle of expansion

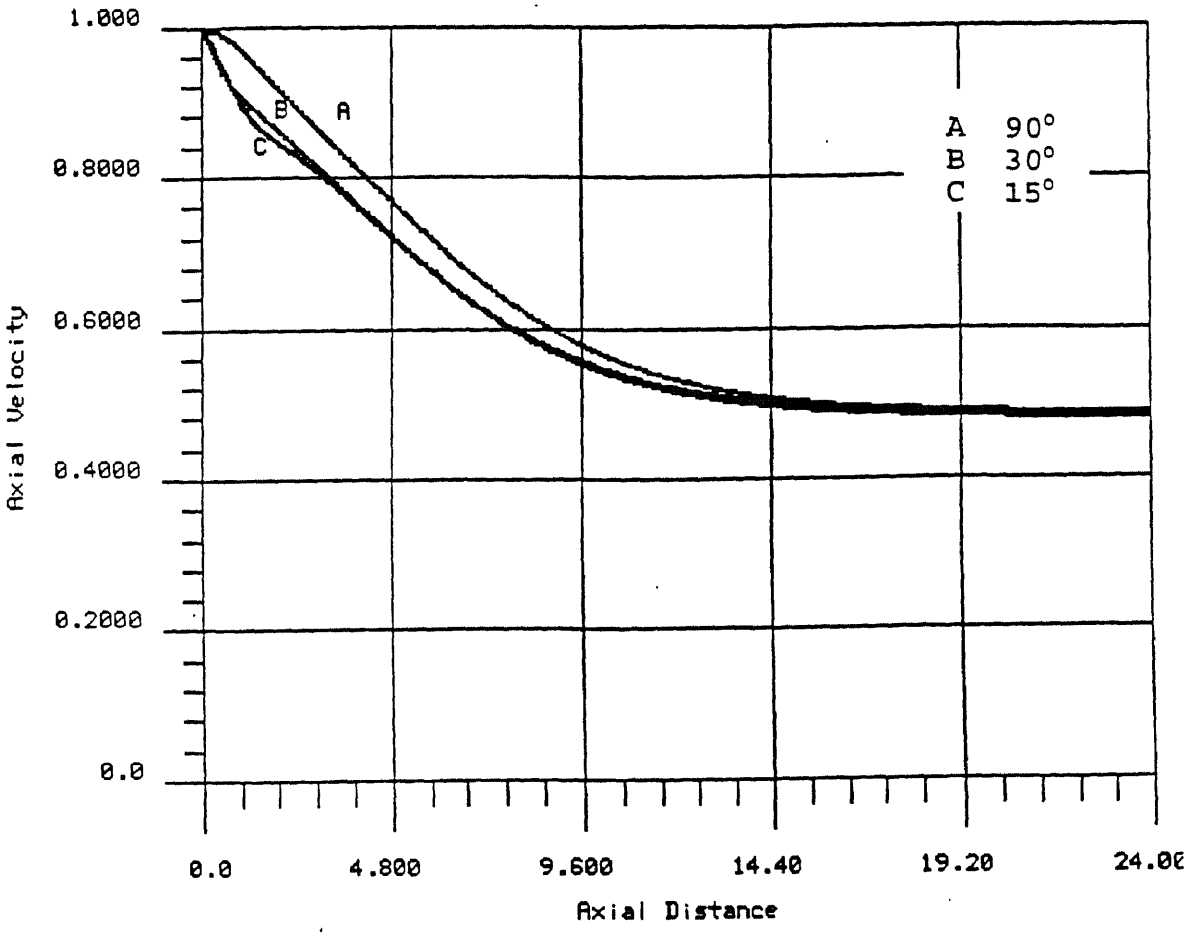

Figure 19 Centerline axial velocity distribution for various half angles of expansion

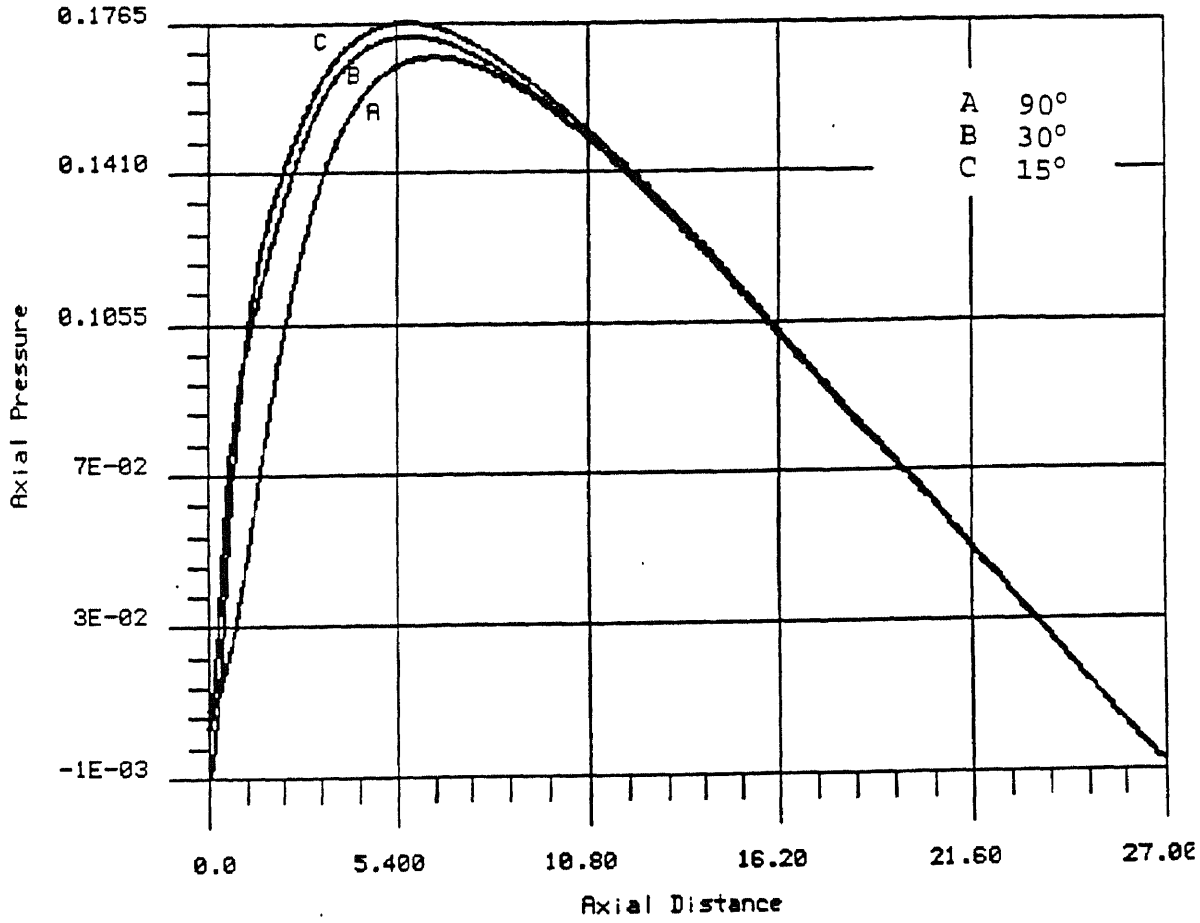

Figure 20 Centerline pressure distribution for various half angles of expansion

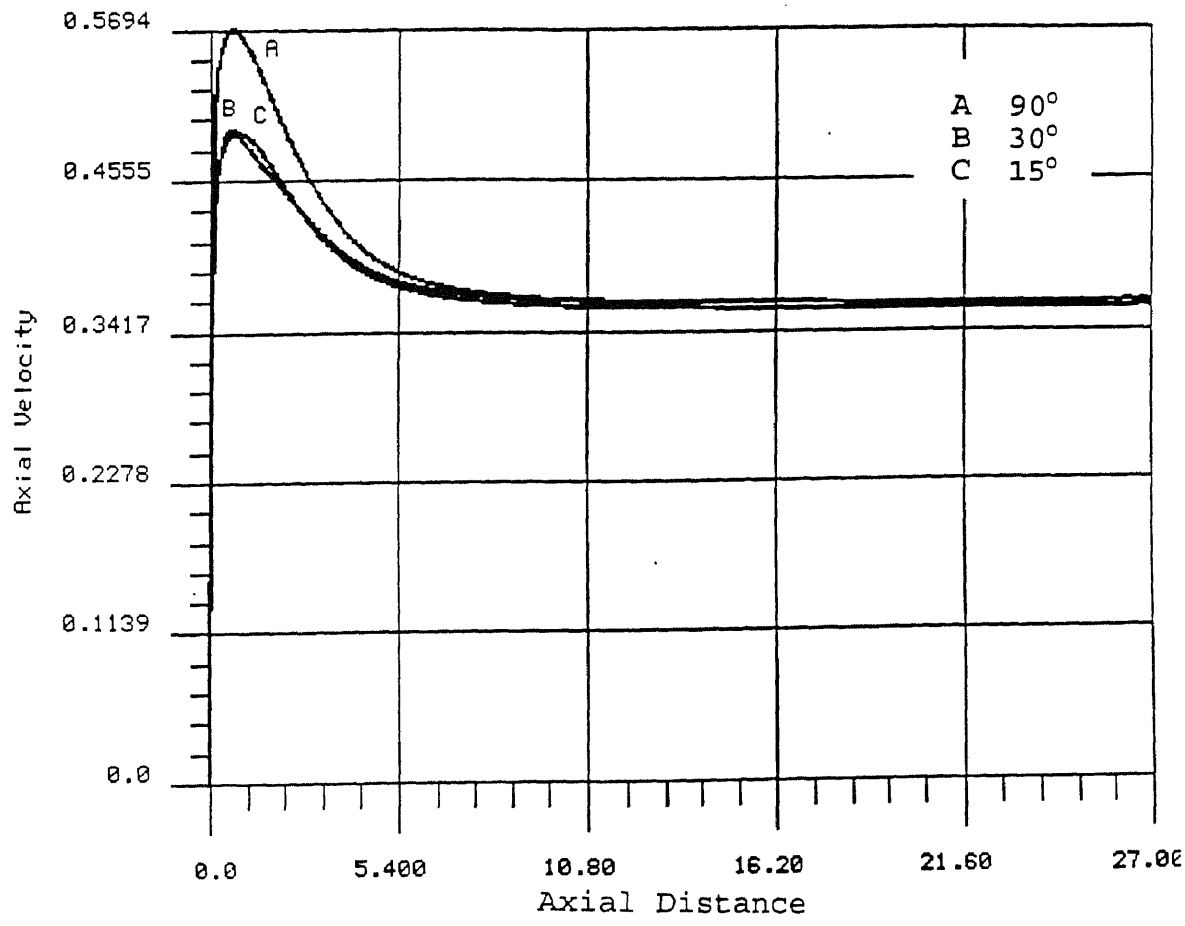

Figure 21 Axial velocity distribution along the shear layer for various half angles of expansion

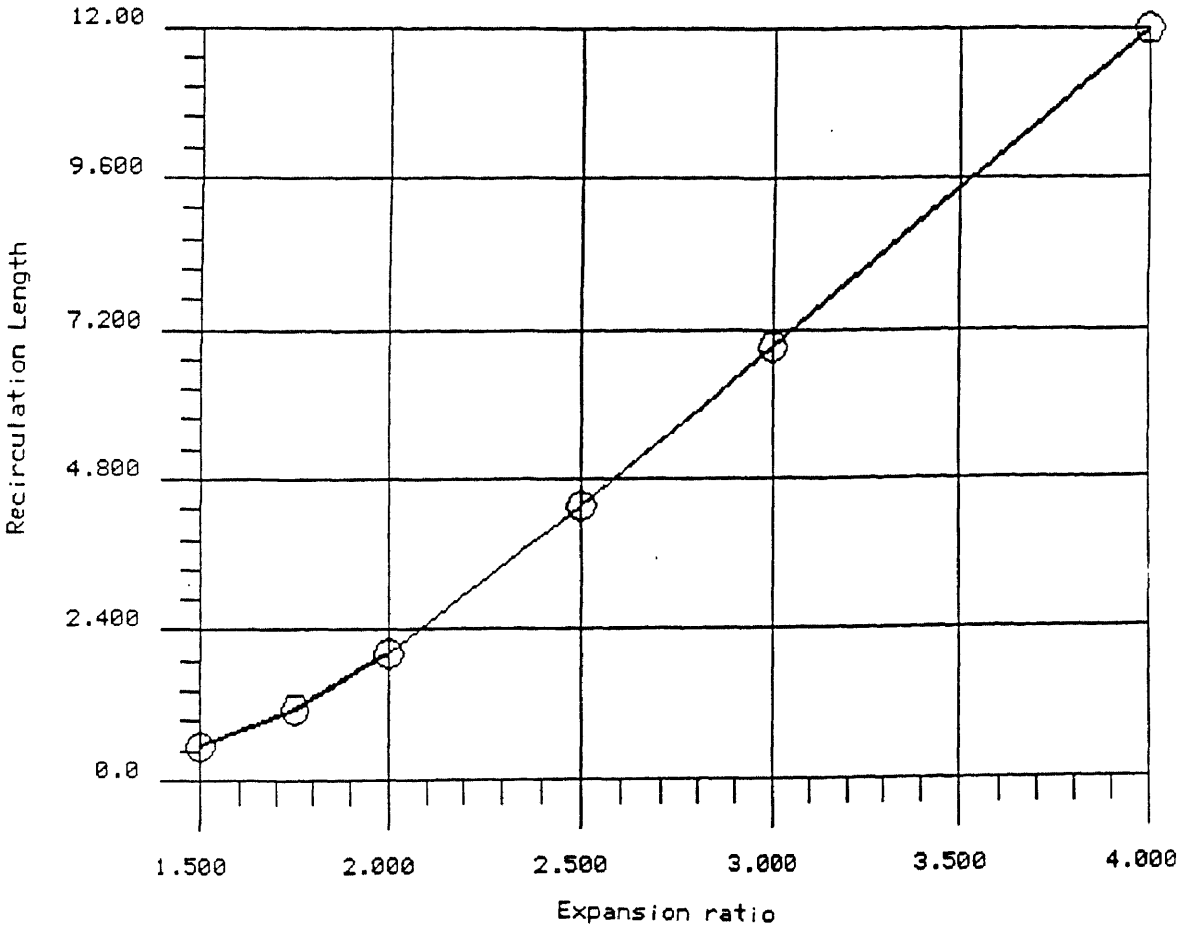

Figure 22 Variation of recirculation length with expansion ratio

APPENDIX II

RESULTS FOR TURBULENT FLOW

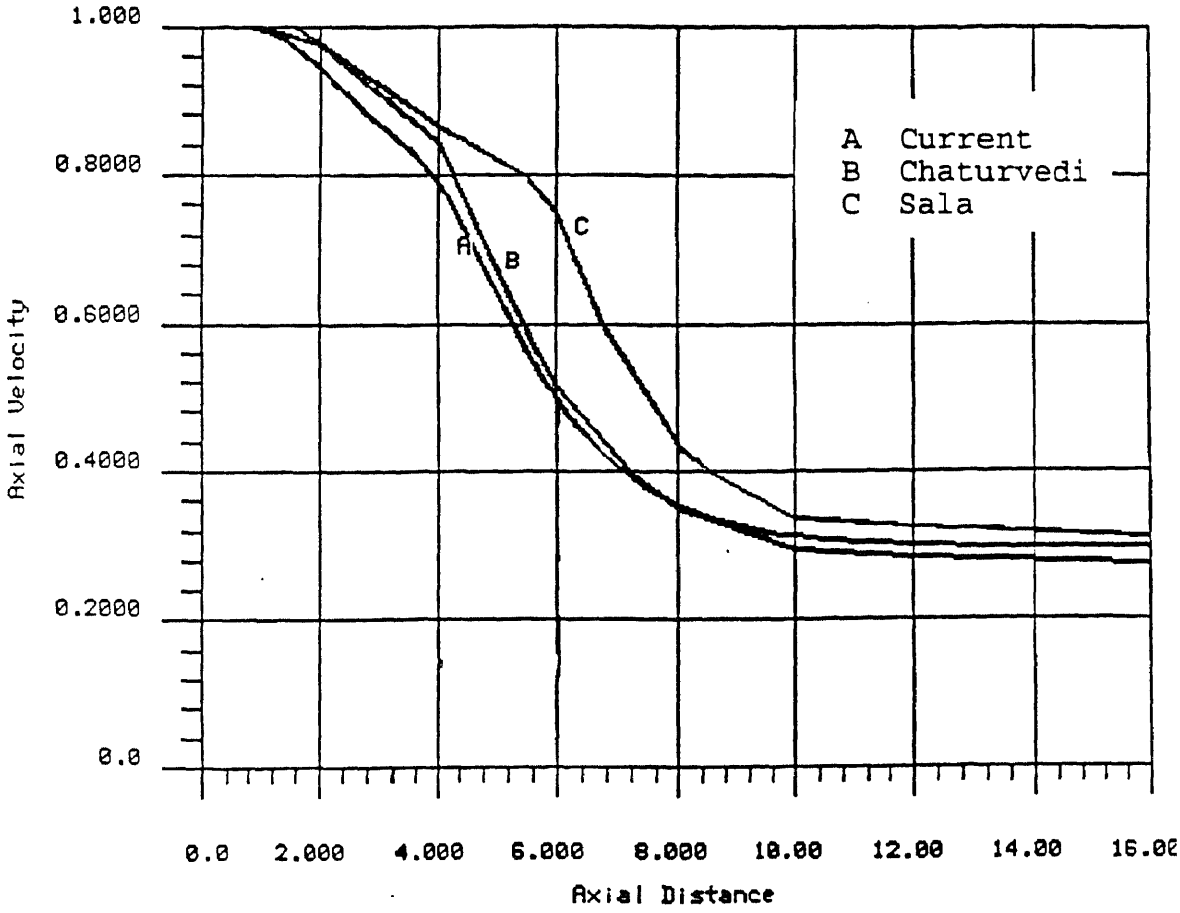

Figure 23 Centerline axial velocity distribution for half angle of expansion of 90°

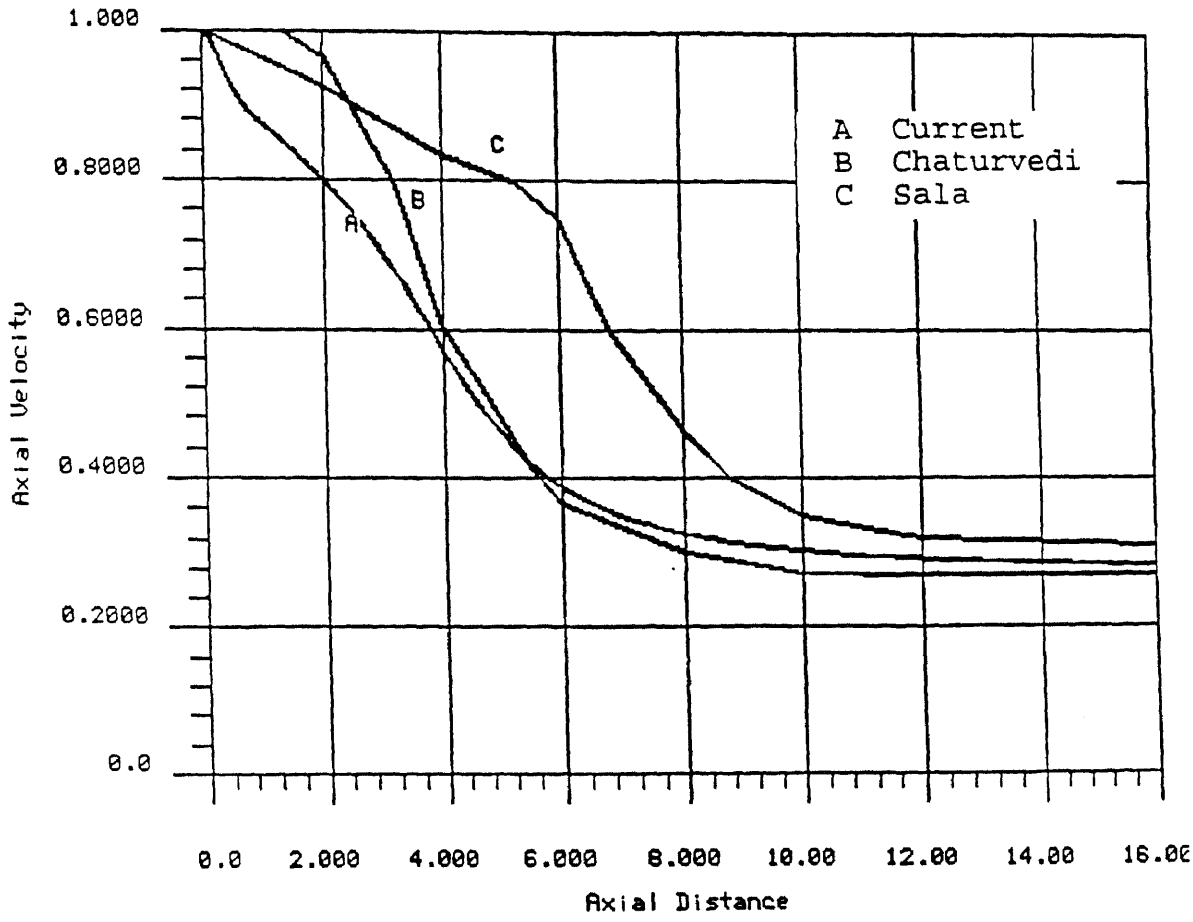

Figure 24 Centerline axial velocity distribution for half angle of expansion of 30°

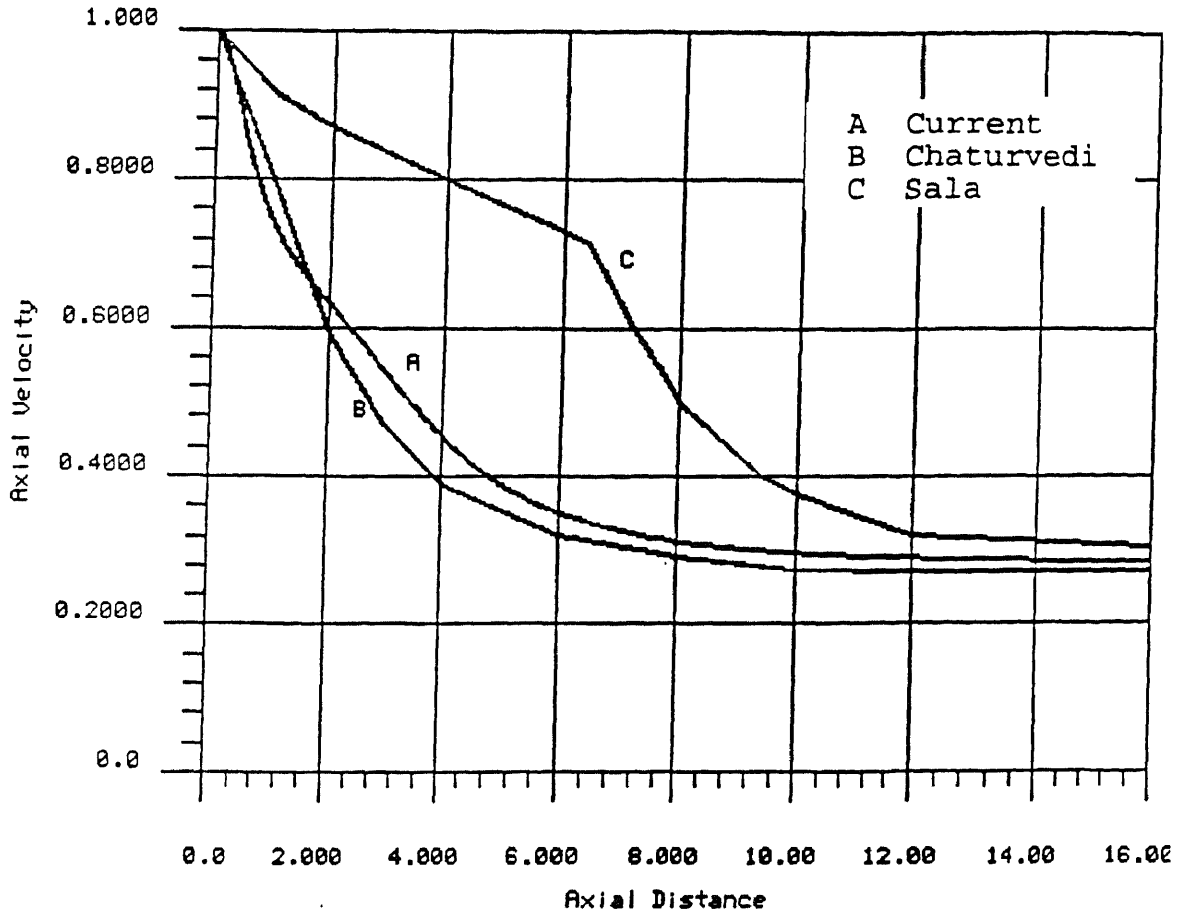

Figure 25 Centerline axial velocity distribution for half angle of expansion of 15°

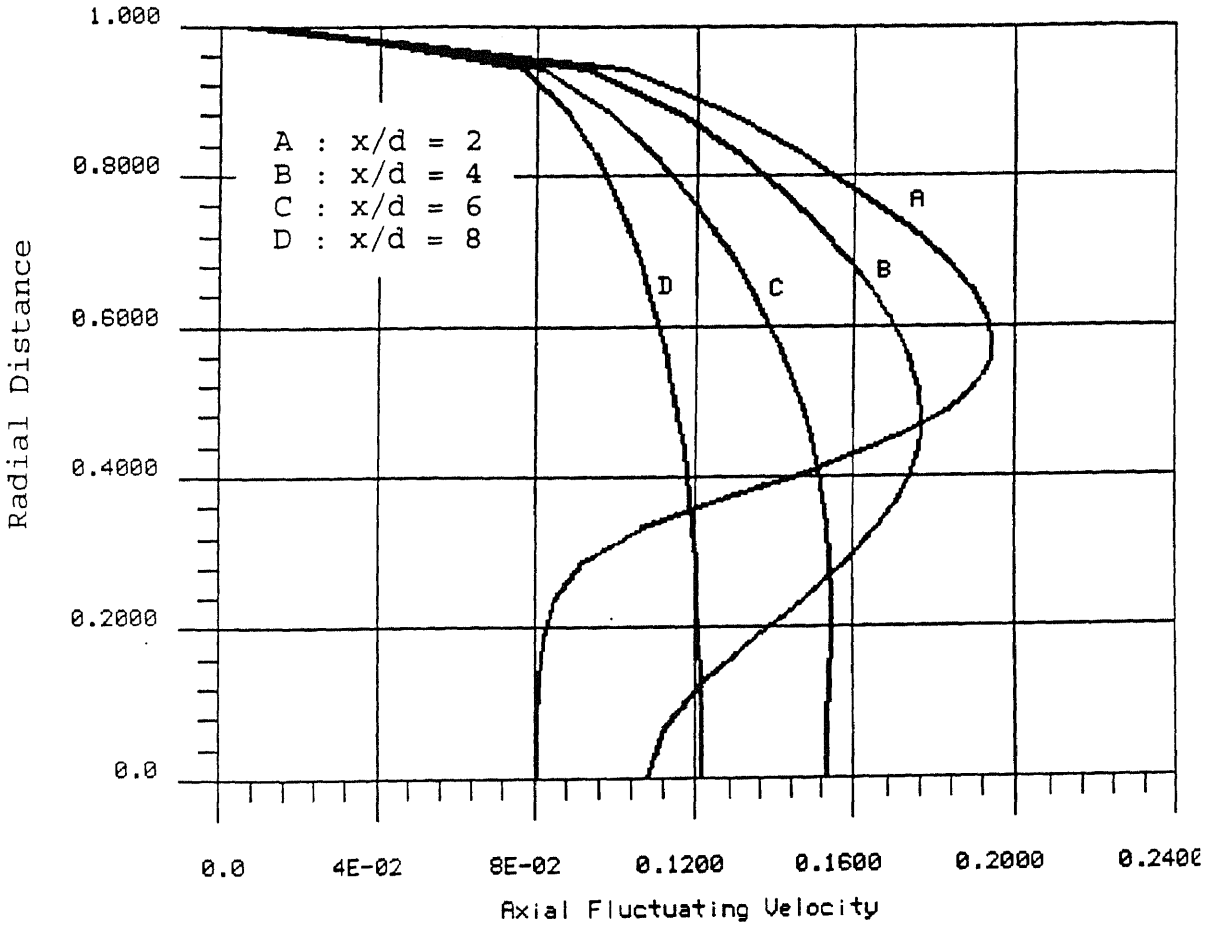

Figure 26 Profiles of fluctuating axial component of velocity at various cross sections for half angle of expansion of 90°

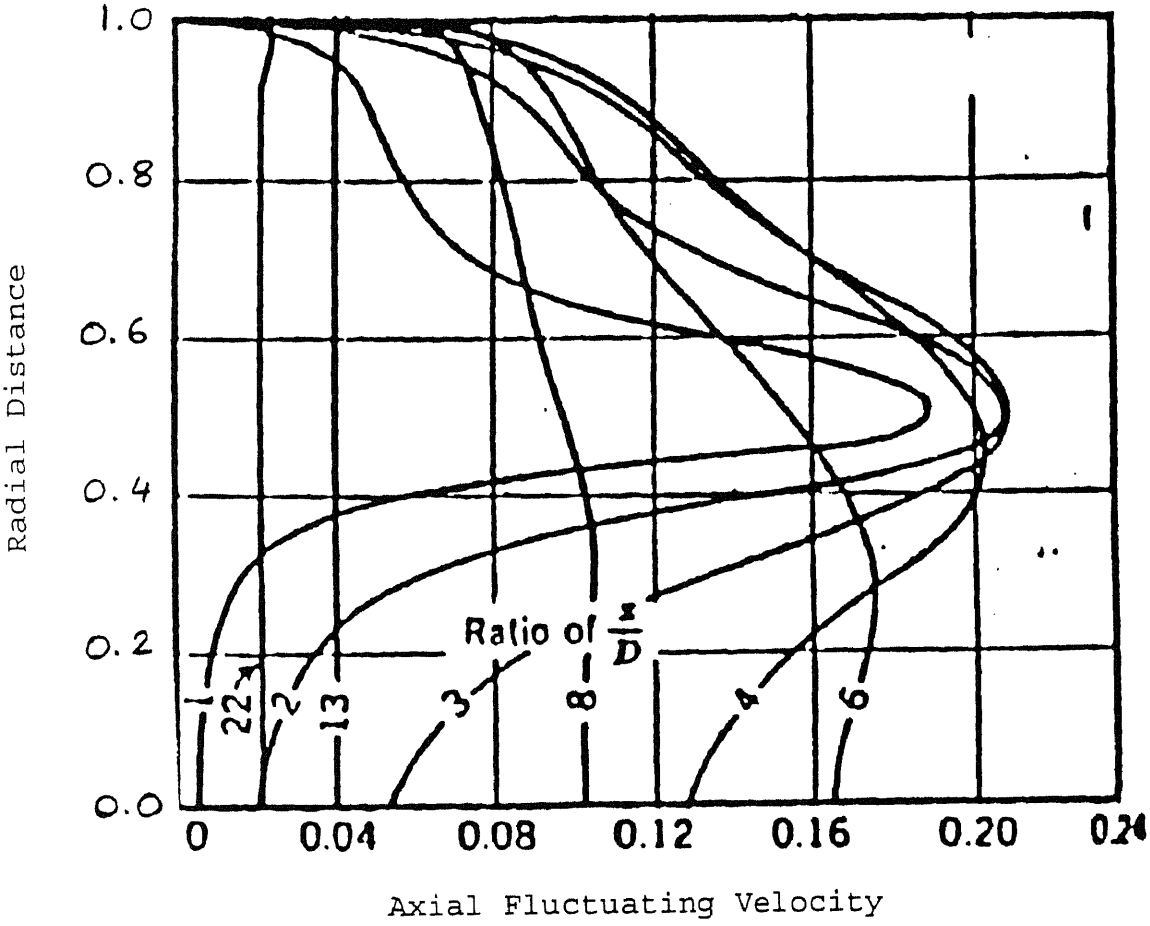

Figure 27 Experimental results for profiles of fluctuating axial component of velocity at various cross sections for half angle of expansion of 90°

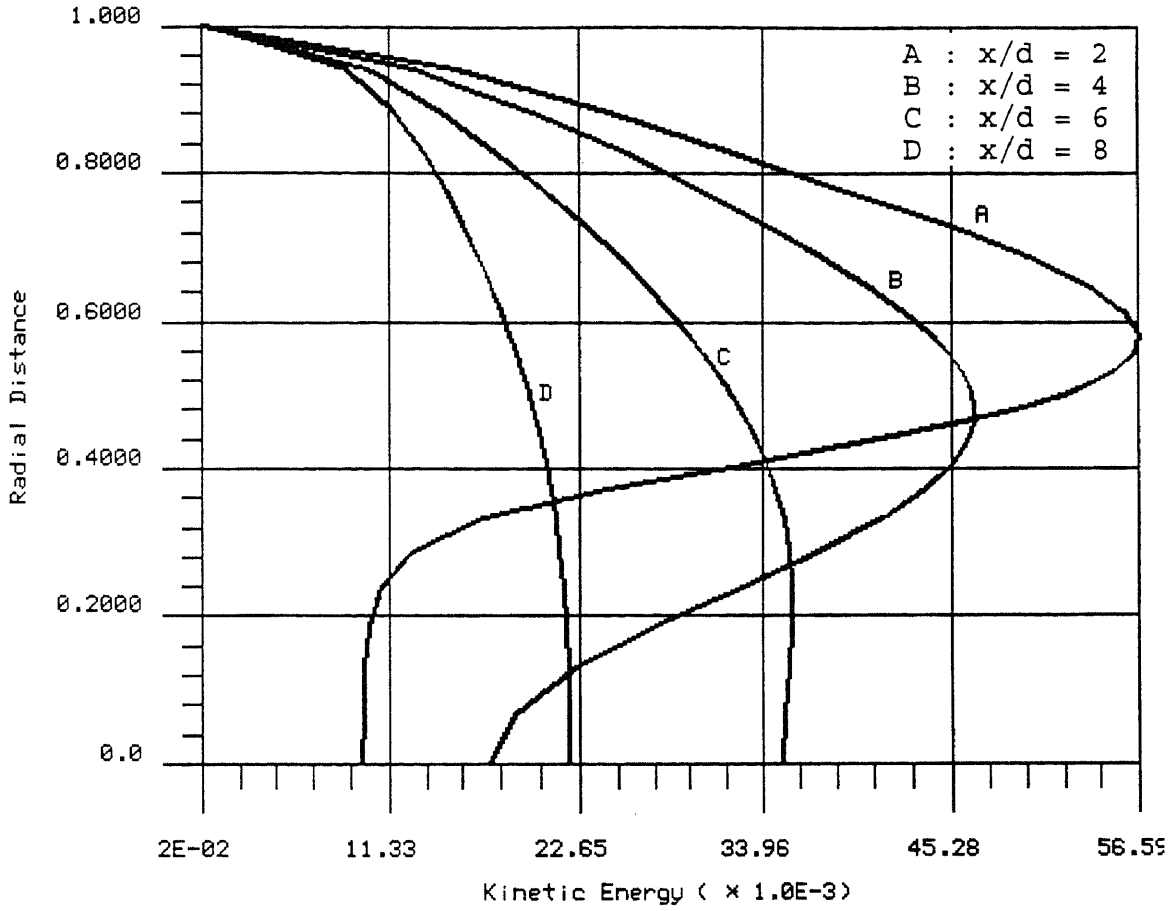

Figure 28 Profiles of turbulent kinetic energy at various cross sections for half angle of expansion of 90°

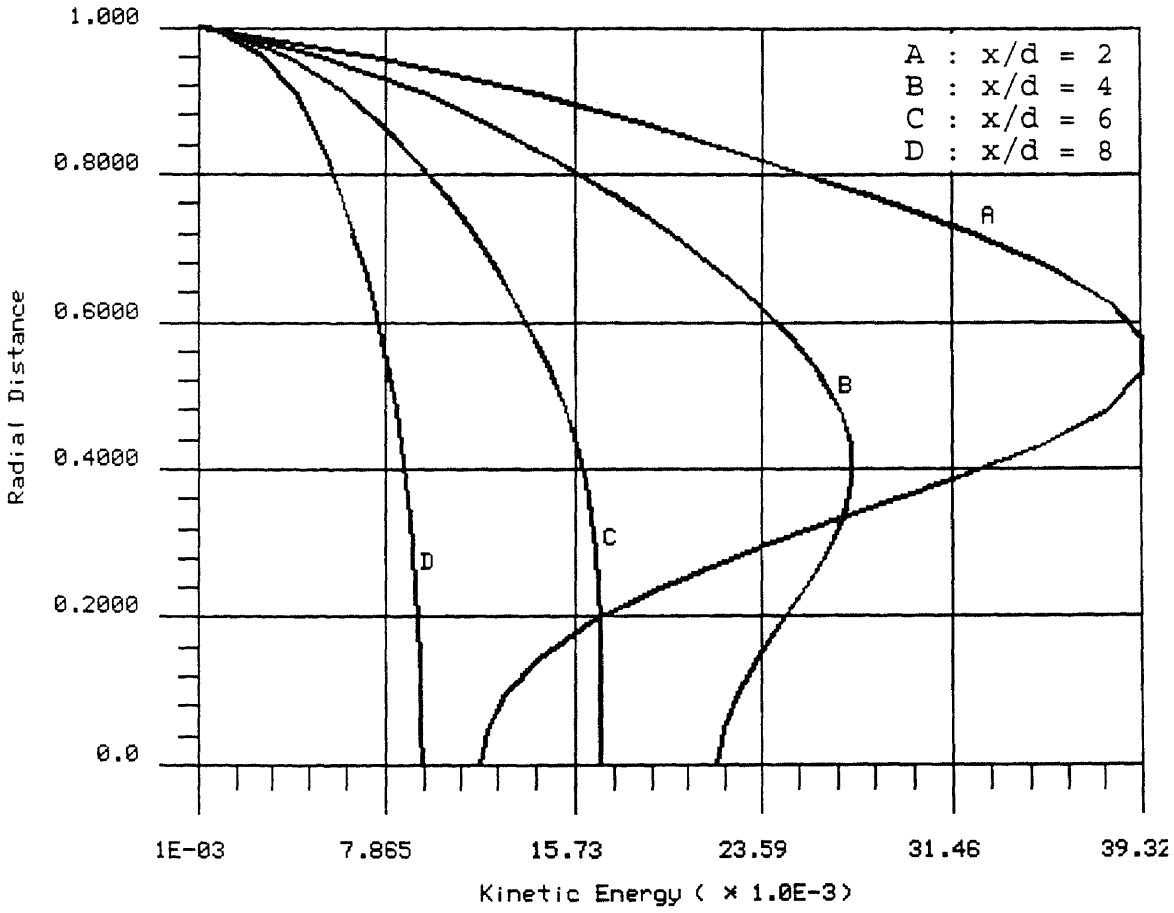

Figure 29 Profiles of turbulent kinetic energy at various cross sections for half angle of expansion of 30°

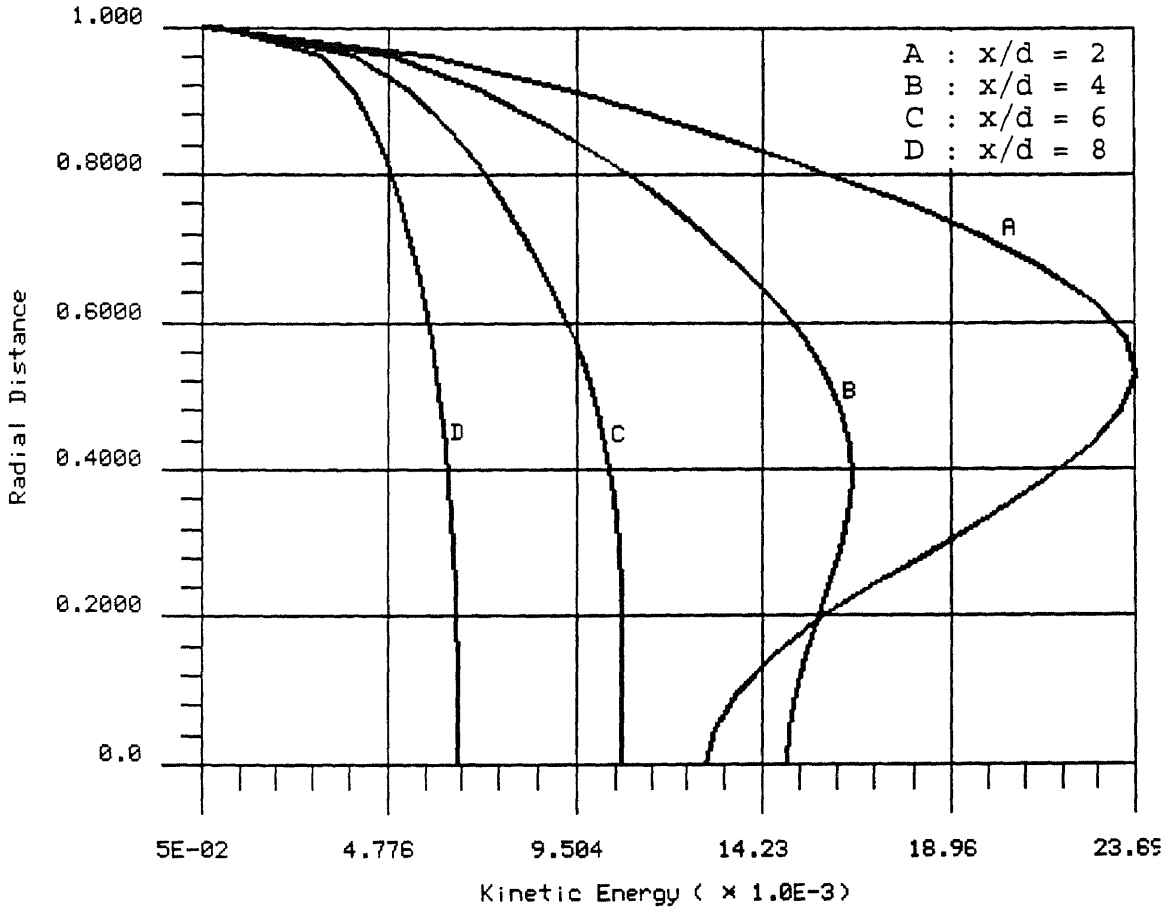

Figure 30 Profiles of turbulent kinetic energy at various cross sections for half angle of expansion of 15°

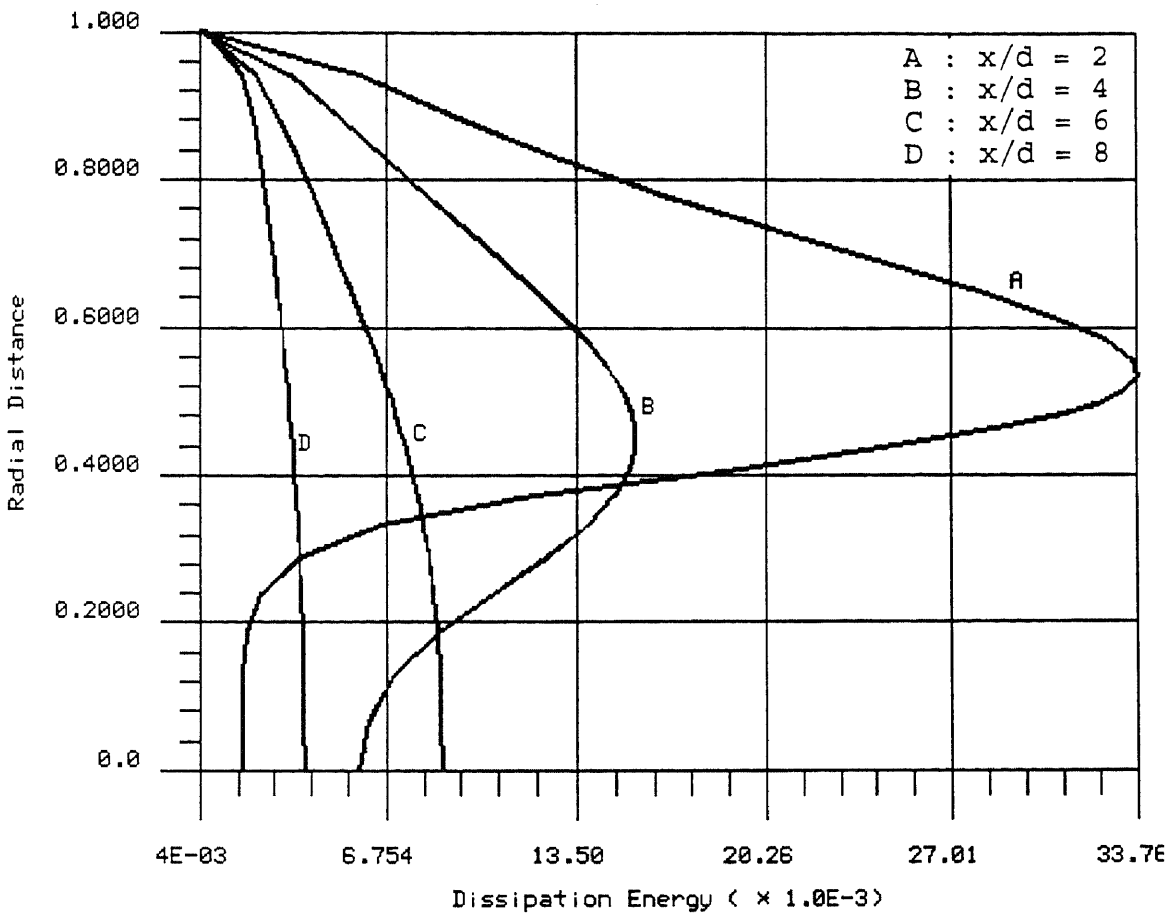

Figure 31 Profiles of turbulent dissipation energy at various cross sections for half angle of expansion of 90°

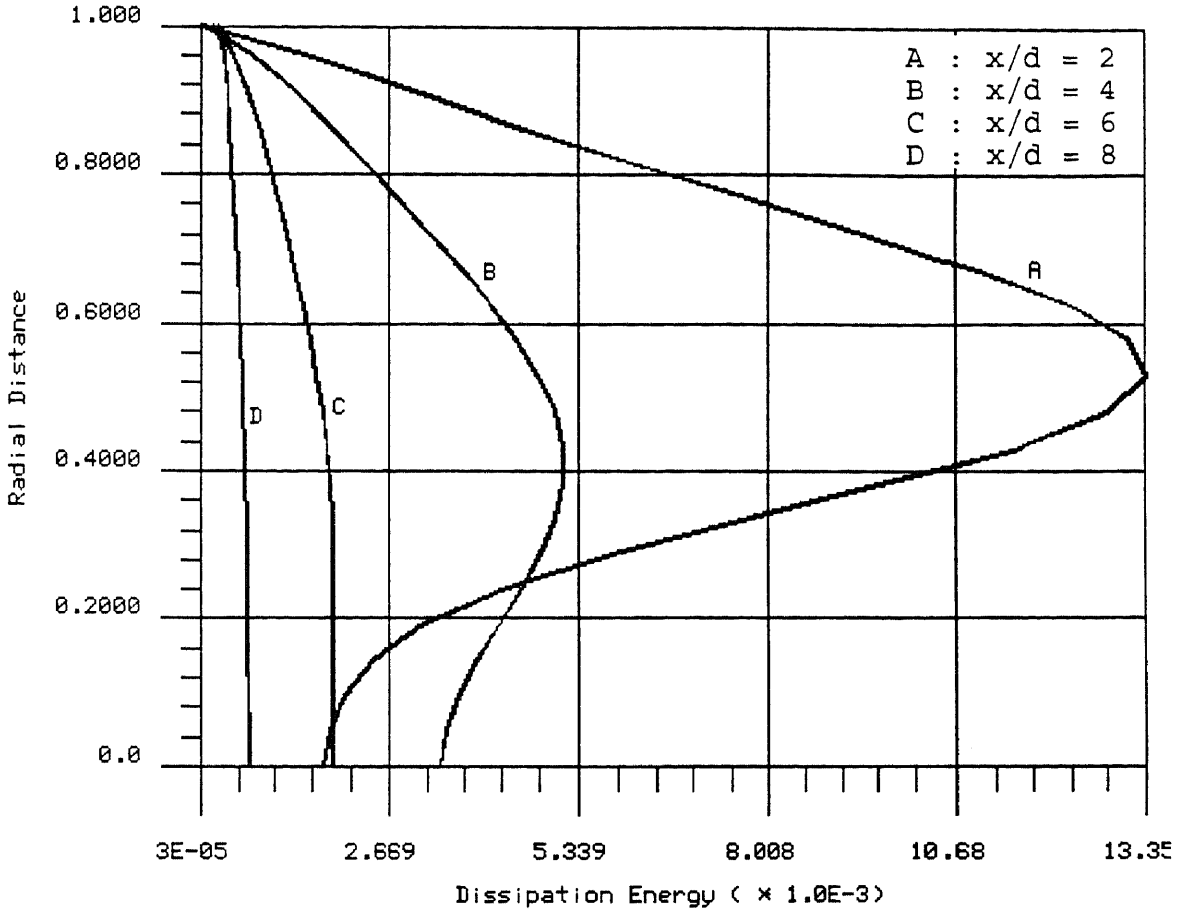

Figure 32 Profiles of turbulent dissipation energy at various cross sections for half angle of expansion of 30°

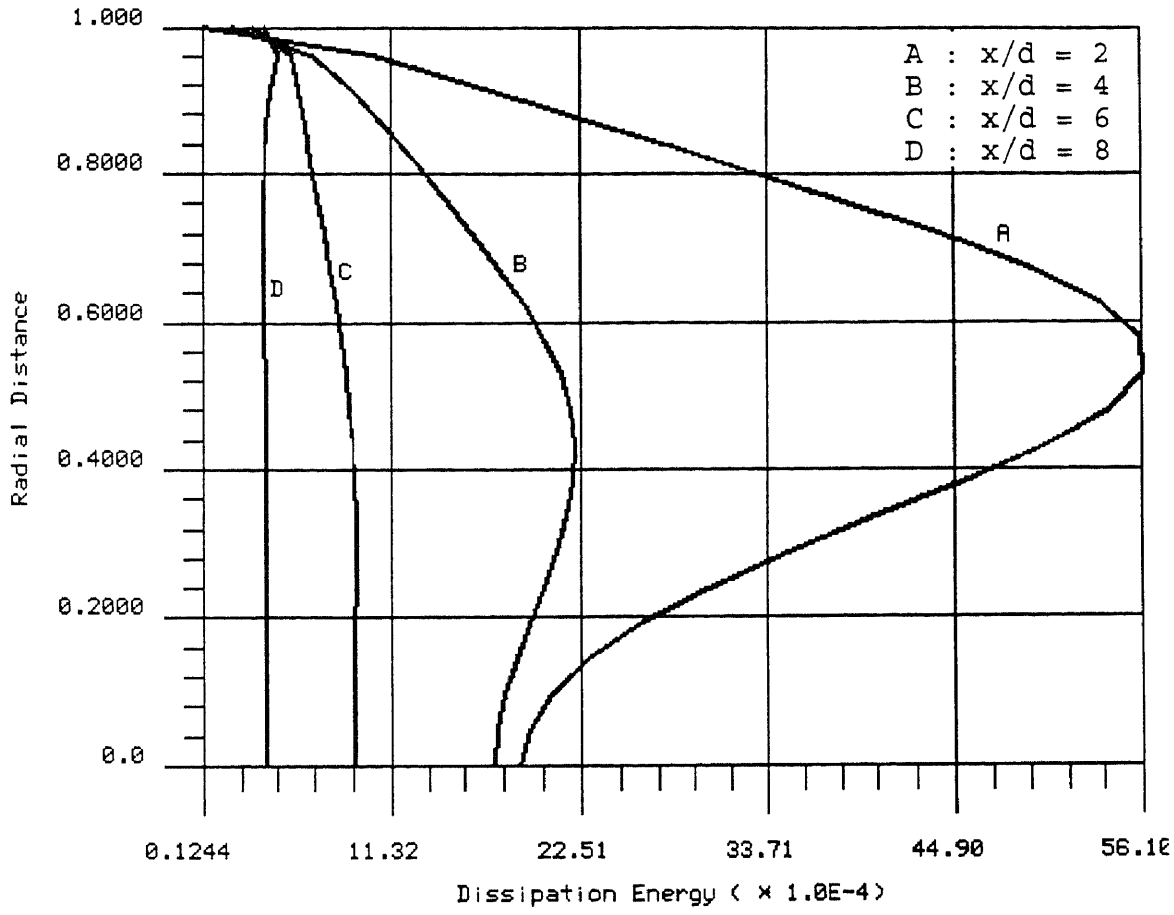

Figure 33 Profiles of turbulent dissipation energy at various cross sections for half angle of expansion of 15°

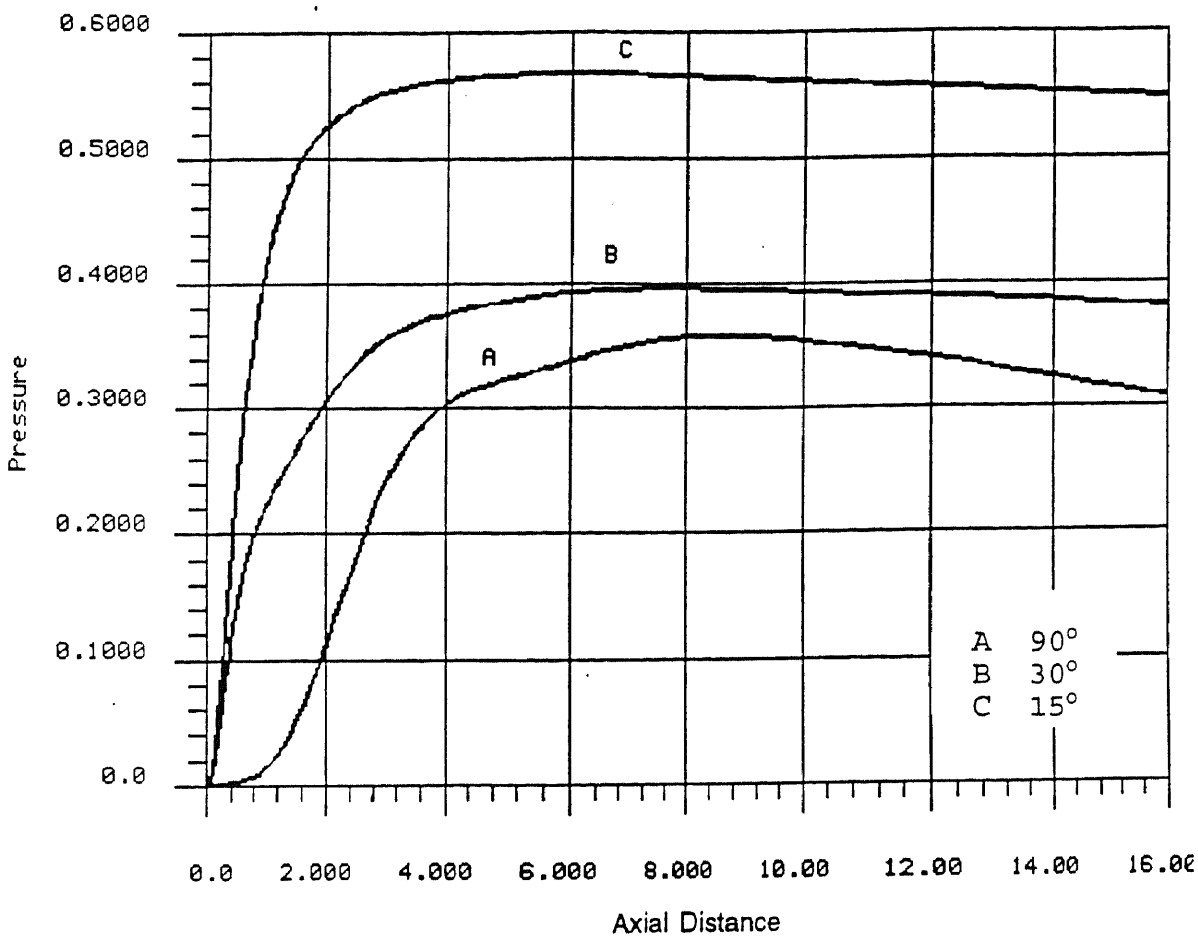

Figure 34 Centerline pressure distribution for various half angles of expansion

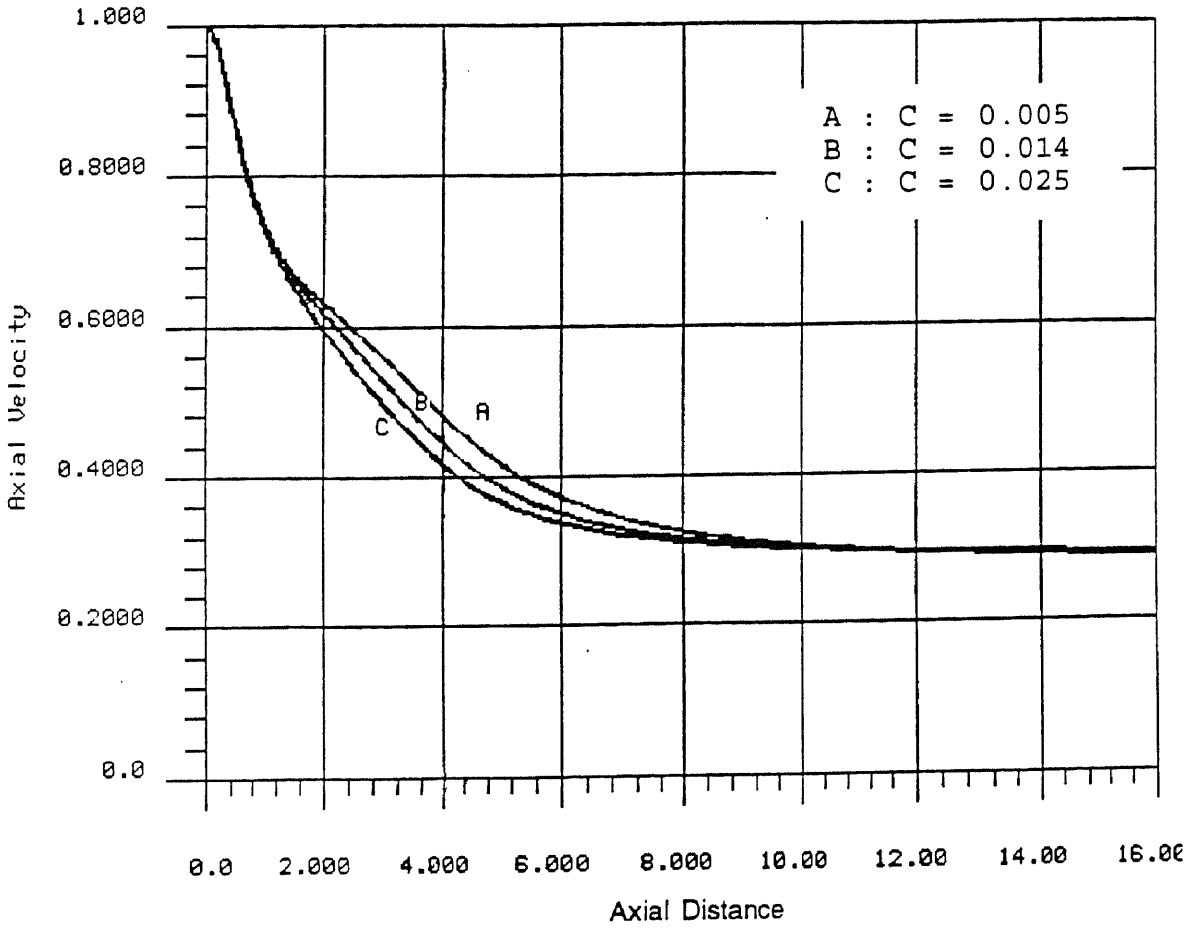

Figure 35 Centerline axial velocity distribution for different inlet kinetic energy boundary conditions (half angle of expansion = 15°)

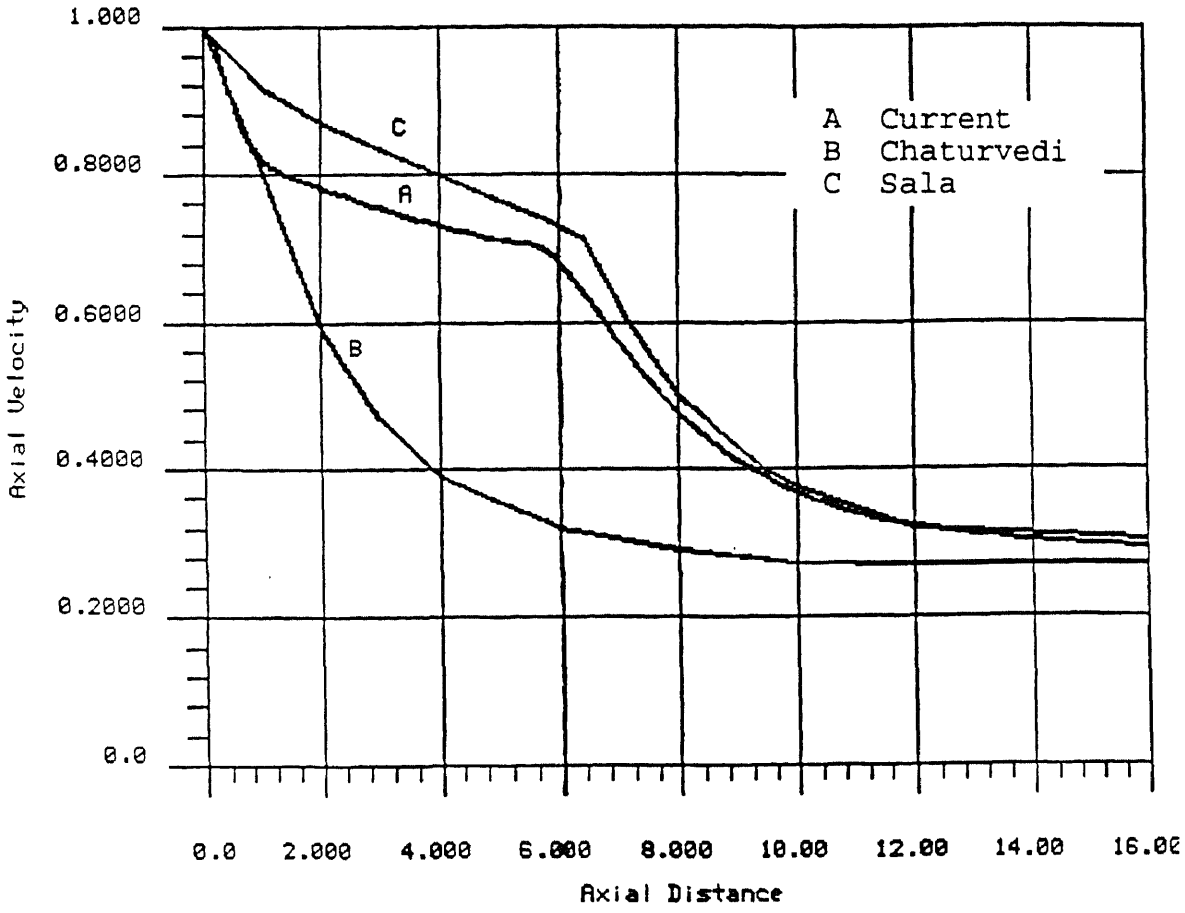

Figure 36 Centerline axial velocity distribution for increased dissipation energy at the inlet (half angle of expansion = 15°)

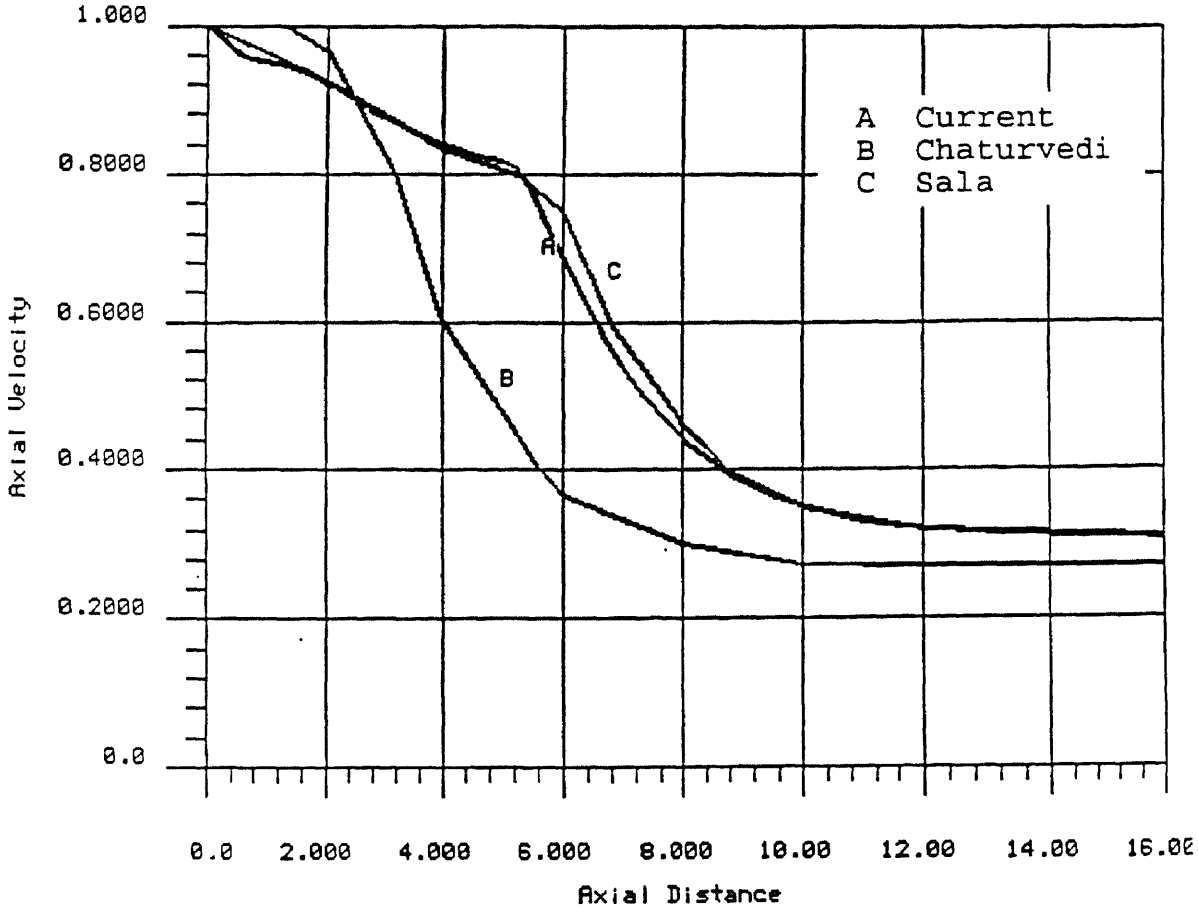

Figure 37 Centerline axial velocity distribution for increased dissipation energy at the inlet (half angle of expansion = 30°)

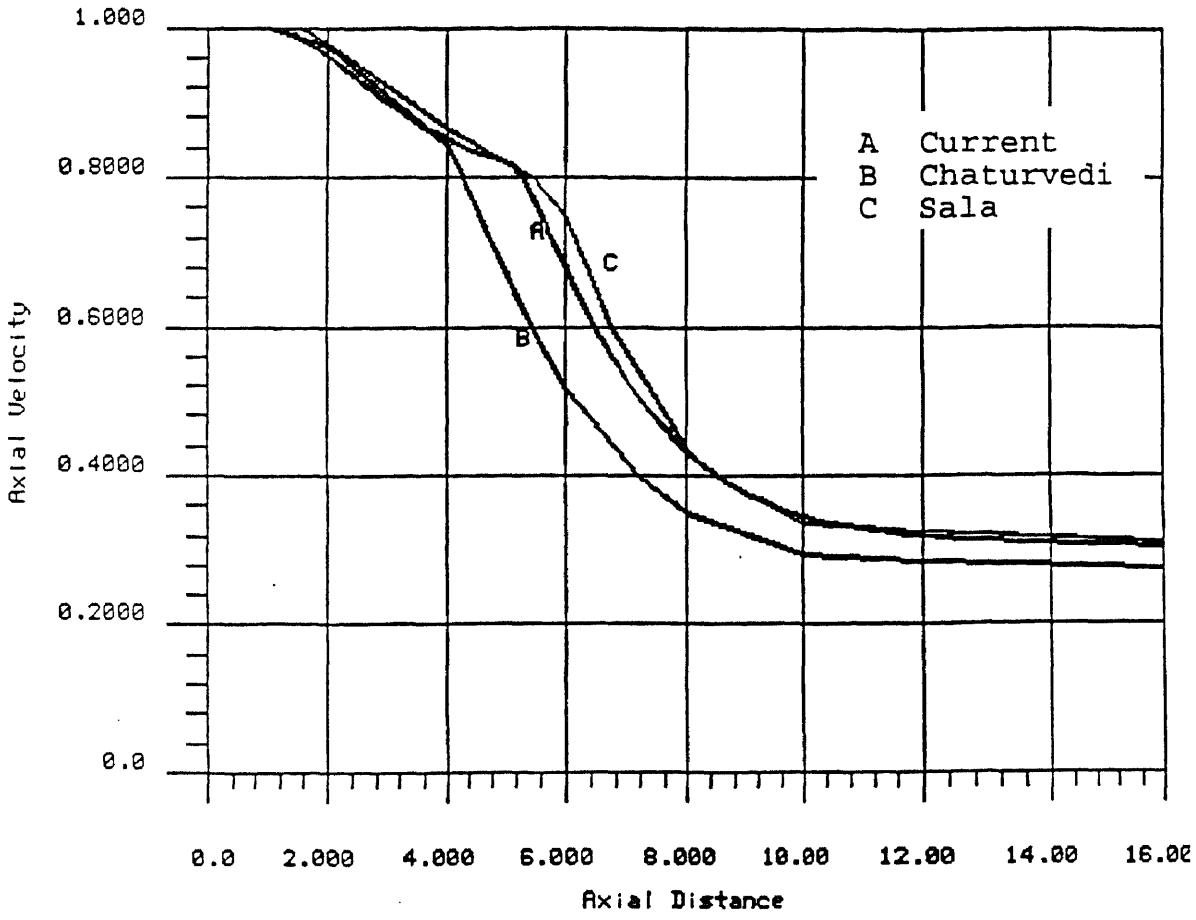

Figure 38 Centerline axial velocity distribution for increased dissipation energy at the inlet (half angle of expansion = 90°)

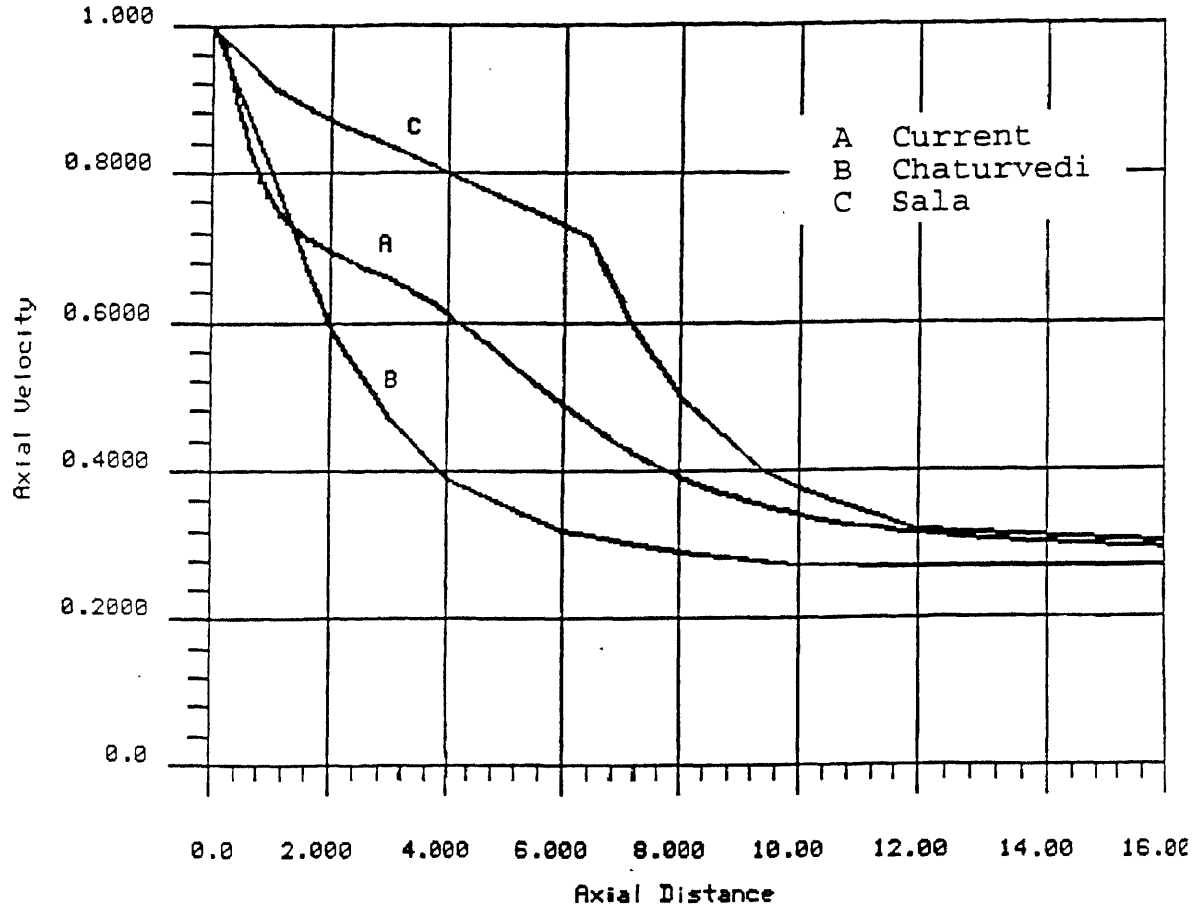

Figure 39 Centerline axial velocity distribution for half angle of expansion of 15° for C_{μ} = 0.045

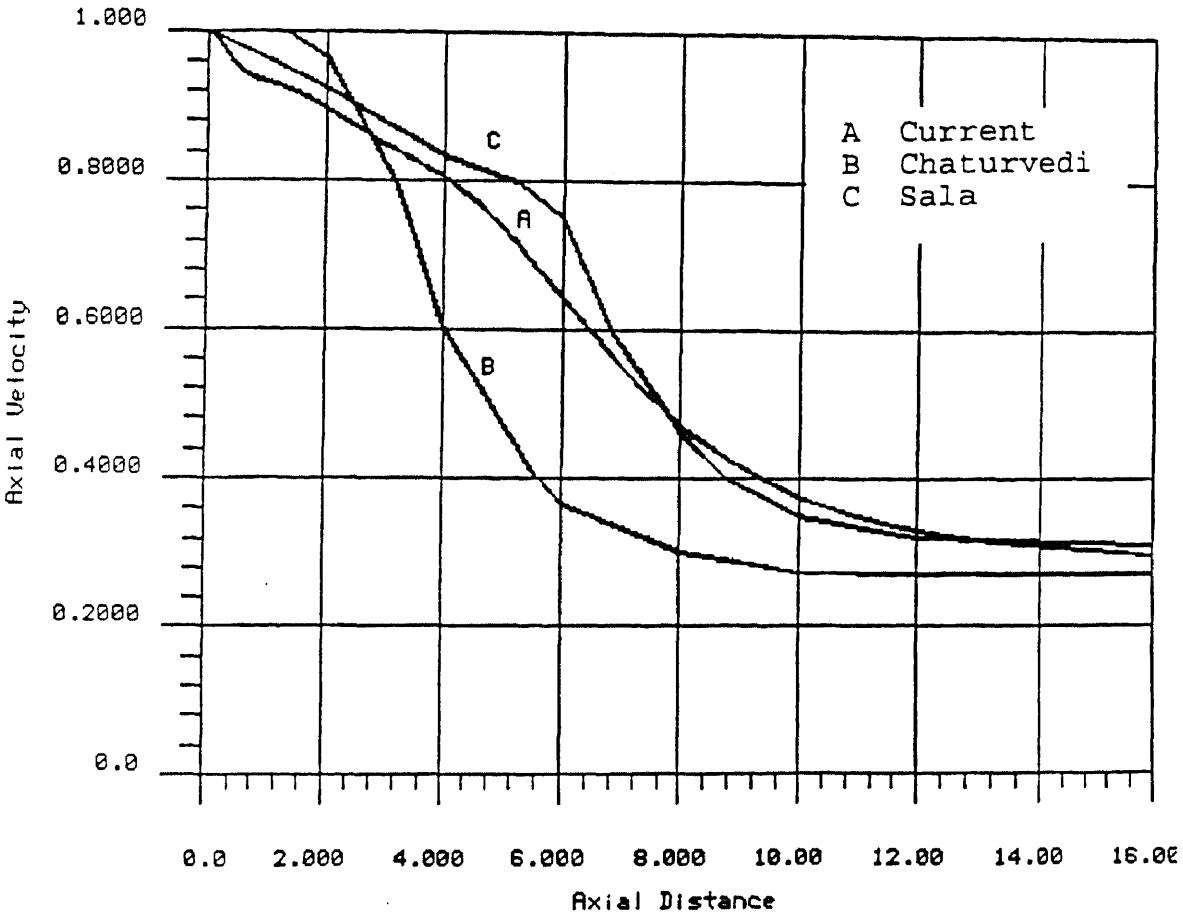

Figure 40 Centerline axial velocity distribution for half angle of expansion of 30° for C_μ = 0.045

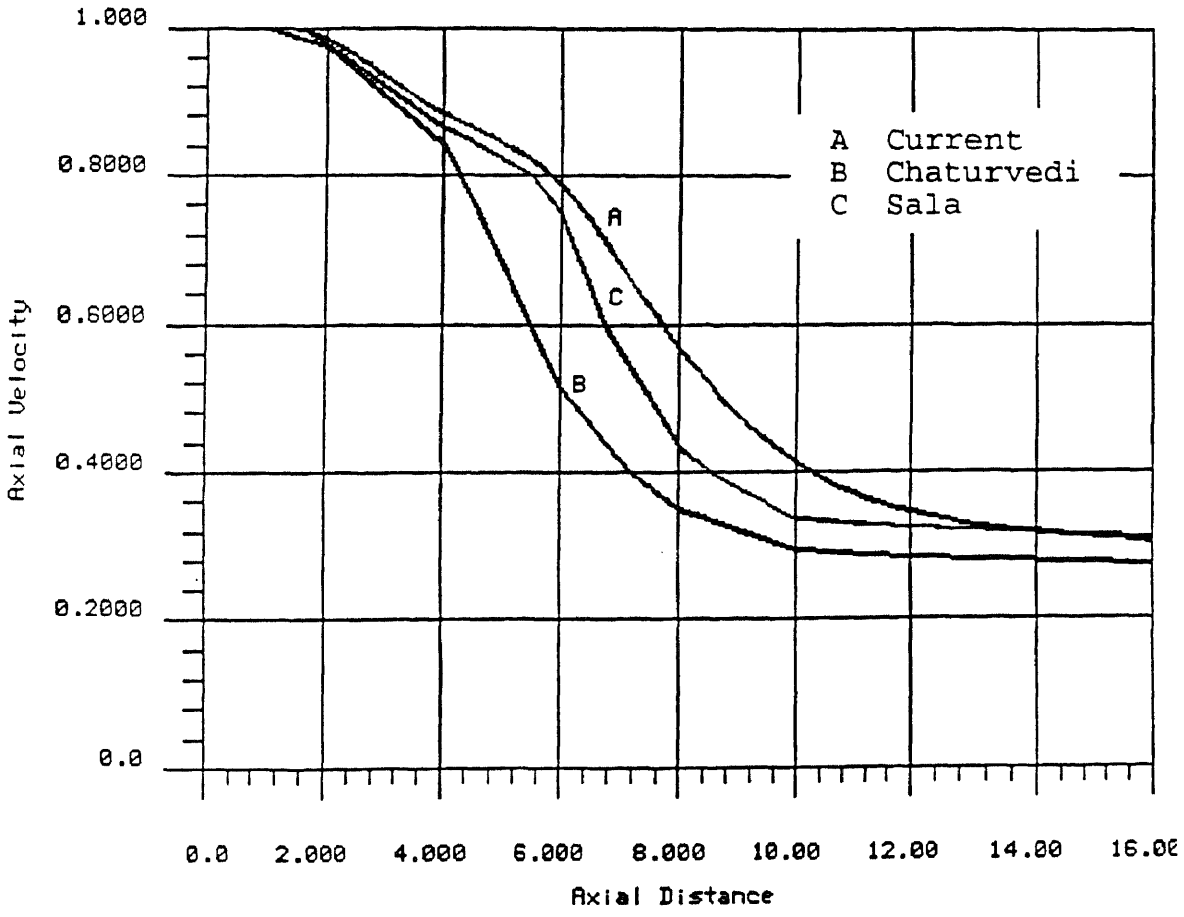

Figure 41 Centerline axial velocity distribution for half angle of expansion of 90° for C_μ = 0.045

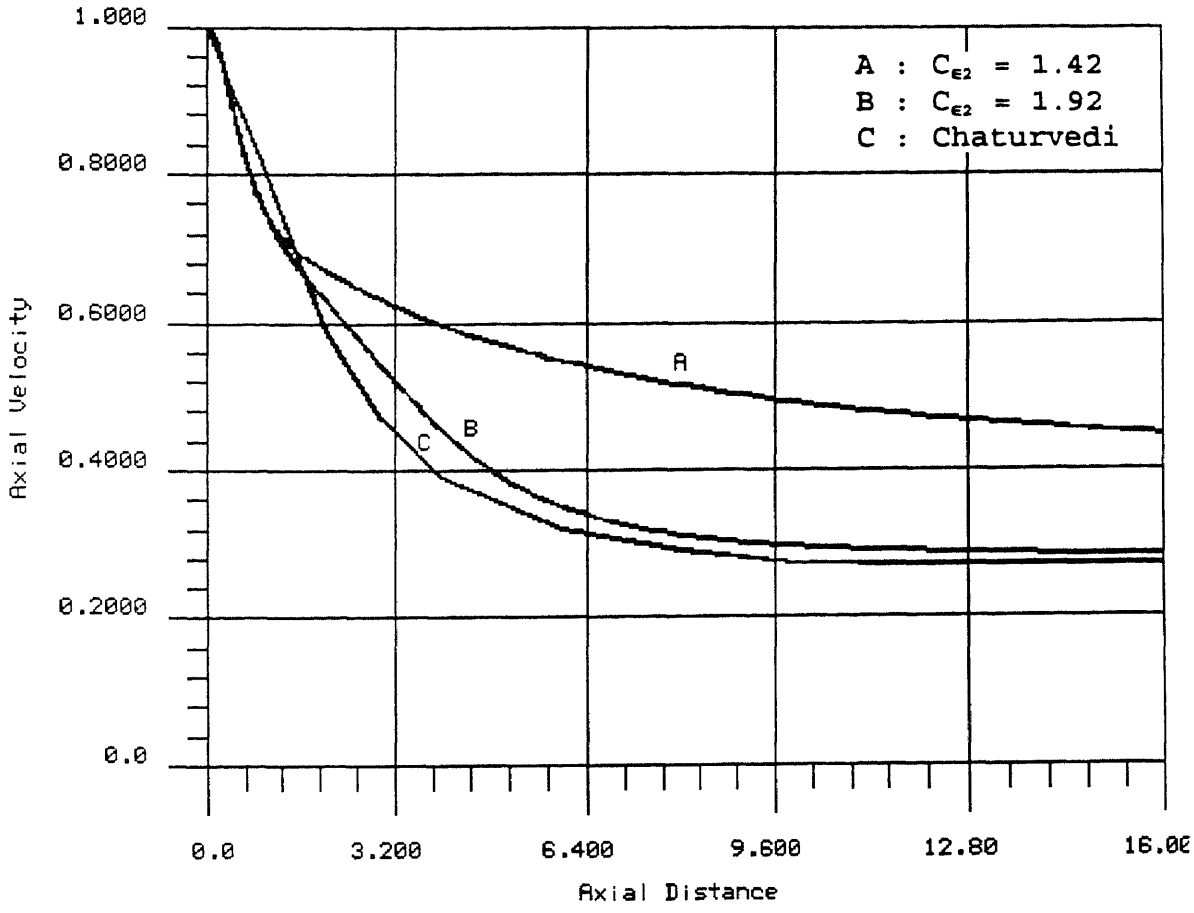

Figure 42 Comparison of centerline axial velocity distribution for different values of coefficient $C_{\epsilon 2}$

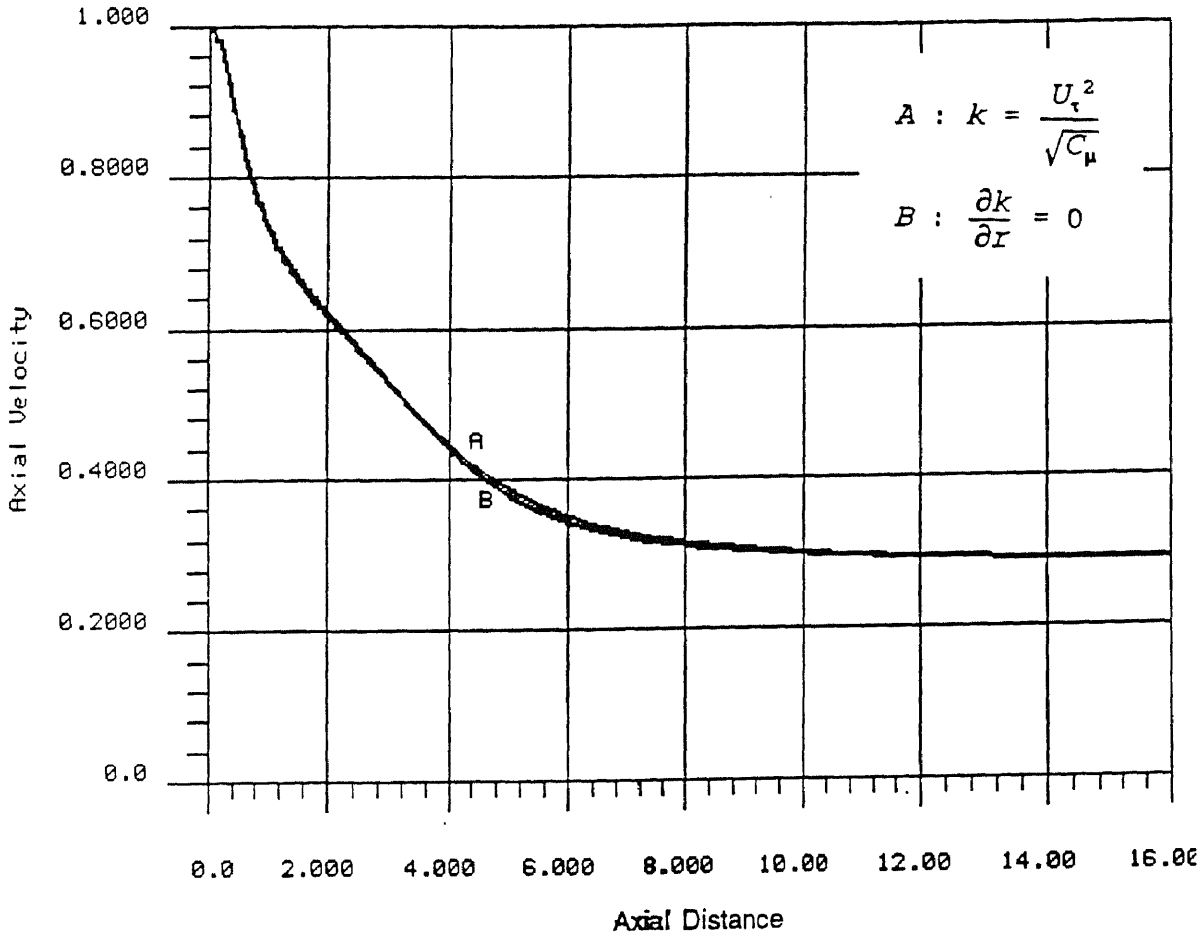

Figure 43 Comparison of centerline axial velocity distribution for different boundary condition of turbulent kinetic energy at the wall

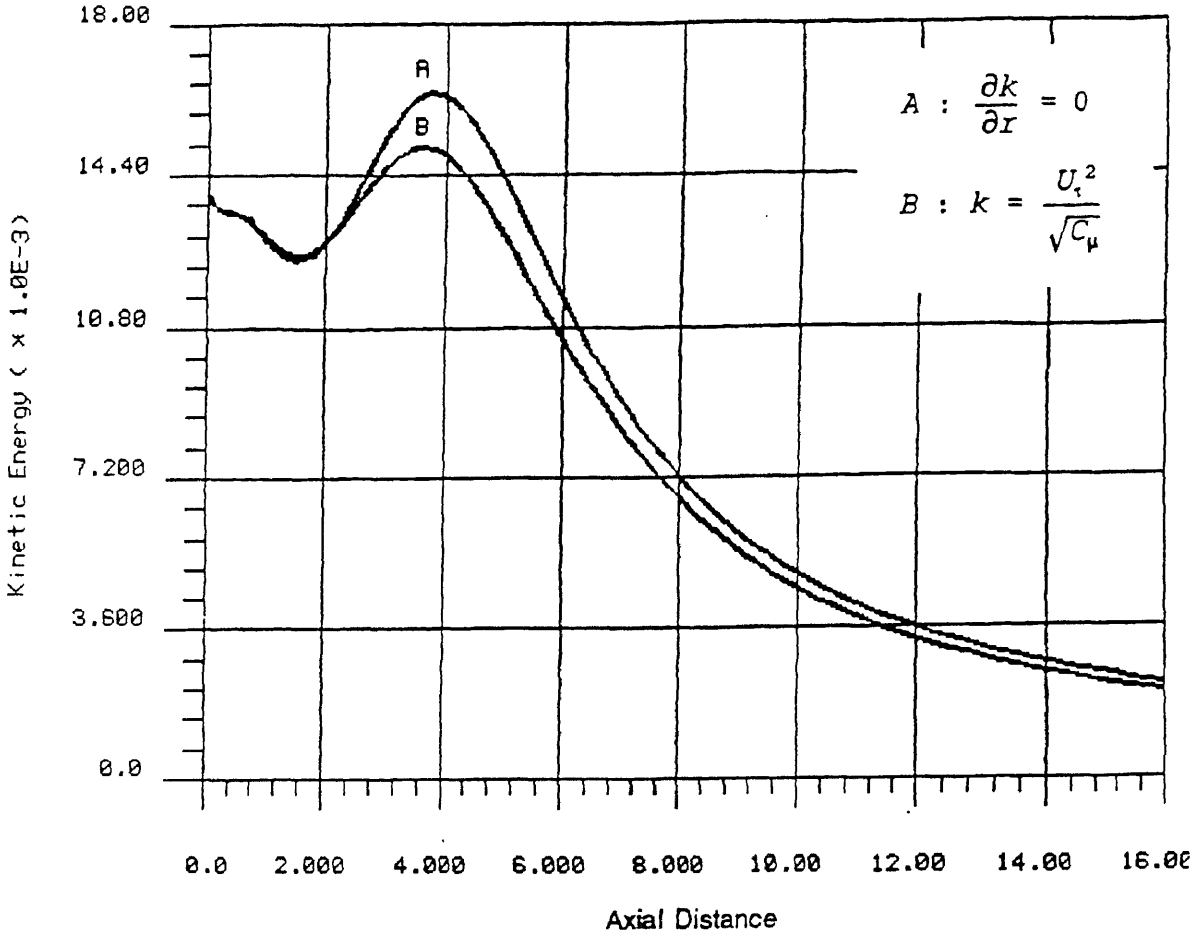

Figure 44 Comparison of centerline turbulent kinetic energy distribution for different boundary condition of turbulent kinetic energy at the wall

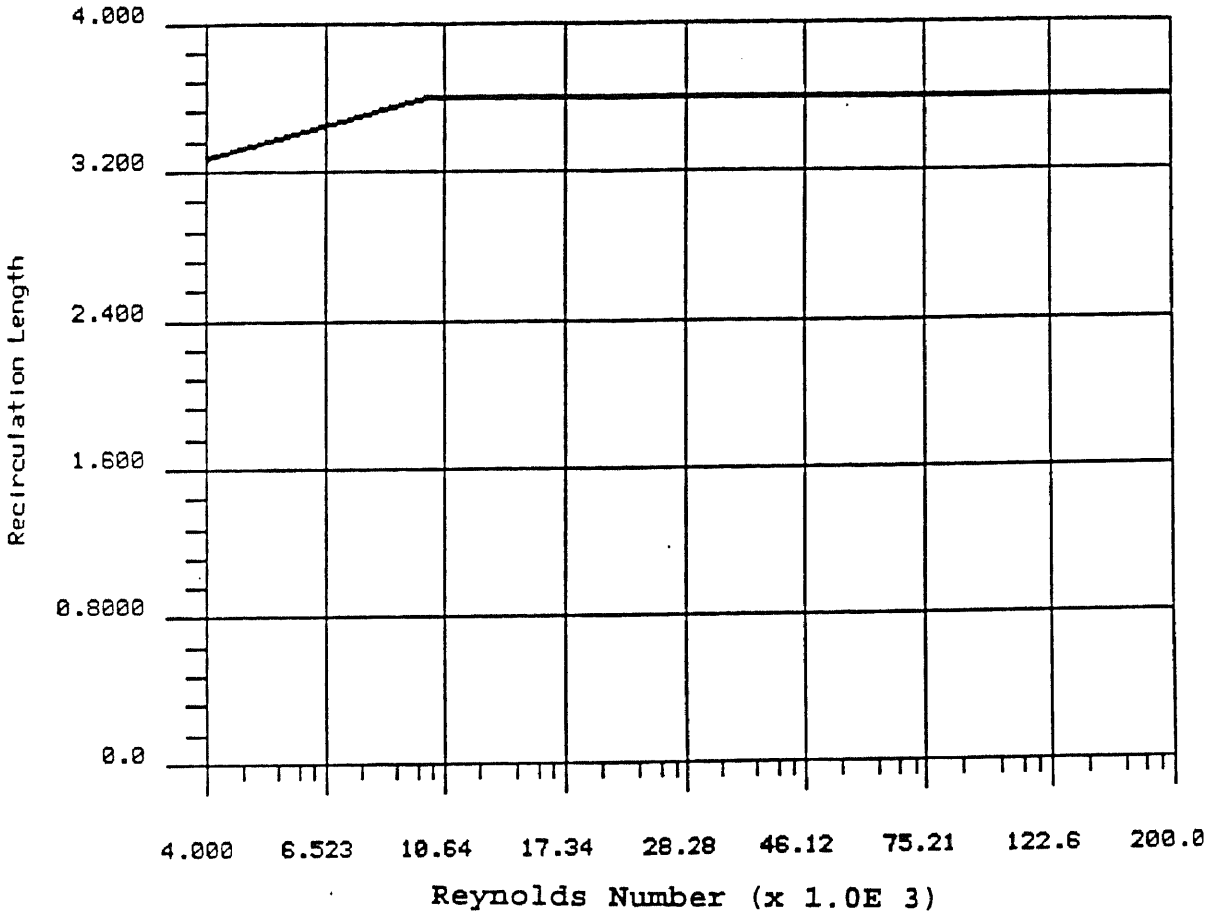

Figure 45 Variation of recirculation length with Reynolds number

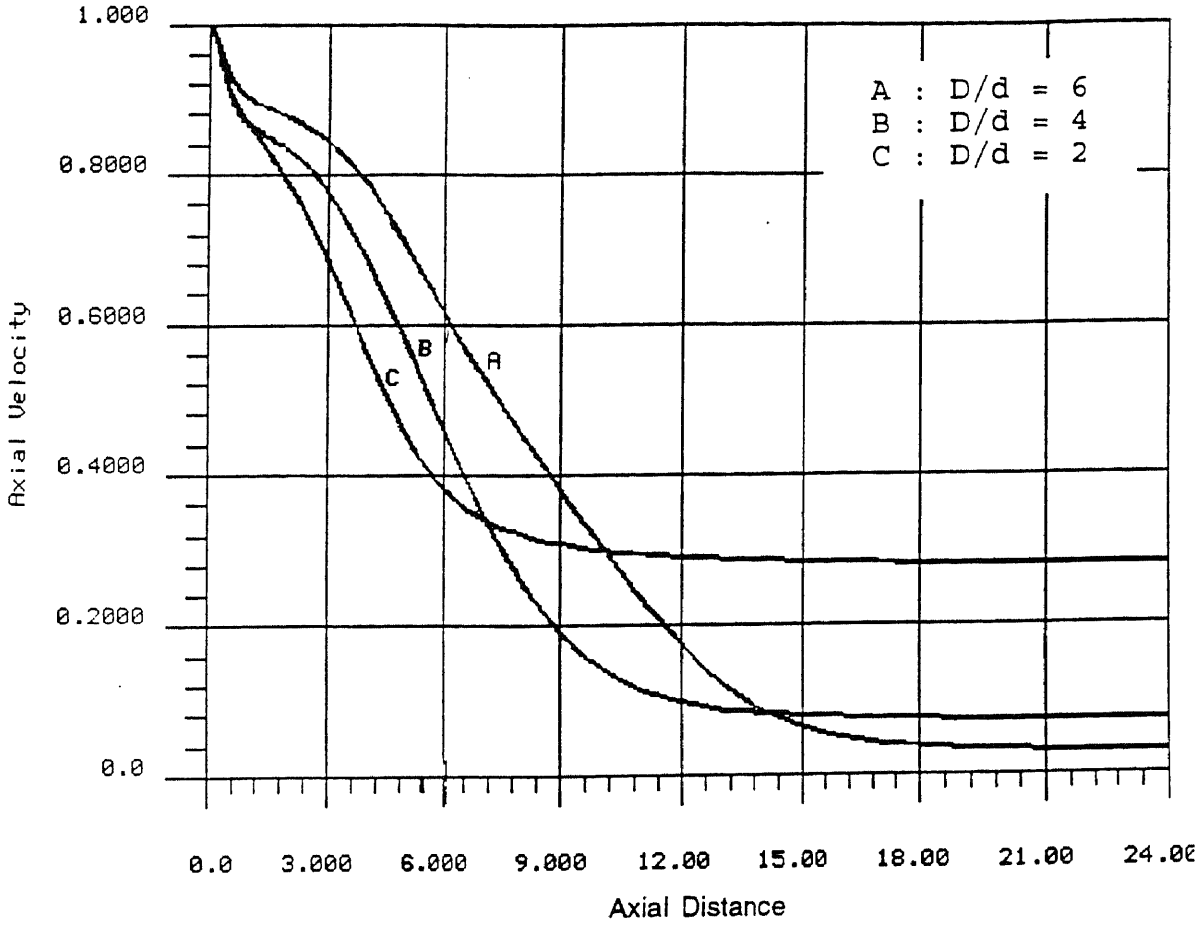

Figure 46 Centerline axial velocity distribution for different expansion ratios

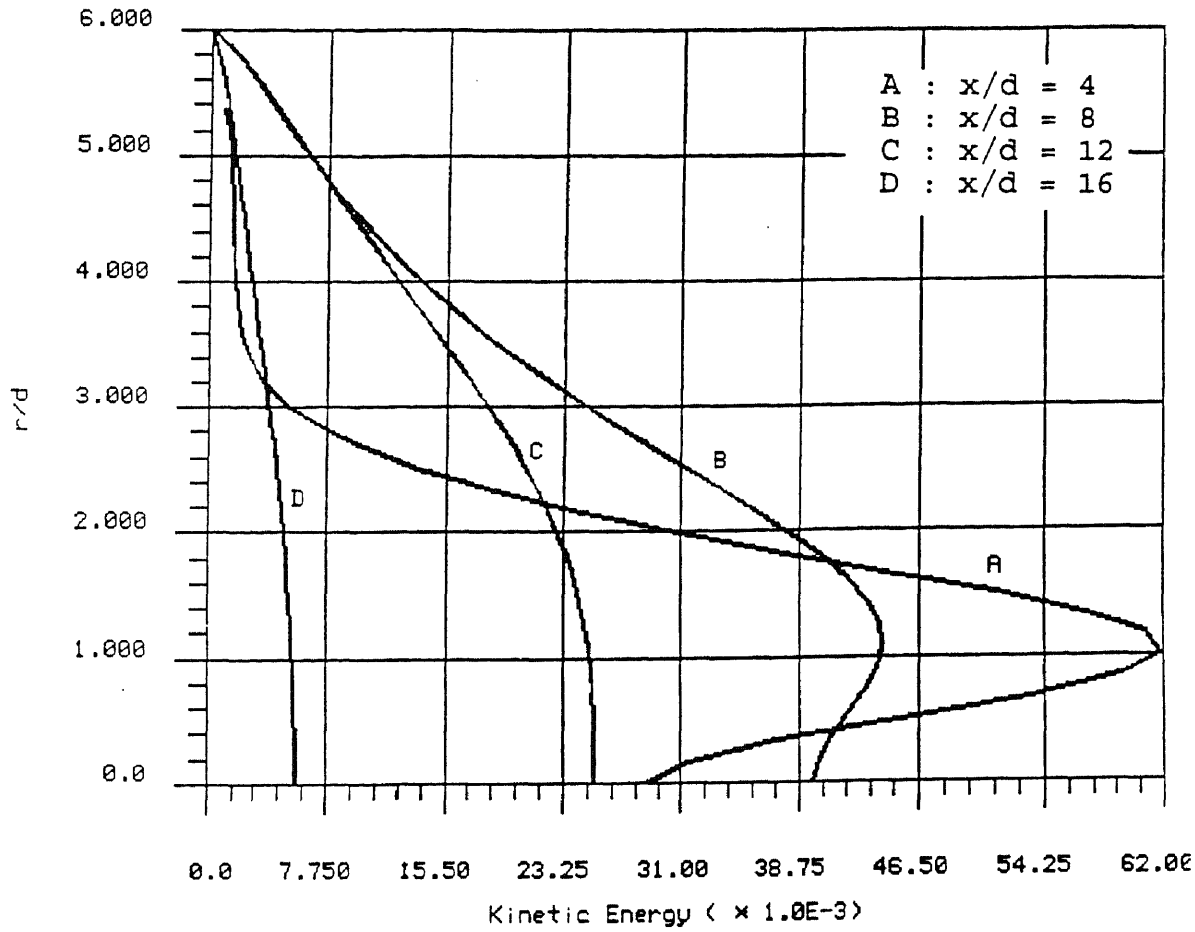

Figure 47 Turbulent kinetic energy profiles at different cross sections for expansion ratio of 6.0

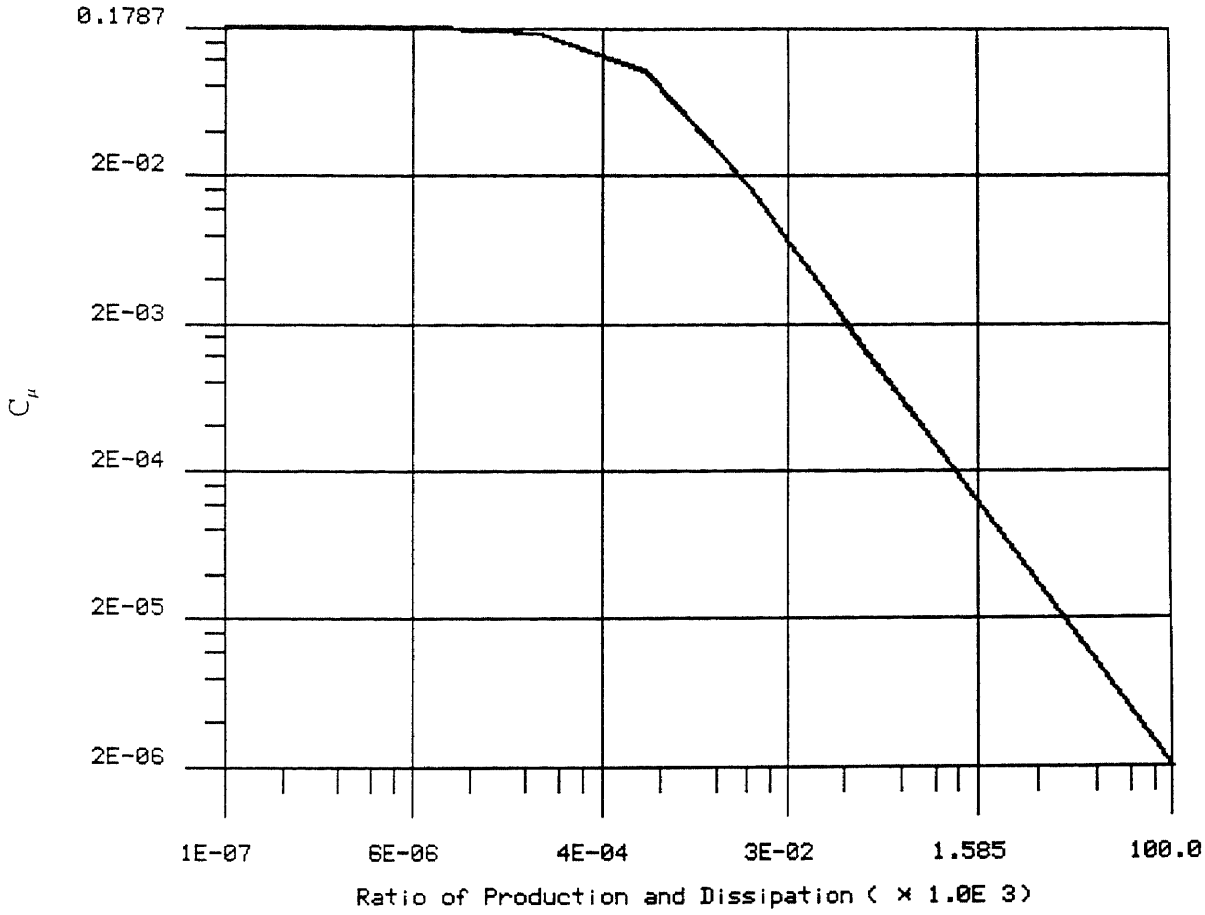

Figure 48 Variation of C_μ with ratio of production and dissipation of turbulent kinetic energy

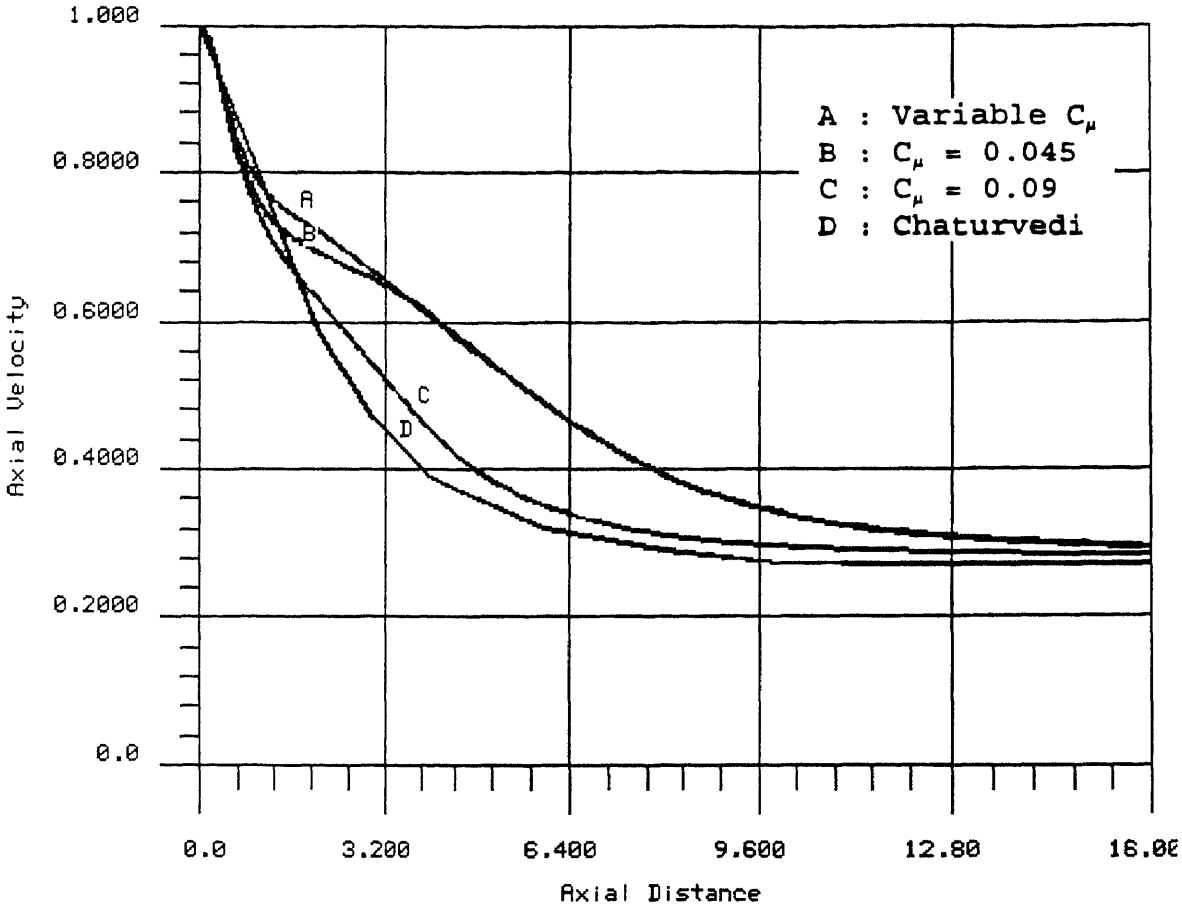

Figure 49 Centerline axial velocity distribution for different values of the coefficient C_μ (half angle of expansion = 15°)

REFERENCES

Argyris, J.H., and Kelsey, S., 1960, Energy Theorems and Structural Analysis, Butterworth Scientific Publications, London.

Autret, A., Grandotto, M., and Dekeyser, I., 1987, "Finite Element Computation of a Turbulent Flow over a Two-Dimensional Backward Facing Step", Int. J. for Numer. Methods in Fluids, Vol. 7, pp. 89-102.

Back, L.H., and Roaschke, E.J., 1972, "Shear-Layer Flow Regimes and Wave Instabilities and Reattachment Lengths Downstream of an Abrupt Circular Channel Expansion", Journal of Applied Mechanics, Trans. ASME, Vol. 94E, Sept., pp. 677 - 681.

Badekas, D., and Knight, D.D., 1992, "Eddy Correlation for Laminar Axisymmetric Sudden Expansion Flows", ASME J. of Fluids Engineering, Vol. 114, pp. 119-121.

Baskarone, E. A., 1991, "Finite Element Analysis of Turbulent Flow in Annular Exhaust Diffusers of Gas Turbine Engines", ASME J. of Fluids Engineering, Vol. 113, pp. 104-110.

Benim A.C., and Zinser, W., 1985,"Investigation into the Finite Element Analysis of Confined Turbulent Flows Using A k-ϵ Model of Turbulence", Computer Methods in Applied Mechanics and Engineering, Vol. 51, pp. 507-523.

Betts, P.L., and Haroutunian. V., 1985, "k-ϵ Modelling of Turbulent Flow Over a Backward Facing Step By a Finite Element Method; Comparison with Finite Volume Solutions and Experiment", Paper published in Proceedings of IV International Conference on Numerical Methods in Laminar and Turbulent Flow, held at Swansea,Uk,9th-12th July.

Bhatia, K., Rahman, M., Agarwal, B., 1993, "Analysis of Three Benchmark Problems Using NISA/3D-FLUID", Paper published in the Proceedings of "The Fluids Engineering Conference of ASME", Washington, D.C.

Chaturvedi, M.C., 1963, "Flow Characteristics of Axisymmetric Expansions", J. Hydraulics Div., Proc. Am. Soc. Civil Eng., Vol. 89.

Chou, P.V., 1945, "On Velocity Correlations and the Solution of the Equations of Turbulent Fluctuations", Quard. J. Appl. Math. 3, 1, pp. 8-54.

REFERENCES
(Continued)

Chung, T.J., 1978, "Finite Element Analysis in Fluid Dynamics", Mcgraw Hill.

Clough, R.W., 1960, "The Finite Element Method in Plane Stress Analysis", J. Struct. Div., ASCE, Proc. 2nd Conf. Electronic Computation, pp. 345-378.

Courant, R., 1943, "Variational Methods for the Solution of Problems of Equilibrium and Vibration", Bull. Am. Math. Soc., Vol. 49, pp. 1-43.

Davidov, B.I., 1961, "On the Statistical Dynamics of an Incompressible Turbulent Fluid", Dokl. AN SSSR, 136, 47.

Fletcher, D., Maskel, S., and Patrick, M., 1985, "Heat and Mass Transfer Computations for Laminar Flow in an Axisymmetric Sudden Expansion," Computers and Fluids, Vol. 13, pp. 207-221.

Habib, M.A. and Whitelaw, J.H., 1982, "The Calculation of Turbulent Flow in Wide-Angle Diffusers", Numerical Heat Transfer, Vol. 5.

Harlow, F.H. and Nakayama, P.I., 1967, "Turbulent Transport Equations", The Physics of Fluids, 10, pp. 2323.

Hinze, O., 1959, Turbulence, Mc. Graw Hill, New York.

Hrenikoff, A., 1941, "Solution of Problems in Elasticity by the Framework Method", J. Appl. Mech. Trans. ASME, Vol. 8, pp. 169-175.

Hughes, T., Liu, W.K., and Brooks, A., 1979, "Finite Element Analysis of Incompressible Viscous Flows by the Penalty Function Formulation", Journal of Computational Physics, vol. 30, pp. 1-60.

Irons, M.B., 1970, "A Frontal Solution Program For Finite Element Analysis", Int. J. for Numerical Methods in Fluids, pp. 5-32.

Jones, W.P., 1971, "Laminarisation in Strongly Accelerated Boundary Layers", Ph.D Thesis, Univ. of London.

Jones, W.P. and Launder, B.E., 1972, "The Prediction of Laminarization with a Two Equation Model of Turbulence", Int. J. Heat and Mass Transfer, 15, 301.

REFERENCES
(Continued)

Keller, L. and, Friedmann, A. 1924,"Differential gleichungen, fUr die turbulente Bewegung einer Kompressiblen Flussigkeit", Proc. Ist Int. Congress Appl. Mech., Delft, pp. 395-405.

Kolmogorov, A.N., 1968, "Equations of Turbulent Motion of an Incompressible Fluid", Imperial College, Mech. Eng. Dept. Rept. ON/6, 1968.

Krall, K.M. and Sparrow, E.M., 1966, "Turbulent Heat Transfer in the Separated Reattachment and Redeveloped Region of a Circular Tube", Journal of Heat Transfer, Trans. ASME, Vol. 88c, February, pp. 131-136.

Lai, M.K.Y., Vijay, M.M. and Zou, C., 1991, "Computational Fluid Dynamics Analysis of Submerged Cavitating Water Jets", Proc., 6th American Water Jet Conference, Aug., 24-27, pp. 411-426.

Launder, B.E. and Spalding, D.B., 1972, Lecture in Mahematical Models of Turbulence, Academic Press.

Launder, B.E. and Spalding, D.B., 1974, "The Numerical Computations of Turbulent Flows", Computer Methods in Applied Mechanics and Engineering, Vol. 3.

Leonard, B.P., 1979, "A Stable and Accurate Convective Modeling Procedure Based on Quadratic Upstream Interpolation", Comput. Methods Appl. Mech. Eng. 19, 59.

Macagno, E., and Hung, T.-K., 1967, "Computational and Experimental Study of a Captive Annular Eddy", Journal of Fluid Mechanics, Vol. 28, pp. 43-64.

Moon, L.F. and Rudinger, G., 1977, "Velocity Distribution in an Abruptly Expanding Circular Duct", ASME J. of Fluids Engineering.

Mosavi, R.K., 1987, "Comparing Laser and Waterjet Cutting", Lasers and Optronics.

Pai, B.R., Richter, W. and Lowes T.M., 1975, "Flow and Mixing in Confined Axial Flows", J. Inst. Fuel, 48, pp. 185-196.

Prandtl, L., 1925, "Uber die ausgebildete Turbulenz", ZAMM 5, pp. 136.

REFERENCES
(Continued)

Prandtl, L., 1945, "Uber ein neues Formelsystem fUr ausgebildete Turbulenz", Nachr. Akad. Wiss., Gottingen Math.-Phys. Klasse, pp. 6.

Raithby, G.D., 1976, "Skew Upstream Differencing Schemes for Problems Involving Fluid Flow", Comput. Methods Appl. Mech. Eng., 9, 153.

Rodi, W., 1971, "On the Equation Governing the Rate of Turbulence Energy Dissipation", Imperial College, Mech. Eng. Rep. TWF/TA/A/14.

Rodi, W., 1976, "A New Algebraic Relation for Calculating the Reynolds Stress", ZAMM 56, T219-T221.

Rodi, W., 1980,"Turbulence Models and their Applications in Hydraulics-A State of the Art Review", Report, University of Karlsruhe, Karlsruhe, Germany.

Rotta, J.C., 1968, "Statistical Theory of turbulence", Imperial College, Dept. of Mech. Eng.,Reports TWF/TN/ 38, 39.

Runchal, A.K., 1971, "Mass Transfer Investigation in Turbulent Flow Downstream of Sudden Enlargement of a Circular Pipe for Very High Schmidt Numbers", International Journal of Heat and Mass Transfer, Vol. 14, pp. 781-791.

Saffman, P.G., 1970, "A Model for Inhomogeneous Turbulent Flow", Proc. Roy. Soc., Ser. A, 317, pp. 417.

Sala, R., Vivarelli, P.L., and Garuti, G., 1980, "Numerical Analysis of Wide-Angled Diffusers in Turbulent Flow", J. of Hydraulics Div., Proc. ASCE, Vol. 106, pp. 629-647.

Schlichting, H., 1979, Boundary Layer Theory, McGraw-Hill, New York.

Scott, P., and Mirza, M., 1986, "A Finite Element Analysis of Laminar Flows Through Planar and Axisymmetric Abrupt Expansions", Computers and Fluids, Vol. 14, pp. 423-432.

Spalding, D.B., 1971, "The KW Model of Turbulence", Imperial College, Dep. of Mech. Eng., Report (TM/TN/A/16).

REFERENCES
(Continued)

Stieglmeier, M., Tropea, C., Weiser, N., and Nitsche, W., 1989, "Experimental Investigation of the Flow Through Axisymmetric Expansions", ASME J. of Fluids Engineering, pp. 464-471.

Szabo, B.A., and Lee, G.C., 1969, "Derivation of Stiffness Matrices for Problems in Plane Elasticity by Galerkin's Method", Int. J. Numer. Methods Eng., Vol. 1, pp. 301-310.

Tenneskes, H. and Lumley, J.L., 1972, A First Course in Turbulence, MIT-Press, Cambridge, Mass.

Tong, G.D., 1983, "A Treatment of Wall Boundaries for k-ε Turbulance Modeling Within An Integral (Finite Element) Formulation", Finite Element Methods in Fluids, Vol. 5, pp. 227-236.

Tsui, Y-Y and Lee, S-Y, 1992, "Calculation of Turbulent Flow through Engine Inlet Ports", Int. J. Heat and Fluid Flow, Vol. 13, No. 2, pp. 232-240.

Turner, M., Clough, R., Martin, H. and Topp, L., 1956, "Stiffness and Deflection Analysis of Complex Structures", J. Aero Sci., Vol. 23, pp. 805-823.

User's Manual, NISA/3D-FLUID, 1992.

Visser, W., 1965, "A Finite Element Method for the Determination of Nonstationary Temperature Distribution and Thermal Deformations", Proc. Conf. Math. Methods Struc. Mech., Air Force Institute of Technology, Dayton, Ohio.

Yung, C., Keith, Jr., T.G., and DeWitt, K.J., 1989, "Numerical Simulation of Axisymmetric Turbulent Flow in Combustors and Diffusers", Int. J. Num. Meth. in Fluids, Vol. 9.

Zienkiewicz, O.C., and Cheung, Y.K., 1965, "Finite Elements in the Solution of Fluid Problems", The Engineer, pp. 507-510.

Zienkiewicz, O.C., 1971, The Finite Element Method in Engineering Science, Mc Graw-Hill (UK), London.